THE EFFECT OF CONTROLLED NANOMATERIAL DEPOSITION TOWARDS ELECTRODES FOR MICROBIAL FUEL CELLS AND ELECTROLYSIS CELLS

by

BRYAN STEINHOFF

DISSERTATION

Submitted in partial fulfillment of the requirements
for the degree of Doctor of Philosophy at
The University of Texas at Arlington

August, 2019

Arlington, Texas

Supervising Committee:

Hyejin Moon, Committee Chair and Supervising Professor
Sunand Santhanagopalan, Co-advisor
Jiechao Jiang
Daejong Kim
Wen Shen

ACKNOWLEDGEMENTS

This work is supported by the National Science Foundation Award #1444473 as well as the University of Texas at Arlington Graduate School via the 2019 Summer Dissertation Fellowship.

I would like to whole-heartedly thank my committee members, Dr. Hyejin Moon, Dr. Wen Shen, Dr. Daejong Kim, Dr. Sunand Santhanagopalan, and Dr. Jiechao Jiang for their valuable insights and perspectives for this work. In particular, I would like to thank Dr. Jiang, and by extension the Characterization Center for Materials and Biology, for his guidance on the characterization equipment.

I would like to especially thank Dr. Hyejin Moon for pushing me along with my research and dissertation, even when I thought I was not ready. Thank you Dr. Moon for believing in me when I doubted myself.

I would like to thank Dr. Erian Armanios and the Mechanical and Aerospace Engineering department for all their assistance over the years and their aid in making my PhD a reality at the University of Texas at Arlington.

A special thank you to former members of the MuSES lab at Michigan Technological University and here at UTA (Ryan Lemmens and Hanfei Zhang in particular) for their friendship and insights during all the years I spent working on this research.

Words cannot express enough how much I would like to thank Dr. Sunand Santhanagopalan for his role in my research and my process in acquiring this degree. You are more than just an advisor or friend to me Sunand, you are a brother and I cannot thank you enough for pushing me to be the best I could be and always being there to cheer me up when I was too stressed to move forward. You are an amazing mentor and are always there to show me how the best way to do things are, even when I think my own way is the right way. I hope going forward I will be able to be as driven as you are and I will always strive to be a better researcher like you.

DEDICATION

This dissertation is dedicated to my family, my parents Karen and Steve and my brothers Erik, Gary, and Steven. Thank you for all of your support over the years and your endless love, even in the darkest times. You guys have, and will always be, my guiding light.

ABSTRACT

The Effect of Controlled Nanomaterial Wettability on Electrodes
For Microbial Fuel Cells and Electrolysis Cells

Bryan Steinhoff, Ph.D.

The University of Texas at Arlington, 2019

Supervising Professor(s): Dr. Hyejin Moon; Dr. Sunand Santhanagopalan

Microbial fuel cells (MFCs) and microbial electrolysis cells (MECs) are relatively new energy harvesting technologies that utilize the bacteria in wastewater or other organic-rich aqueous media to produce either electricity or hydrogen gas, respectively. Given that MFCs and MECs are newer technologies, there has been many works over the past two decades that have provided understanding into how modifying electrode surface chemistry can improve these cells. It has been widely known that increasing the surface functional groups of MFC anodes, either chemically or thermally, causes the cell power density to increase dramatically. Since MFCs and MECs use the same anodes, a corresponding increase in power density for a MFC will cause an increase in hydrogen generation if the anode is used in a MEC. Previous studies have also demonstrated that increasing the hydrophobicity of anode electrodes causes a corresponding decrease in output voltage and increases the necessary start-up time for MFCs. However, these studies do not correlate whether increasing hydrophilicity of anodes is of any benefit and there has been little study of how hydrophilicity can affect the MEC cathode where hydrogen generation takes place.

In this work, a one-step electrophoretic deposition (EPD) process is undertaken to deposit carbon nanotubes (CNTs) with variable wettability for MFC/MEC anodes and MEC cathodes. The EPD process allowed for the controlled wettability of the CNT depositions by changing the composition of the organic solvent used to disperse the nanomaterials, from hydrophilic to hydrophobic, without changing the applied voltage or nanomaterial concentration. Scanning electron microscopy images and Fourier-transform infrared spectroscopy were used to characterize these depositions and understand how changing the deposition solvent causes the corresponding change in surface wettability. The CNT depositions allowed previously poor performing bare metals, such as stainless steel, to express significantly increased volumetric power density and Coulombic efficiencies. A novel radial EPD technique was developed to deposit nanomaterials uniformly on stainless steel brushes to create a cost-effective, hierarchical three-dimensional anode for MFCs/MECs. All anodes were extensively studied electrochemically at each step of the cell wastewater inoculation process, when the bacteria colony is developed on the anode, as well as during the steady-state operation using either a conventional phosphate buffered solution or an amended wastewater.

TABLE OF CONTENTS

LIST OF FIGURES

LIST OF TABLES

I. General Introduction

1.1 Background and Motivation

According to Ricard E. Smalley, of the top 10 problems humanity faces for the next 50 years, energy takes precedence over all, even over the likes of war, poverty, and disease[1]. In today's society, fossil fuels continue to supply the plentiful energy society demands for continued global industrialization and economic growth. In fact, fossil fuels were used to meet almost 90 percent of the global energy needs throughout the last 50 years, with 60 percent of the overall needs met by oil and gasoline alone[2]. However, ever since its first widespread uses during the Industrial Revolution beginning in the late 18^{th} century, this consumption of fossil fuel as had devastating effects on the planetary ecosystem in the form of greenhouse gas emissions, which have caused detrimental widespread effects such as global warming, which has induced consequences such as melting artic ice caps and rising sea levels to name a few. More often than not, researchers are contemplating the impacts of 1.5-2^{o}C increases in the global temperature as an eventuality rather than a simple thought experiment[3].

As a result of normality of global warming and its impact on the environment, and by extension the economy from the eventual depletion of fossil fuels, researchers have begun to investigate and commercialize alternative energy sources to lessen the dependency on fossil fuels. Some of the more mainstream and commercially available alternative energy technologies are batteries, solar power, wind power, and fuel cells[4], [5]. The U.S. Department of Energy has a comparison of the more common fuel cells technologies and lists proton exchange membrane fuel cells (PEMFCs), solid oxide fuel cells (SOFCs), direct methanol fuel cells (DMFCs), alkaline fuel cells

(AFCs), phosphoric acid fuel cells (PAFCs), and molten carbonate fuel cells (MCFCs) as noteworthy. While these fuel cell technologies are good renewable energy technologies, they do not combat both the need of renewable energy and wastewater management that is necessary for future societal needs.

In addition to the crisis onset by humanity's dependence on fossil fuel as its main energy source and the occurrence of global warming, there is an increasing concern in the area of water management and urban growth. Energy may be the number one problem humanity faces, but according to Smalley, water and water management is a close second[1]. By 2025 over 5 quadrillion gallons of water will be consumed globally, all of which must be treated if it is to be reused for either residential or commercial use. In the United States alone there are over 14,000 publicly owned treatment works (POTWs) that service 238 million people. These POTWs generate over 8 million tons of sludge. In order to treat the sludge, a wastewater treatment plant can spend, depending on the source, upwards of 30 percent of the its total consumed electricity and upwards of 60 percent of its total operating costs[6][7]. Compounding this issue is the fact that wastewater treatment plants and urban sewer systems must be operated in perpetuity in order to meet society's daily need of safe, potable water. Therefore, repairing sewer systems and upgrading wastewater plants is a costly necessity, which can cost a currently estimated $150 billion[6]. As such, it is imperative to either reduce the workload on wastewater treatment plants or find ways to minimize the amount of sludge that is needed to be disposed of at the end of the treatment process.

There is however one type of fuel cell that is missing from the U.S. Department of Energy list, or rather a type of alternative energy system, and that is the bioelectrochemical systems (BES). This type of energy system uses microbes that produce electrons when consuming organic matter, called exoelectrogens, to create electricity, hydrogen, methane, or some other valued added product. BESs take advantage of the microbial metabolism in the form of extracellular electron transfer (EET), where bacteria directly or indirectly emit excess electrons to an electrode, typically the anode, where they are then harvested for the appropriate process[8]. The direct process of EET requires direct contact of microbes on an electrode's surface in order to transfer the electron through the c-type cytochromes of the outer membrane of the bacteria while indirect EET processes include transfer of electrons through conductive pili, conductive biofilm matrixes made up of c-type cytochromes, and shuttling of electrons through oxidation and reduction reactions of microbes coming into contact with the electrode surface[9]. Bioelectrochemical systems can aid the ongoing struggle society has with water management and wastewater disposal since the microbes in these cells can break down the sludge in order to provide clean, renewable energy source.

One particular type of BES is the microbial fuel cell (MFC), and is defined as a cell which contains a sustainable process of microbes catalyzing electron generation, which are then consumed at the cathode[10]. It is important to clarify that electrochemical cells that do not catalyze electrons directly from bacteria or enzymes created directly from bacterial activity are not called MFCs and are instead designated as enzymatic fuel cells (EFCs)[11]. The first reported use of a MFC dates back to 1911 with Potter, who used pure cultures of the *Saccharomyces* bacteria to decompose a commercial yeast to produce maximum voltages between 0.3 and 0.5 volts[12]. The technology

was largely abandoned until modern times where the necessity for renewable energy sources made MFCs an attractive candidate for research, in the form of an energy harvesting technology[13].

Microbial fuel cells can also be converted into microbial electrolysis cells (MECs), which take advantage of the same cell architecture, but instead of utilizing the typically used air-breathing cathode in MFCs to produce electricity via the oxygen reduction reaction (ORR), the MEC is operated in a completely anaerobic environment. By applying a small voltage, traditionally 0.4V to 1V, and combining this voltage with electrons supplied by the bacterial colony, hydrogen gas can be generated and captured for other uses[14], [15]. This process has been named electrohydrogenesis and does not actually involve the splitting of water, even though electrolysis is part of the overall cell name[15]. Microbial electrolysis cells provide a unique opportunity to create hydrogen gas at voltages below that of conventional water electrolysis, though current limitations of cells include low hydrogen production, mixing of hydrogen with other gas byproducts such as methane, and lack of scalable designs[16].

Since electron transfer to the anode of the MFC or MEC is critical for effective cell performance, choosing the proper electrode material is of great importance, if not the most important decision when constructing and operating a MFC or MEC. However, electrode material is by no means the only factor that effects cell performance in either of these cells and overall cell performance is a combination of many factors. Reactor configuration, operating temperature, electrolyte conductivity and pH, inoculation source and method, and catalyst can all have major impacts on MFC and MEC start-up and final output performance[17]–[19]. All of these parameters, and others, have been extensively studied, but there are many questions remaining and more

comprehensive analysis is needed to provide a full picture of how MFCs and MECs can optimally function.

Since their reintroduction into the forefront of alternative energy research, many different materials have been utilized as anode materials. Early concept works of both MFCs and MECs were dominated by two-chamber cells utilizing two-dimensional carbon based materials such as carbon paper, carbon cloth, graphite rods, and graphite granules while traditionally maintaining a carbon cloth cathode using a 10% weight Pt/C catalyst[20]–[22]. Eventually cells moved towards a single chamber design, however, kept the same cathode and catalyst configuration[14], [23]. All of these studies exposed flaws in the two-dimensional carbon substrates, in the fact that they have higher internal resistances, high mass-transfer overpotential, and relatively low surface area[24]. In order to create high performance MFCs, high surface area three-dimensional anodes are required to larger colonies of bacteria, and in turn, generate more electrons for to be reduced on the cathode from the oxygen reduction reaction (ORR). However, despite their limitations, carbon based materials do provide good biocompatibility for promoting bacterial colony growth, so creating a three-dimensional carbon based anode was of upmost importance to initial MFC research. This was achieved when the first graphite fiber brush (GFB) anode was created and this particular anode remains the current standard as one of the highest power performing anodes in MFCs[25].

Since the inception of the graphite fiber brush, research has branched in numerous new directions, some of which include anode surface modifications and while others focus on the development of more cost-efficient materials. The current drawback to incorporating graphite fiber brushes into

all MFCs is that they are an expensive and time-consuming anode to fabricate. The current methodology of making a GFB consists of taking a sheet of carbon fiber and cutting the sheet repeatedly to manufacture micron sized fibers. These fibers are then woven around a titanium wire core, which acts as the anode's current collector, using a specific brush making machine that can accommodate the small fibers. All of this has been traditionally done to order, or made in house, for the specific studies that use them.

In order to reduce the lead time of making these brushes, and in general reduce the overall cost of anodes, the MFC and MEC research community has turned its attention to bare metals. Once thought as unsuitable for use as MFC anodes because of their poor biocompatibility, tendency to corrode, and high overpotential, some researchers have claimed that copper, stainless steel, and nickel are suitable bare metal electrodes for MFC and MEC anodes[26]–[28]. Stainless steel (SS) has been rising in popularity and is generally accepted as a suitable bare metal to experiment with, but copper is controversial due to its high corrosion in the presence of bacteria and the corrosion of copper has been demonstrated to provide a large initial cell voltage which is not sustainable over the course of the cell lifetime[29]. However, even though it is generally accepted as a low-cost alternative to carbon based anodes, bare SS electrodes produce cell output voltages that are orders of magnitude less than even two-dimensional carbon materials[30].

As such, stainless steel needs to undergo a surface modification in order to compete with other carbon based materials and carbon composite structure anodes. Some of the earliest surface modifications included the ammonia gas treatment of GFBs and their follow-up acid and heat treatments[31], [32]. Both studies showed that the treatments improved the power production of

the GFBs by over 30 percent and that, due to its simplicity and lower cost, the acid and heat treatments were the preferred surface modification methods. Flame oxidation is one method to create carbon nanostructures on SS electrodes and has been shown to greatly improve SS performance as MFC anodes, but the process removes the protective oxidation layer of the bare metal, leaving it susceptible to corrosion in pure wastewater[33], [34]. Therefore, in order to simultaneously protect the bare SS from corrosion while increasing its biocompatibility decreasing its overpotential, researchers focused on the deposition of carbon nanomaterials, in particular carbon nanotubes and graphene[35]–[38]. Deposition methods varied from water based electrophoretic deposition to traditional pasting of nanomaterials, combined with a conductive polymer, or Nafion or other nonconductive binders.

Hydrophilic surface modifications of MFC and MEC electrodes are under-utilized in the research community, stemming mostly from the way most surface modifications are currently applied. Many studies employ the use of dip-coating and binders, Nafion in particular, to adhere the altering nanomaterial or substance to the desired electrode, which intrinsically increases the hydrophobicity of the electrode[39],[30]. As a side-effect, the electrical conductivity of the electrodes decreases as a result of these binders. Current studies elaborate on the importance of anode wettability in the improvement of overall MFC power performance or start-up time, however, these wettability modifications are generally due to the intrinsic increased wettability of the added material and not via a controlled modification process[40]–[44]. Therefore, it is important that surface modifications, if desired to be hydrophilic, avoid the use of dip-coating and binders in order to have the high conductive necessary to promote facile EET from the bacterial colony to the cathode electrode. While it is generally well known in the PEMFC community that

wettability has a large impact on fuel cell performance, it is currently not known to what extent wettability has on MFCs and MEC performance, and if at all there is an optimal wettability for MFC anodes[45], [46].

One deposition method that has demonstrated controlled wettability of carbon nanotubes is electrophoretic deposition (EPD). At its core, EPD is a versatile process where nanoparticles are suspended in a liquid media and deposited onto a conductive substrate using an applied electric field. In general, the only typical downside of EPD, when compared to other methods such as slurry-coating or dip-coating, is its use in aqueous media. For a water based EPD, the water will undergo electrolysis and the hydrogen or oxygen evolution at the deposition electrode can significantly degrade the quality of the film surface[47]. Water EPD has been done extensively however, and the electrolysis can generally be mitigated if deposition voltages are kept below 20V[48].

The migration of the nanoparticles can only occur when the nanoparticles have enough charge in the liquid media they are suspended in[49]. If nanoparticles do not have enough charge to make a stable colloidal suspension, surfactants or charging salts can be added, though the latter is preferred since the former can induce higher film resistances, much like binders in traditional pasting techniques. The deposited charging salts from the EPD process have shown to act as a holding layer for deposited nanoparticles and the EPD process has been shown to be able to control the wettability of carbon nanotubes from hydrophilic to superhydrophobic while dramatically increasing the electrode's electrochemical performance [50]–[52]. While EPD has been sparingly used for cathode deposition in MFCs, with no reported downside, it has not been utilized to

generate well covered, nanoparticle decorated carbon nanotube films for bacterial growth on anodes[38]. Since EPD can provide the controlled wettability and good coverage to protect bare SS anodes, it will be used extensively throughout this work as the main deposition method for all nanomaterial dispersions.

1.2 Outline of Chapters

Chapter 2: Theory of Microbial Fuel Cells and Microbial Electrolysis Cells

This chapter explains the theoretical concepts of how both MFCs and MECs operate. The focus of this chapter is to give an in-depth view of the functional mechanisms of how MFCs and MECs use bacteria to produce electricity and hydrogen, respectively, schematically and the reactions that take place during typical research conditions in laboratories. An overview of the design evolution of MFCs and MECs will be discussed and a discussion of the historical advantages and challenges of each system design is provided. A thorough explanation of the calculation methods of MFCs in particular are established, ranging from the introduction of Coulombic efficiency and how it is determined from cell voltage curves to an explanation of the shape of the cyclic voltammetry (CV) and what potential peaks can signify to a discuss of power overshoot and means of correcting it during cell cycle operation. Additional discuss is provided specifically for MECs with

Chapter 3: Effect of Controlled Surface Modification via Electrophoretic Deposition of Carbon Nanotubes on Microbial Fuel Cell Performance

This chapter aims to demonstrate and characterize the ability to control wettability on anodes that are used for MFCs and MECs. In this work, anodes are made by depositing carbon nanotubes onto stainless steel sheet electrodes by utilizing an organic solvent based electrophoretic deposition.

The organic solvent is varied from pure ethanol to equal parts ethanol and isopropyl alcohol (IPA), which significantly changes the wettability of the anode from hydrophilic with no IPA present, to hydrophobic with increasing IPA content. The overall goal of this work is to show the effect of wettability on cell performance, as well as the overall effect of CNT depositions onto stainless steel for use in wastewater inoculated MFCs. At each point of the inoculation phase, from abiotic to wastewater inoculation to phosphate buffer solution steady-state, extensive electrochemical testing is undergone to understand how the EPD anodes operate in MFCs and how other factors besides wettability are affecting EPD anode MFC performance.

Chapter 4: Versatility of Developed Electrophoretic Deposition Technique to Fabricate Scalable Anodes for Microbial Fuel Cells

This chapter aims to demonstrate the versatility of the EPD process of depositing carbon nanotubes exhibited in Chapter 3 to create, for the first time via radial EPD, a hydrophilic, highly conductive and high surface area stainless steel brush type anode. This anode was compared, in 30 mL MFCs, to the stainless steel sheet type anode used in Chapter 3, along with a stainless steel mesh anode developed as the in-between for the 2D and 3D types. Some investigation into how various of the parameters of EPD parameters affect the deposition of carbon nanotubes on the bristle surface when using radial EPD with some explanation as to why the deposition differs compared to traditional planar EPD. After this investigation, a larger brush was used to create one of the largest known MFCs utilizing an EPD anode, a 275 mL MFC, which was operated solely in unamended wastewater to provide a realistic determination of the performance of these EPD anodes in wastewater treatment plants.

Chapter 5: Controlled Wettability via Electrophoretic Deposition and the Effect on Catalytic Performance for Microbial Electrolysis Cell Cathodes

This chapter aims to provide, for the first time, a demonstration of electrophoretically deposited carbon nanotube based catalysts for improved hydrogen generation in MECs. For this work, an electrochemical study using linear sweep voltammetry (LSV) of two different catalyst wettabilities, one hydrophobic and one hydrophilic, was conducted on stainless steel sheet. The role of wettability is investigated and how the wettability correlates to performance differences during the LSV study. After this, the better performing hydrophilic CNT based catalyst was deposited on stainless steel mesh and subjected to a platinum galvanic replacement as a means to show improved catalytic performance and demonstrate the ability to modify EPD based carbon nanotube films after their initial deposition.

Chapter 6: Conclusions

This chapter contains a brief summary of the highlights of the dissertation work and contains some discussion of potential work that can be investigated from the results presented in this dissertation.

II. Chapter 2: Theory of Microbial Fuel Cells and Microbial Electrolysis Cells

2.1 Theory of MFC and MEC Bacteria

As was stated in the introduction, bioelectrochemical systems, including both microbial fuel cells and electrolysis cells, use microbes that produce electrons when consuming organic matter, called exoelectrogens. These exoelectrogens can be cultivated onto the anodes of either of these cells either by transferring pre-cultured pure strains or by introducing media such as wastewater to induce multiple, or mixed-culture, strains onto the anode. The former method is good for investigations into specific reactions with a bacterium or evaluating specific gene modifications while the latter is more practical for evaluation of how MFCs or MECs will behave in a commercial environment.

Of all the bacteria strains present in mixed-culture communities, microorganisms in the *Geobacteraceae* family, and in particular the *Geobacter sulfurreducens* strain, can be highly enriched on both sediment and wastewater MFC anodes and be used in the breakdown of organic matter[53]. Together with the strain *Shewanella oneidensis*, these two strains make up the most studied exoelectrogens used in MFCs and MECs as their entire gene sequences have been known since almost the onset of modern MFC and MEC research[54]. These strains have been used to breakdown substrates such as acetate, cellulose glucose, lactate, propionate, sucrose, and a variety of wastewaters ranging from sources from swine farms to paper recycling centers to wineries

In order for bacteria strains such as *Geobacter sulfurreducens* and *Shewanella oneidensis* to transfer electrons to the MFC or MEC anode, the bacteria must undergo a process called

extracellular electron transfer (EET), where the bacteria directly or indirectly emit excess electrons to an electrode where they are then harvested for either electricity in MFCs or hydrogen in MECs[8]. The direct process of EET requires direct contact of microbes on an electrode's surface in order to transfer the electron through the c-type cytochromes of the outer membrane of the bacteria while indirect EET processes include transfer of electrons through conductive pili, conductive biofilm matrixes made up of c-type cytochromes, and shuttling of electrons through oxidation and reduction reactions of microbes coming into contact with the electrode surface[9]. Bioelectrochemical systems can aid the ongoing struggle society has with water management and wastewater disposal since the microbes in these cells can break down the sludge in order to provide clean, renewable energy source.

Electrochemical testing can be used in order to detect bacterial growth in MFCs and MECs, as well as potentially study the reaction kinetics between bacteria and electrodes. This study of reaction kinetics is important as surface modifications become more pervasive in MFC and MEC studies and how bacteria interact with these environments[55]. While the methods of EET have been proposed, many of these processes have complex interactions with the anode surface, cell electrolyte, and even between the bacteria colony itself, making it difficult to prove the assumptions of the EET models[56]. As such, electrochemical testing methods, in particular cyclic voltammetry, can provide a wide-range view of the electrochemical activity of the bacteria and provide the potentials, or range of potentials, of specific redox reactions happening within the bacteria's c-type cytochromes.

The shape of the CV curve is what is known as a reverse-catalytic curve, which indicates that as the catalyst or reactive element of the system gains or loses electrons, the catalyst is regenerated by its operation in the system itself[57]. For MFCs, the bacteria continually emit electrons and from cytochromes in their outer cell membrane, which are replenished by the break-down of the acetate. This anodic reaction can be seen in the following equation:

$$CH_3COO^- + 4H_2O \rightarrow 2HCO_3^- + 9H^+ + 8e^-, \qquad E_0 = 0.187V \qquad (1)[58]$$

This constant emission of electrons drives the catalytic reversible curve towards its characteristic "S" shape until the point where bacterial electron production can no longer sustain the increase in current where the current will fall and later plateau. For *Geobacter sulfurreducens*, the c-type cytochrome has a reduction potential of -350 mV vs. SCE and an oxidation peak of -420 mV vs. SCE (-305 mV and -375 mV vs. saturated Ag/AgCl respectively), when exposed to concentrations of a ferrihydrite suspension[59]. Additional studies have shown a slightly lower reduction potential for pure culture *G. sulfurreducens* of -170 mV vs. NHE (-370 mV vs. saturated Ag/AgCl), indicating that reduction potentials for mixed cultures primarily consisting of *G. sulfurreducens* should have CV reduction peaks close to these voltages[53]. Another method of verification of redox potentials, if there are no discernible peaks in the reversible catalytic wave, is to take the first derivative of the CV curve. By doing so, the noticeable peak between 350 mV and 370 mV versus Ag/AgCl can be seen, which again corresponds to the of the reduction potential of c-type cytochromes[24].

2.2 Theory of Microbial Fuel Cells

As was stated in Chapter 1, a microbial fuel cell is an energy system which, after an inoculation process, contains a sustainable production of electrons from microbes catalyzing an electron donor. These electrons are then transferred through a circuit with a load bearing resistor, used to measure the voltage and thereby the current when the resistor is fixed, where they are consumed on the cathode. The typical circuit diagram for a MFC is seen in Figure 1.

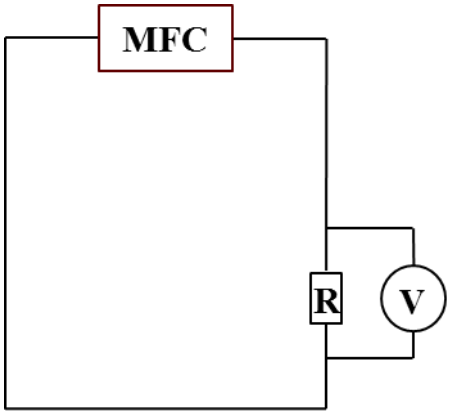

Figure 4: Typical Circuit Diagram of a Microbial Fuel Cell

The first MFCs built in the 1990s and early 2000s focused primiarily on two-chamber designs, and consisted generally of two bottles, typically H-bottles, or a two-chamber cell connected by either a salt-bridge or cation exchange membrane (CEM)[60]–[62]. However, these configurations, while good for parameter studies or concept validation, where quickly discarded due to their low power densities and high internal resistances generated by the salt bridges[58]. As such, researchers have moved away from two-chambered designs and have instead in modern times been focusing on one-chamber MFCs utilizing a variety of three-dimensional or nanomaterial decorated anodes to generate high power performance.

Cathodic reactions in MFCs are typically broken down into two categories, either the oxygen reduction reaction (ORR) or non-ORR reactions. In modern MFCs, virtually all cells use the ORR reaction on the cathode since oxygen as the electron acceptor as it is a well-established and known reaction kinetics, is a fuel source that can be easily replenished from the atmosphere, and provides one of the highest available cathodic potentials for operating fuel cells. The equation and standard reaction potential of the ORR reaction can be seen in Equation 2.

$$O_2 + 4H^+ + 4e^- \rightarrow 2H_2O, \qquad E_0 = 1.229V \qquad (2)[58]$$

However, due to the operating conditions of MFCs, typically at a pH near 7 and with the air containing approximately 20 percent oxygen, the actual cathodic potential of a MFC is 0.805V

For early MFCs, MnO_2 with and without ferricyanide, were used as the alternative to oxygen reduction as wet-proofed carbon cloth cathodes with an outer layer gas diffusion layer had not been readily established. The integration of the wet-proofed carbon cloth cathode, coupled with the fact that both MnO_2 and ferricyanide deplete over the course of the MFC lifetime and the movement towards one chamber MFCs, led to these two cathode materials to eventually be phased out of most laboratory studies. Ferricyanide in particular has been readily avoided because its use as an electron acceptor would create conditions that would not exist in practical applications[63]. The equations for both of these materials can be seen in Equations 3 and 4 respectively.

$$MnO_2(s) + 4H^+ + + 2e^- \rightarrow Mn^{2+} + 2H_2O, \qquad E_0 = 1.230V \qquad (3)[58]$$

$$Fe(CN)_6^{3-} + e^- \rightarrow Fe(CN)_6^{4-}, \qquad E_0 = 0.361V \qquad (4)[58]$$

For modern fuels cells incorporating the use the ORR and acetate as the electron donor, the theoretical OCV of a MFC becomes 1.042V by subtracting the theoretical anodic potential in Equation 1 from the cathodic potential in Equation 2. However, due to the operating conditions of MFCs, typically at a pH near 7 with the air containing approximately 20 percent oxygen and bicarbonate and acetate concentrations of 5 mM, the actual theoretical OCV of a MFC is 1.1V, with typical OCV seen in MFCs being approximately 0.8V[58], [64].

Microbial fuel cells are typically started up in a batch process mode, where inoculation fluid is added to the abiotic cell and bacteria is allowed to proliferate on the anode until a threshold voltage is achieved. This threshold voltage can be varied, depending on the strength of the inoculation media, but typically ranges between 20 and 200 mV[25], [65], [66]. Batch start-up can be conducted via multiple cycles, i.e changing inoculation media at fixed time intervals, or by allowing one cycle until noticeable depreciation of cell voltage is recorded.

Microbial fuel cells typically report three types of data as a means of characterizing cell performance. This characterization is represented as a cell voltage curve, the Coulombic efficiency, and the cell polarization curve. The cell voltage curve is plotted with the measured cell voltage across the external resistor in the circuit, with respect to time, typically in either hours or days depending on the length of the study. A minimum of three reproducible cycles should be reported in order to verify that current generation is stable and that no galvanic currents are causing additional voltage, especially when using bare metal anodes[63].

The Coulombic efficiency, C_{eff}, is a measure of how many Coulombs are actually produced from breakdown of the provided substrate against how many Coulombs could theoretically be produced from the complete breakdown of said substrate, and can be represented by Equation 5. The calculation of the theoretical number of Coulombs, C_T, can be seen in Equation 6 where *F* is Faraday's constant (96,485 C/mol electrons), *b* is the number of moles of electrons produced per mole of substrate, *S* (g/L) is the substrate concentration in grams per liter, *v* (L) is the liquid volume of the cell in liters, and *M* is the molar mass of the substrate.

$$C_{eff} = \frac{C_{act}}{C_T} \quad (5)[65]$$

$$C_T = \frac{FbSv}{M} \quad (6)[65]$$

To calculate the actual number of Coulombs produced by the bacteria, C_{act}, the current provided by the cell voltage curve, calculated using Ohm's Law since voltage is measured across a fixed resistor, is integrated with respect to time, as represented in Equation 7.

$$C_{act} = \int_{t_o}^{t} I \, dt \quad (7)$$

Polarization curves, either a P-I curve, V-I curve, or both, are typical representations of the power density of MFCs. Polarization curves are generally divided into three important areas for characterization. These zones are the increase decrease from OCV to current production where activation losses are dominant, the linear decrease in voltage were ohmic losses are dominant, and the rapid decrease in voltage at high current densities were mass-transport limitations are dominant[58]. In order to conduct polarization curves, which have the current density normalized

to the cathode area or volume of the cell chamber for high surface area anodes, two general methods are employed. The first is via a potentiostat where a slow scan rate linear sweep voltammetry (LSV) between the 0V and OCV for the cell can generate the V-I curve while the second method uses either a variable resistor or resistor box to periodically change the external resistor of the MFC circuit to create a V-I curve. In either case, the power can then be calculated as seen in Equation 8 and plotted against the cell current density, where V_{meas} is the measured cell voltage in volts and R_{ext} is the external resistance in ohms.

$$P = VI = \frac{V_{meas}^2}{R_{ext}} \tag{8}$$

In polarization curves, there are typically two types of power overshoot that can occur, which are Type D and Type M[67], [68]. In Type D overshoot, the power density "doubles back" when the external resistance is decreased to simulate high current density operation while Type M overshoot occurs when the power is overestimated as an error from the polarization testing process. Type M overshoot can be easily corrected by using slower scan rates, if the study is LSV, or by increasing the time before changing the external resistance via the resistor method.

While Type M overshoot is relatively simple to correct and understand, Type D overshoot is more complicated and is not only a MFC problem, but a general fuel cell issue[69]. Some various methods of correcting power overshoot include inoculating bacteria to low external resistances and inoculating anodes at higher fixed potentials[68], [70]. By using either method, bacteria are able to experience much higher oxidation-reduction activity over a larger range of potentials, as denoted by the increased electrochemical area in first derivative CV curves.

2.3 Theory of Microbial Electrolysis Cells

A microbial electrolysis cell is an energy system where, similar to a MFC, microbes catalyze an electron donor to produce electrons. These electrons are then transferred through a circuit with a small current-sensing resistor, where they are consumed on the cathode along with additional electrons provided by an external power source. This entire process, under anaerobic conditions, produces hydrogen gas via the hydrogen evolution reaction and is called electrohydrogenesis[15]. The typical circuit diagram for a MEC is seen in Figure 2.

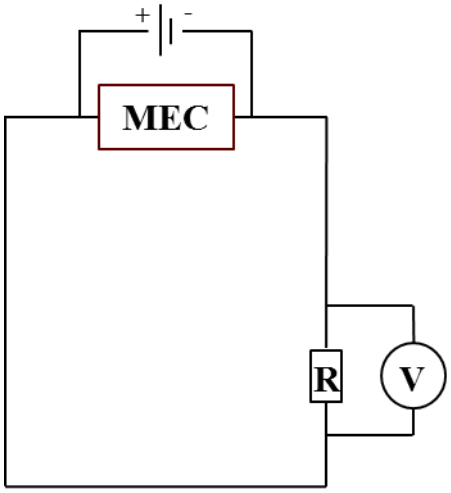

Figure 5: Typical Circuit Diagram of a Microbial Electrolysis Cell

Similar to MFCs, MECs were originally made in a two-chamber design, either the two H-bottles as was previously demonstrated for MFCs, or two chambers made out of a durable material such as poly(methyl methacrylate) (PMMA)[71], [72]. As with original MFCs, these two chambers were separated by a proton exchange membrane (PEM, Nafion 117), which is more important in MECs than it is in MFCs.

For MFCs, a PEM can help transfer protons to the cathodic chamber in a two-chamber configuration, but it largely unnecessary if the two electrode spacing is close. In MECs however, the PEM serves a dual purpose of both proton transfer, as well as preventing hydrogen gas that has been generated from migrating back to the anode. The bacteria can then breakdown the hydrogen gas that was produced on the cathode for additional electrons, a process called hydrogen scavenging, or create methane via a process called methanogenesis[73].

Despite the advantages of a PEM in MECs, ultimately the two-chamber design was discarded for a one-chamber design as what happened to MFCs[74]. This is because the overall hydrogen production rate was fairly low for two-chamber configurations at 1.6 $m^3m^{-3}d^{-1}$ under optimized conditions while preliminary one-chamber configurations were able to produce almost double at 3.12 $m^3m^{-3}d^{-1}$[14], [74], [75]. Both hydrogen scavenging and methanogenesis need to be mitigated when operating one-chamber MECs and is at the forefront of current MEC research.

It should be reiterated that MECs do not undergo the splitting water to create hydrogen, as is done in water splitting. The "electrolysis" in microbial electrolysis cell comes from the fact that a voltage is applied to help make hydrogen from the breakdown of an organic substrate, but the potential applied is not enough to split water alone. The general HER reaction that occurs on the MEC cathode can be seen in Equation 9.

$$2H^+ + 2e^- \rightarrow H_2 \quad (9)$$

When the HER reaction in Equation 9 is combined with the anodic breakdown of acetate seen in Equation 1, the full MEC cell chemical equation can be written. Doing so also allows for the calculation of the Gibbs free energy, to see if the reaction is spontaneous or requires additional energy. The reaction can be seen in Equation 10.

$$CH_3COO^- + 4H_2O \rightarrow 2\,HCO_3^- + H^+ + 4H_2, \qquad \Delta G_r^{o\prime} = 104.6\ kJ/mol \quad (10)[15]$$

With the positive Gibbs free energy, the creation of hydrogen directly from the bacterial composition of acetate is not feasible. Using the Nernst Equation however, the minimum voltage required to create hydrogen can be calculated and is seen in Equation 11. For this calculation, the Gibbs free energy of the reaction is taken from Equation 10, *F* is again Faraday's constant (96,485 C/mole of electrons), and *n* is the number of moles of electrons participating in the reaction, which here is 8.

$$E_{req} = -\frac{\Delta G_r^{o\prime}}{nF} = -0.14V \quad (11)[15]$$

Therefore, the minimum necessary voltage that needs to be applied to a MEC is only 0.14V, much lower than that of traditional water electrolysis for hydrogen generation. Typically however, due to overpotentials in the cell and to increase the hydrogen generation rate, cells are subjected to 0.6 to 1.0V[76].

For microbial electrolysis cells, the overall hydrogen production rate and hydrogen purity are arguably the most important pieces of data to relay to the general scientific community, as these are what practical applications demand. Hydrogen production rates are denoted in $m^3m^{-3}d^{-1}$, which

is short for cubic meters of hydrogen per cubic meter of cell volume per day, while hydrogen purity is reported percentage wise after gas chromatography. Trace amounts of gases are usually ignored and only reported values of hydrogen, carbon dioxide, and methane are reported.

In terms of efficiency calculations, the overall energy efficiency with respect to substrate and energy efficiency with respect to substrate and electricity are the more important parameters to look at for MECs, though latter is the more practical parameter to examine. Due to the how the energy efficiency is calculated, which is the amount of energy produced by burning the generated hydrogen at the upper heating value (UHV), the energy efficiencies of MECs can easily be between 300 and 1000 percent[15]. However, this calculation ignores the participation of the electrical energy input, which drives the HER more as more potential is applied, and as such the efficiency of cell based upon both the electrical input and the substrate breakdown should be considered when evaluating MECs.

III. Chapter 3: Effect of Controlled Surface Modification via Electrophoretic Deposition of Carbon Nanotubes on Microbial Fuel Cell Anode Performance

3.1 Introduction

Microbial fuel cells (MFCs) are a promising technology for the development of electricity from the breakdown of organic matter by anaerobic bacteria[77], [78]. This emerging technology has been primarily associated with the simultaneous electrical generation with wastewater treatment, however, the technology has been adapted to enable hydrogen production, water desalination, heavy-metal ion recovery, and the powering of biosensors[79]–[81]. However, MFCs have seen little commercial development due to their reliance on noble metal catalysts, high material cost and internal resistance, and low power densities with conventional wastewater flows[82], [83]. In particular, high power densities for laboratory MFCs are reliant on high surface area graphite fiber brushes that are custom-made using woven carbon fibers wrapped around a dual titanium wire core[25]. While other carbon anodes have been used in MFCs, including carbon paper, cloth, mesh, graphite granules and blocks, graphite fiber brushes are championed as the low-cost, high power-density anode for large-scale MFC applications[23], [84], [85]. Despite their current high-performance, limited surface modification techniques have been developed that would allow graphite fiber brushes to continue to be at the forefront of MFC technology as a tunable anode electrode[31], [32].

Recently, metals have examined as possible alternatives to the traditionally used carbon-based electrodes in MFCs[28]. In particular, stainless steel has become a material of interest for the anode electrode due to its low-cost, high conductivity, scalability, and many commercially

available morphologies and compositions[26]. The intrinsic downside to stainless steel as an anode material in MFCs stems from its low biocompatibility, high overpotential, and low electron transport caused by the alloy's protective passive oxide layer.

Electrophoretic deposition (EPD) has been explored as a flexible, scalable, and facile method for the binder-less deposition of a range of conductive and non-conductive nanomaterials[47], [49]. Electrophoretic deposition has the unique advantage, as demonstrated in previous works by this lab, of being able to align rod-like particles in a vertical orientation by sequentially dispersing the nanomaterial in a solvent, charging the nanomaterial with a polarizing salt, and then applying a high voltage to deposit the nanomaterial onto the conductive electrode of choice[50], [52], [86]. The vertical deposition of these nanomaterials, as demonstrated with 1D MnO_2 nanorods, provides the necessary increase in surface area and charge-transfer kinetics to be of interest for electrochemical systems applications[51]. Additionally, some of the charging salt during the EPD process is co-deposited as a thin metallic holding layer at the base of the nanomaterial and can be utilized in electrochemical systems as a charge transport pathway even if the electrode has a passive oxidation layer.

In this study, wettability control of carbon nanotubes (CNTs) was investigated to ascertain the effect on parameters such as cell start-up time, steady-state output voltage, and maximum power density. Planar stainless steel sheet (SSS) was used as the anode demonstrate that increased surface roughness and improved surface chemistry provided by the CNTs is enough to overcome the high overpotential and low biocompatibility of the stainless steel to create a well performing MFC anode. In-situ electrochemical testing of working cells was utilized to provide secondary

verification of MFC start-up and cell repeatability, as well as provide insight into the performance of the cell under different output resistances.

3.2 Experimental

3.2.1 Chemicals and Materials

All chemicals were purchased from Sigma-Aldrich (MO, USA) unless specifically stated and deionized (DI) water was collected from a Barnstead Smart2Pure system (Thermo-Fisher Scientific, MA, USA). Commercially available polished 316 stainless steel was purchased (McMaster-Carr, GA, USA) and aligned multi-walled CNTs, 15±5 nm in diameter and 10±5 μm in length, were purchased (denoted Nanoamor CNTs, Nanoamor, Nanostructured & Amorphous Materials, Inc.) and used for the construction of the anodes.

Nanoamor CNTs were refluxed in a 3:1 nitric: sulfuric acid solution for 40 minutes in a round bottom flask in a 90^{o}C heated water bath as previously described[52]. After the refluxing, the CNTs were filtered in DI water until the filtered solution returned to a neutral pH, then dispersed in isopropyl alcohol (IPA), and dried at 80^{o}C in a convection oven (Thermo-Fisher Scientific, MA, USA).

3.2.2 SSS Anode Preparation

As purchased SSS anodes were first cut from a 24” x 12” (length x width) bulk sheet into 4” x 1” blanks, which were then sequentially cleaned in acetone, isopropyl alcohol (IPA), and DI water for 30 minutes each via bath sonication (Branson Ultrasonics, CT, USA) in order to remove any residual organics and debris accumulated from the manufacturing and cutting process. After

cleaning, the SSS blanks were allowed to air dry for 30 minutes at room temperature before being used in other modifications (denoted plain SSS).

Plain SSS anodes were modified exclusively using planar EPD, which can be seen schematically in Figure 1. EPD of Nanoamor CNTs was conducted by creating a 40 mL organic solution of IPA:ethanol (denoted 0:1 for pure ethanol and as appropriately for other ratios) containing 0.05 mg/mL CNTs and 0.05 mg/mL $NiCl_2$, the latter of which was used as a charging salt for the CNTs. First, the Nanoamor CNTs were dispersed via a probe ultrasonicator (Sonics & Materials, Inc., CT, USA) for 15 minutes in a Pyrex beaker. The Pyrex beaker was placed in a cooling bath of room temperature water in order to make sure none of the organic solution was boiled off during sonication. After the CNTs were dispersed, $NiCl_2$ in ethanol was dispersed from a stock solution of 1 mg/mL and the beaker was then filled to 40 mL using ethanol. The solution was then re-dispersed for 15 minutes via the probe ultrasonicator. The IPA volume was varied from 0 to 20 mL at increments of 10 mL and for the pure ethanol sample, CNTs were initially dispersed in 20 mL of ethanol.

EPD of the depositions was conducted immediately after solutions were made via ultra-sonication. A voltage of 400V was applied via a high-voltage power source (Matsusada, Japan) and a graphite foil counter electrode was used for all anode depositions. The time of depositions began with 1 minute for 0:1 solutions and increased to 1.5 and 2 minutes for 1:3 and 1:1 solutions respectively in order to maintain similar mass loadings for all anode depositions. After depositions were complete, anodes were washed in ethanol to remove any excess chloride ions and allowed to dry at room temperature before massing and contact angle measurements.

3.2.3 MFC Construction

30 mL-single chamber, air cathode MFCs were fabricated out of 3 mm acrylic sheet (McMaster-Carr, GA, USA) with fabricated SSS anodes epoxied at the base end of the cell and spaced 3 cm from the cathode with the CNT deposition in parallel with the cathode. Cathodes with a 0.5 mg/cm^2 Pt loading and PTFE gas diffusion layer were constructed as previously described and had a diameter of 3 cm (7.1 cm^2 projected surface area, 23.6 m^2/m^3 cathode specific area), consistent with other standard construction of other 30 mL-single chamber MFCS [10]. MFCs were incorporated into the monitoring circuit by attaching sensing leads to the enlarged tab section of the SSS anode itself and a stainless steel lead wire pressed against the cathode.

3.2.4 MFC Operation

All MFCs were first inoculated using amended domestic wastewater from a primary effluent clarifier (Village Creek Wastewater Treatment Plant, Arlington, TX) and operated in duplicate to demonstrate repeatable results. Amended wastewater was created by adding equal parts wastewater and 50 mM phosphate buffer solution (PBS; 4.58 g/L Na_2HPO_4, 2.45 g/L $NaH_2PO_4 \cdot H_2O$, 0.31 g/L NH_4Cl, 0.13 g/L KCl, produced in-house) containing 1 g/L sodium acetate in order to boost the conductivity and organic content of the wastewater for faster, more repeatable inoculation of the anodes. No other pre-acclimation methods aside from the amended wastewater used to enrich the anodes for increased biocompatibility. Start-up time was defined as the time necessary for all cells to reach 200 mV as had been described previously[66]. After the start-up cycle(s), MFCs were continually fed amended wastewater until 3 steady voltage cycles were achieved, at which point the cells were switched to only being fed a 50 mM PBS solution containing 1 g/L sodium acetate as the consumable organic material. All feed solutions were

replaced once cells dropped below a threshold voltage of 100mV in order to create one full cycle and were operated at room temperature (21 ± 2^{o}C).

3.2.5 Calculations and Measurements

Surface morphologies of the depositions of the stainless steel sheet were taken before and after nanomaterial deposition using a Hitachi S-4800 II field-emission scanning electron microscope (FE-SEM) at a working distance of 8 mm and an accelerating voltage of 5kV. For FE-SEM imaging, depositions were made on 1" x 1" SSS samples using the same parameters as discussed previously for the anodes used in actual MFC operation. An in house-built contact angle measurement stage with commercial optics (Edmund Optics, Barrington, NJ) was utilized to take images of 4 µL water droplets on the anode deposition surfaces. A total of five images were taken for each anode and were then analyzed using the ImageJ software (National Institutes of Health, Bethesda, MD) using the LBDSA plugin to obtain contact angle values[87].

The voltage across an external resistor box (1000Ω unless noted, Elenco Electronics, IL, USA) was measured at 30 minute intervals using DATAQ DI-2108-P data logger and accompanying software (DATAQ, Akron, OH) connected to a personal computer. From the collected voltage, current and power (normalized to the volume of the cell chamber), and Coulombic efficiency (CE) were calculated as have been previously described [10]. Polarization testing was conducted after 4 repeatable cycles of 50 mM PBS operation, for which cells were first filled with fresh 50 mM PBS solution and given 4 hours to reach open-circuit voltage (OCV), which was measured with a Keithley 2110 digital multimeter (Tektronix, Inc., OR, USA). The testing was then conducted by placing the cell in the data logging circuit with 5000, 2500, 1000, 500, 300, 200, 150, 100, 50, 30,

and 10 ohm resistances from the resistor box, with each resistance lasting 30 minutes in order to give the voltage time to stabilize and were subsequently plotted.

Both cyclic voltammetry (CV) and potentiostatic electrochemical impedance spectroscopy (EIS) were conducted using a Gamry Reference 3000 potentiostat/galvnostat (Gamry Instruments, PA, USA). Electrochemical testing using both techniques was performed before wastewater inoculation (abiotic), after wastewater inoculation but before only 50 mM PBS operation (1000 ohm WW), and after 50 mM PBS operation but before polarization testing (1000 ohm PBS). Additionally, all testing was performed on fully constructed MFCs incorporating an Ag/AgCl reference electrode in 50 mM PBS containing 1 g/L sodium acetate. Cyclic voltammetry was conducted for 4 cycles between -0.6V and 0.4V at a scan rate of 2 mV/s with the fourth cycle reported and EIS was conducted using a frequency of 100 kHz to 10 mHz with an AC voltage of 10 mV, 10 points per decade, and zero DC voltage component.

3.3 Results and Discussion

3.3.1 Stainless Steel Sheet CNT Deposition Wettability Study

Contact angles for the SSS anodes can be seen in Figure 1 and the contact angle values are tabulated in Table 1. Figure 1a, 1c, and 1e represent the wettabilities of the anodes designated as "MFC Set 1" throughout this study and Figures 1b, 1d, and 1f represent the wettabilities of the anodes designated as "MFC Set 2." All samples were made in duplicate. As is shown in Figure 3, as the content of IPA in the solution is increased, the contact angle appreciably increases. This phenomenon has been demonstrated previously and is explained by a combination of the following possibilities[52]. The first reason for the change in wettability is that the polar groups

that are innately present on the Nanoamor CNTs, or provided by the refluxing process, are removed by metal ions, which in this case happens to be the Ni^{2+} ion provided by the $NiCl_2$ charging salt. The Ni^{2+} ions readily remove the H^+ ions of the polar groups, thereby leaving only hydrophobic non-polar groups present on the surface of the deposition[88].

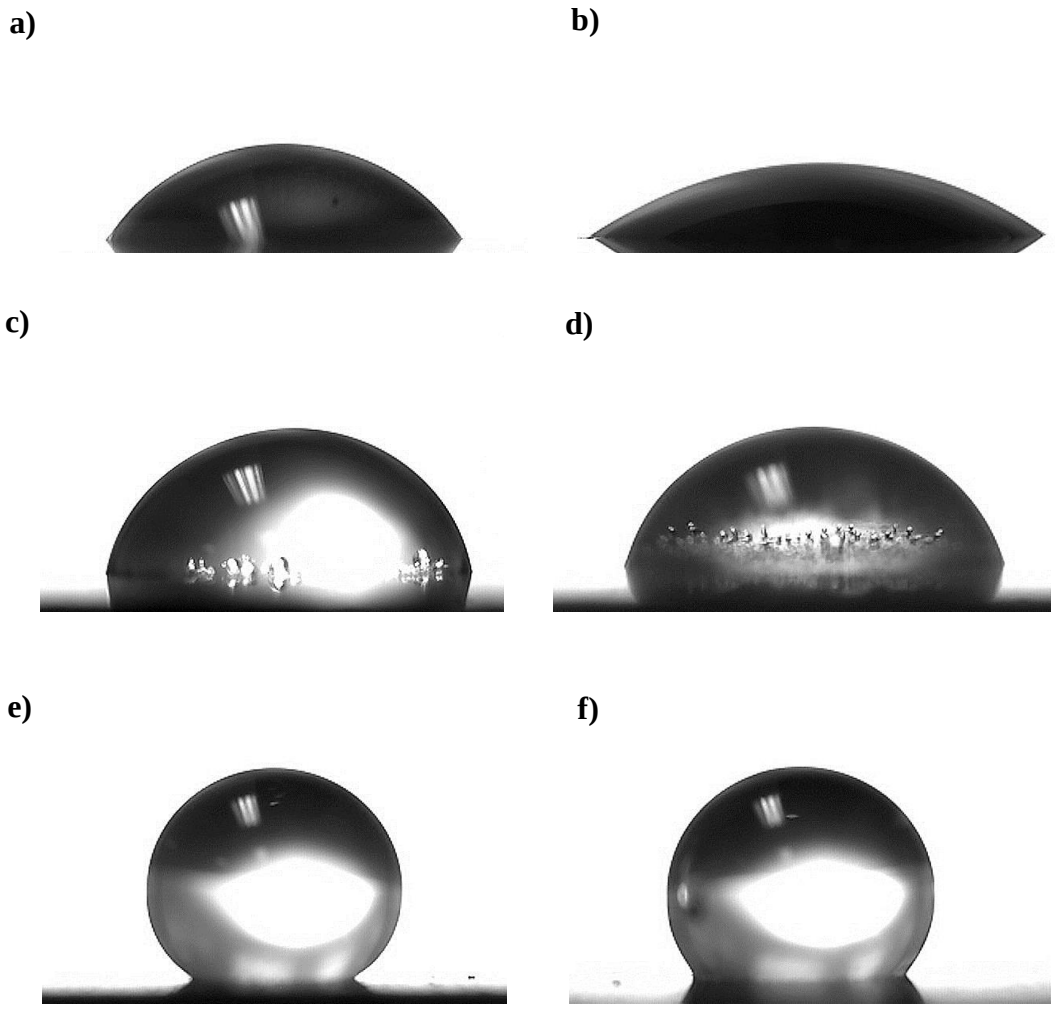

Figure 3: Wettability of EPD SSS MFC anodes made at 400V using IPA:EtOH ratios of a-b) 0:1, c-d) 1:3, and e-f) 1:1

Another reason could be is that the CNTs are receiving hydrophobic groups from the dispersion media, which primarily happens when the CNTs are being dispersed under high ultrasonication, as is done in this work. Increasing the IPA content provides more opportunity for hydrophobic groups and has been previously demonstrated with superhydrophobic CNT coatings made in acetone dispersions[52], [89].

Table 1: Contact Angle Measurements of CNT Anode Depositions

	Contact Angle (º)	**Standard Deviation (º)**
0:1 #1	55.3	8.2
0:1 #2	35.8	5.0
1:3 #1	74.4	3.2
1:3 #2	73.8	4.3
1:1 #1	145.1	8.5
1:1 #2	131.3	8.0
Plain SS #1	70.6	4.0
Plain SS #2	75.2	4.5

While all both of these explanations would shine light as to why the 1:3 and 1:1 increase in hydrophobicity the more IPA is increased, this does not necessarily explain why the pure ethanol sample remains hydrophilic. A possible explanation comes from the binder layer of ethanol deposit, which is likely nickel hydroxide and not nickel metal nanoparticles as are in the 1:3 and 1:1 samples. When nickel is deposited in ethanol, the small amount of water present in the ethanol undergoes electrolysis, providing –OH free radicals to the dispersion. These free radicals adhere

to the nickel as it forms the holding layer for the CNTs, hence creating nickel hydroxide, which is hydrophilic in nature[90], [91].

3.3.2 Stainless Steel Sheet CNT Deposition Morphology Study

FE-SEM images for all three CNT depositions can be seen at 4kX magnification in Figure 4 and 50kX magnification in Figure 5.

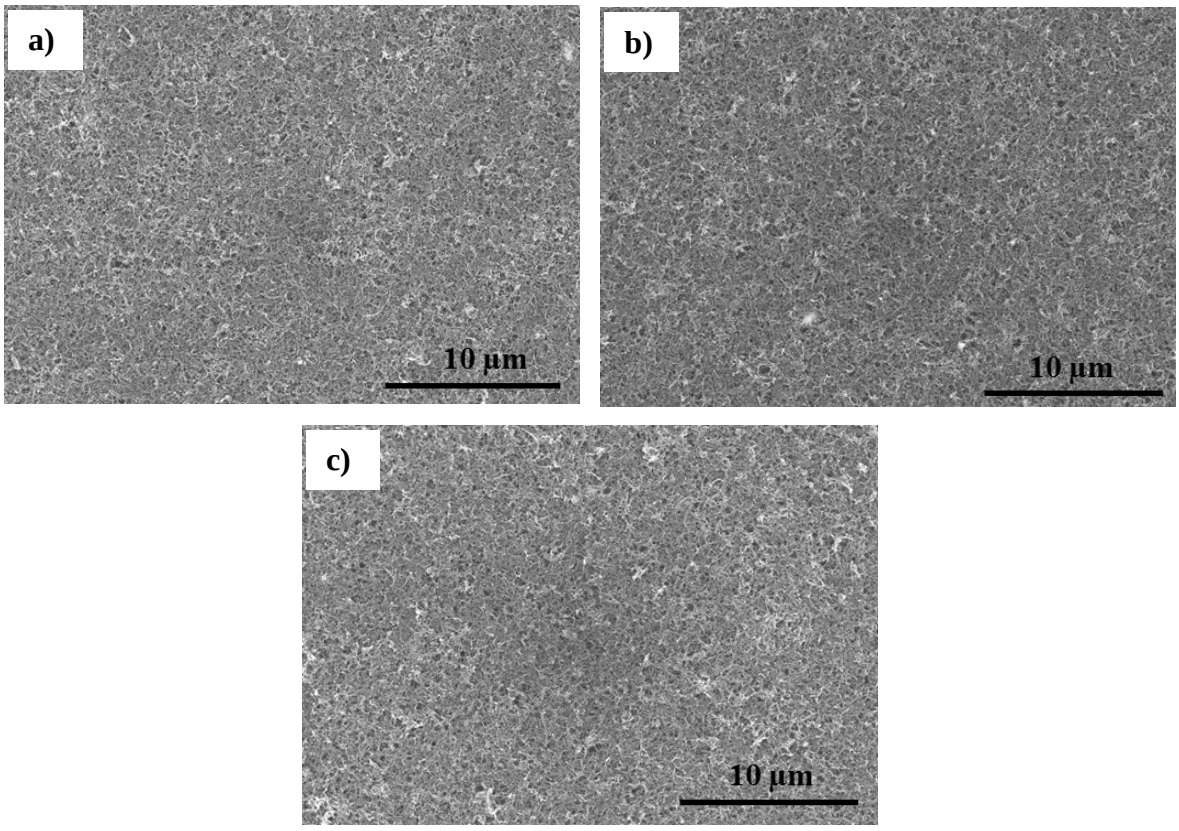

Figure 15: FE-SEM Images at 4kX Magnification of a) 0:1, b) 1:3, and c) 1:1 CNT Anode Depositions

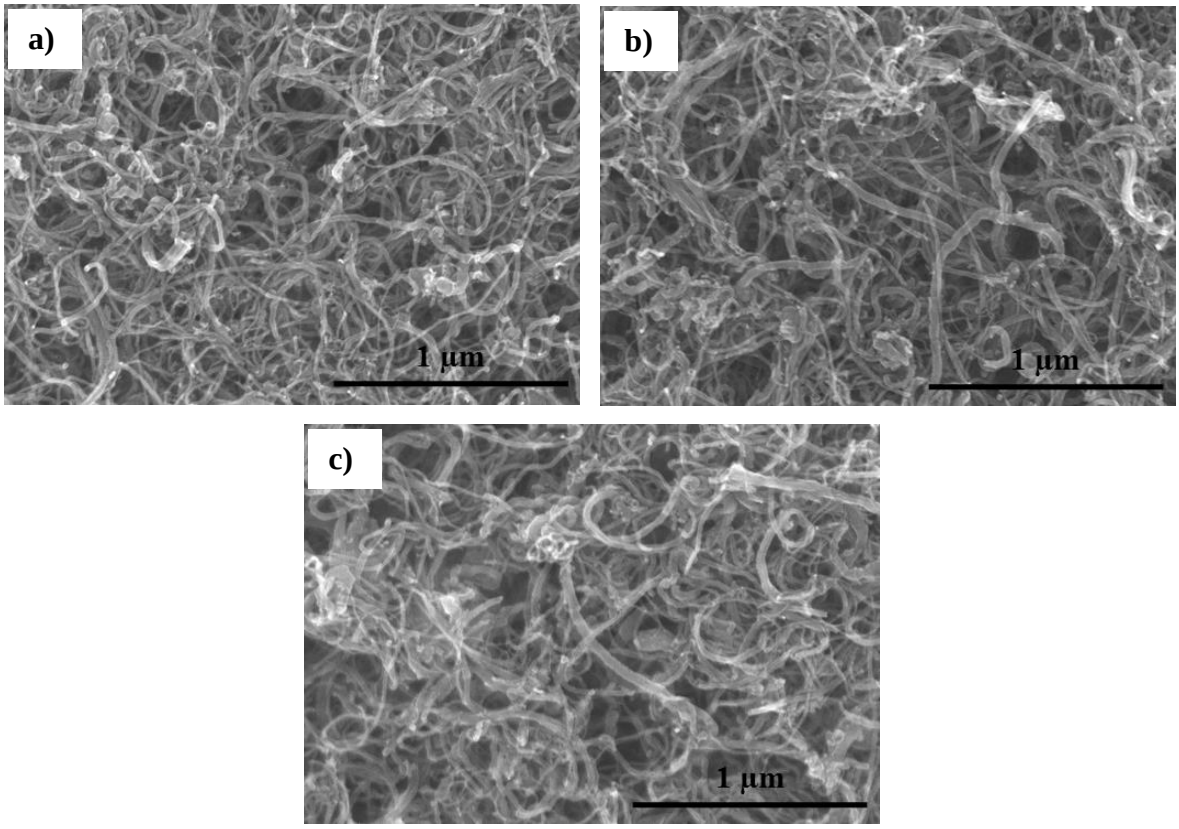

Figure 16: FE-SEM Images at 50kX Magnification of a) 0:1, b) 1:3, and c) 1:1 CNT Anode Depositions

As can be seen in both figures, all three of the depositions have the same morphologies, regardless of the solvent used in the deposition itself. All of the depositions completely cover the stainless steel sheet with a dense mat of intertwined CNTs on which bacteria will be grown upon when the anode is used in a MFC.

Along with investigating the physical morphology, energy dispersive X-ray spectroscopy (EDS) was performed on the depositions to gain insight into the elemental composition of the surfaces. The breakdown of the elemental compositions can be seen in Figure 6.

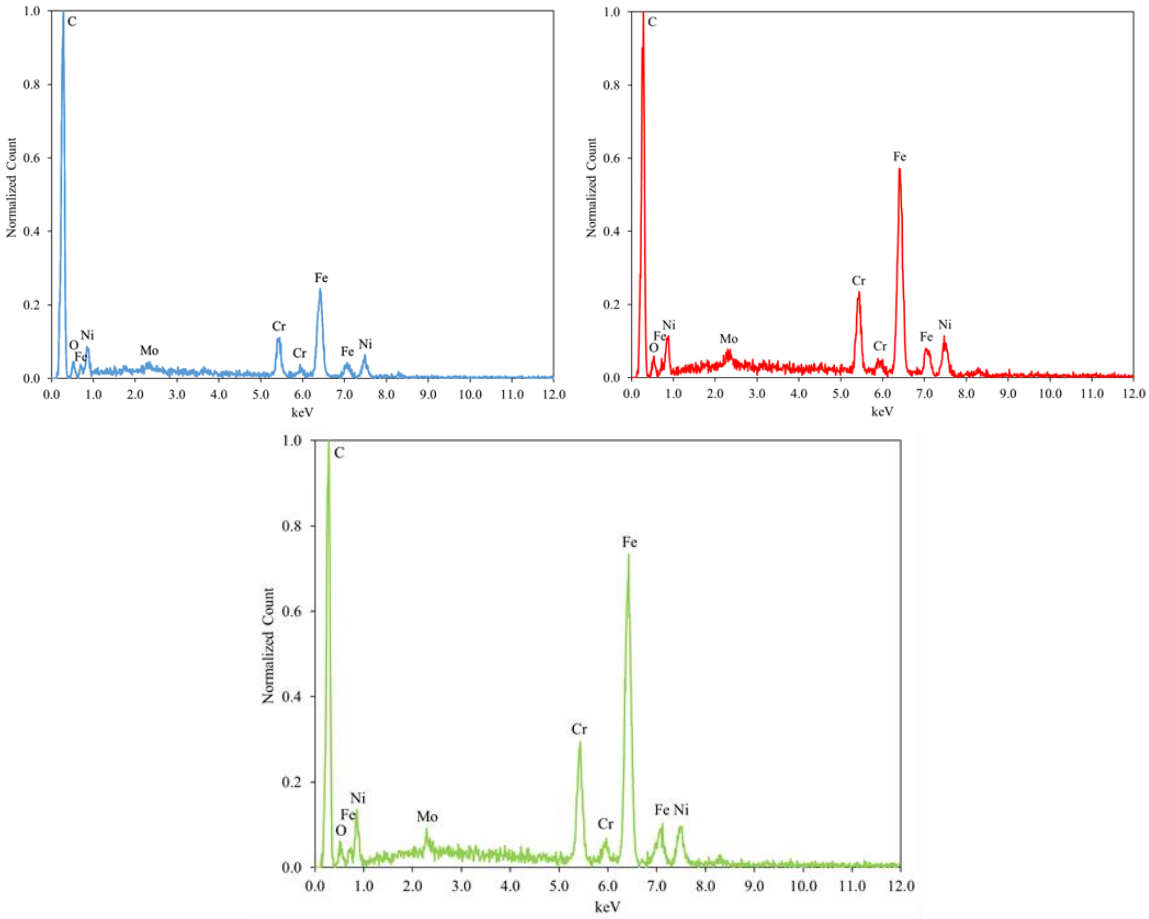

Figure 17: EDS Analysis of a) 0:1, b) 1:3, and c) 1:1 CNT Anode Depositions

Akin to the results displayed from the FE-SEM images shown Figures 4 and 5, the EDS shows that the elemental compositions of all three depositions are similar in nature, with the 1:3 and 1:1 depositions containing slightly higher nickel concentrations than the 0:1 deposition. The higher nickel concentration should lead to lower internal resistance in an operational MFC due to the higher conductivity of deposition. However, since quantitative EDS is not a definitive method for evaluating elemental compositions in depositions, electrochemical impedance spectroscopy (EIS) will be used during cell operation to determine the internal resistance of the MFCs during start-up and steady-state operation.

3.3.3 Abiotic Testing and Wastewater Start-up

Initial abiotic CV curves for all cells can be seen in Figure 7. Both of the plain SSS anodes showed considerably less electrochemical activity, determined from the much smaller area between the oxidation and reduction curves of the CV, when compared to the CNT depositions. All CNT depositions were very similar in the measured current and demonstrated between 100 to 200 μA under positive voltages against the Ag/AgCl reference electrode while exhibiting much more negative currents, -275 to -400 μA, when negative voltages were applied. Only one of the anodes, 400V 1:3 #1 exhibited any peaks, which is an unknown free radical, likely adsorbed during the EPD process.

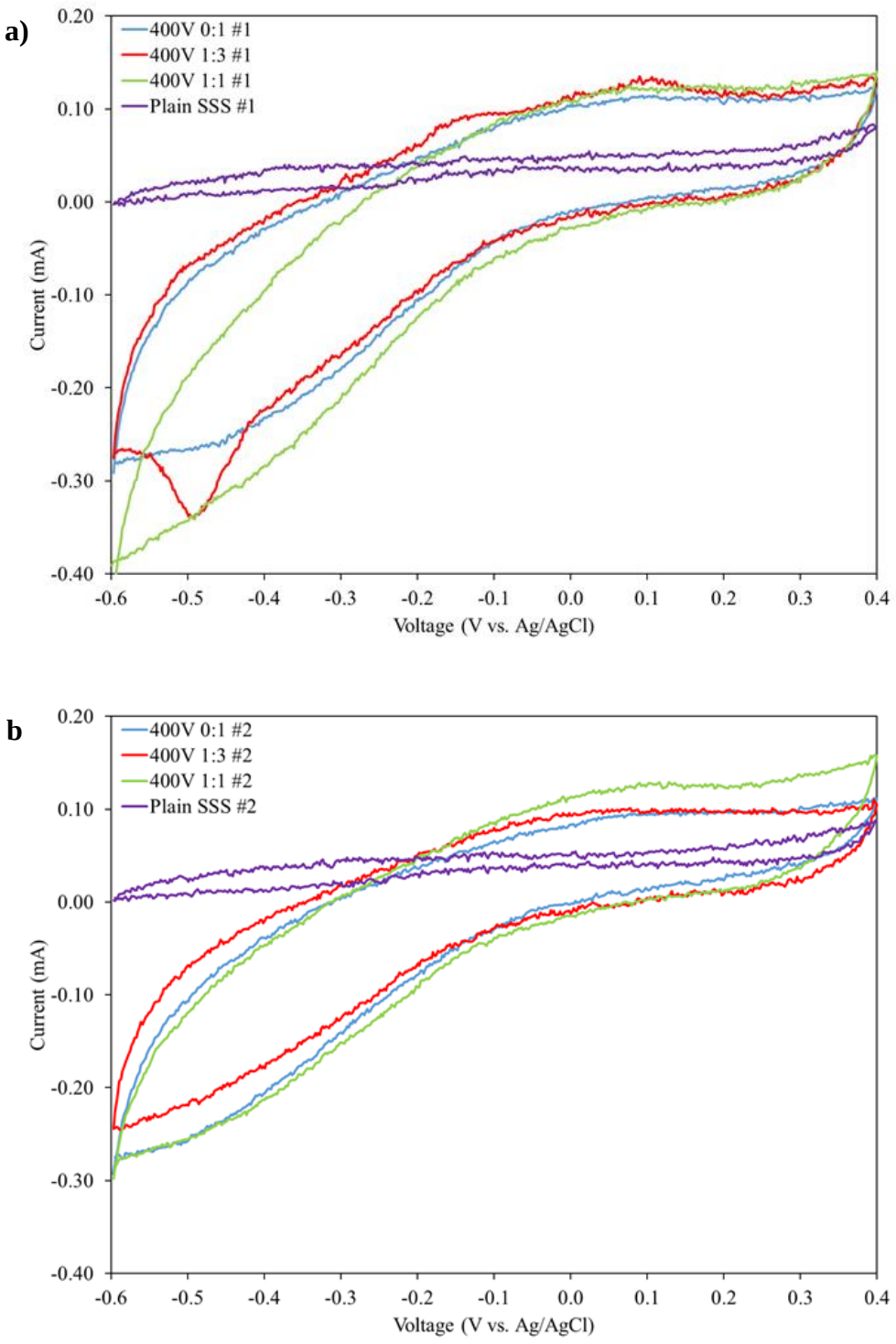

Figure 7: Abiotic Cyclic Voltammetry of a) SSS MFC Set #1 and b) SSS MFC Set #2

For the EIS, all of the CNT depositions, regardless of their deposition solution chemistry, demonstrated an approximately 200-250Ω charge transfer resistance before wastewater inoculation, as seen in Figure 8. The charge transfer resistance was taken to be the end of the of the plateau before the beginning of the second time constant, representing Warburg diffusion due to the use of a gas diffusion layer for the air-breathing cathode, and subtracting off the solution resistance[92]. For all EIS measurements across all anodes, the solution resistance which was approximately 30Ω and a marginally higher resistance for the 0:1 and 1:3 samples can be seen for MFC set #1 in Figure 8a, at around 50Ω while all of the resistances for MFC set #2 seem to be very similar in Figure 8b.

Considering that the surface chemistry is different between all three anodes, given from their initial wettability and probable nickel hydroxide formation, in the pure ethanol sample especially, it is currently unknown why the initial internal resistances for the 1:3 and 1:1 samples are not lower than that of the 0:1 anode. One possibility is that contact resistances for the cathode, in particular the contact resistance between the stainless steel lead wire and the cathode and the contact resistances between the electrochemical work station and the cathode lead, could be causing enough variation to mask any small changes in the internal resistance due to the increasing nickel metal nanoparticles that are being added from using higher IPA content dispersions. These contact resistances, and other factors along with the change in the surface chemistry, could also be the reason the EIS curves end near 550-600Ω for set #1 and in the 700-800Ω range for set #2.

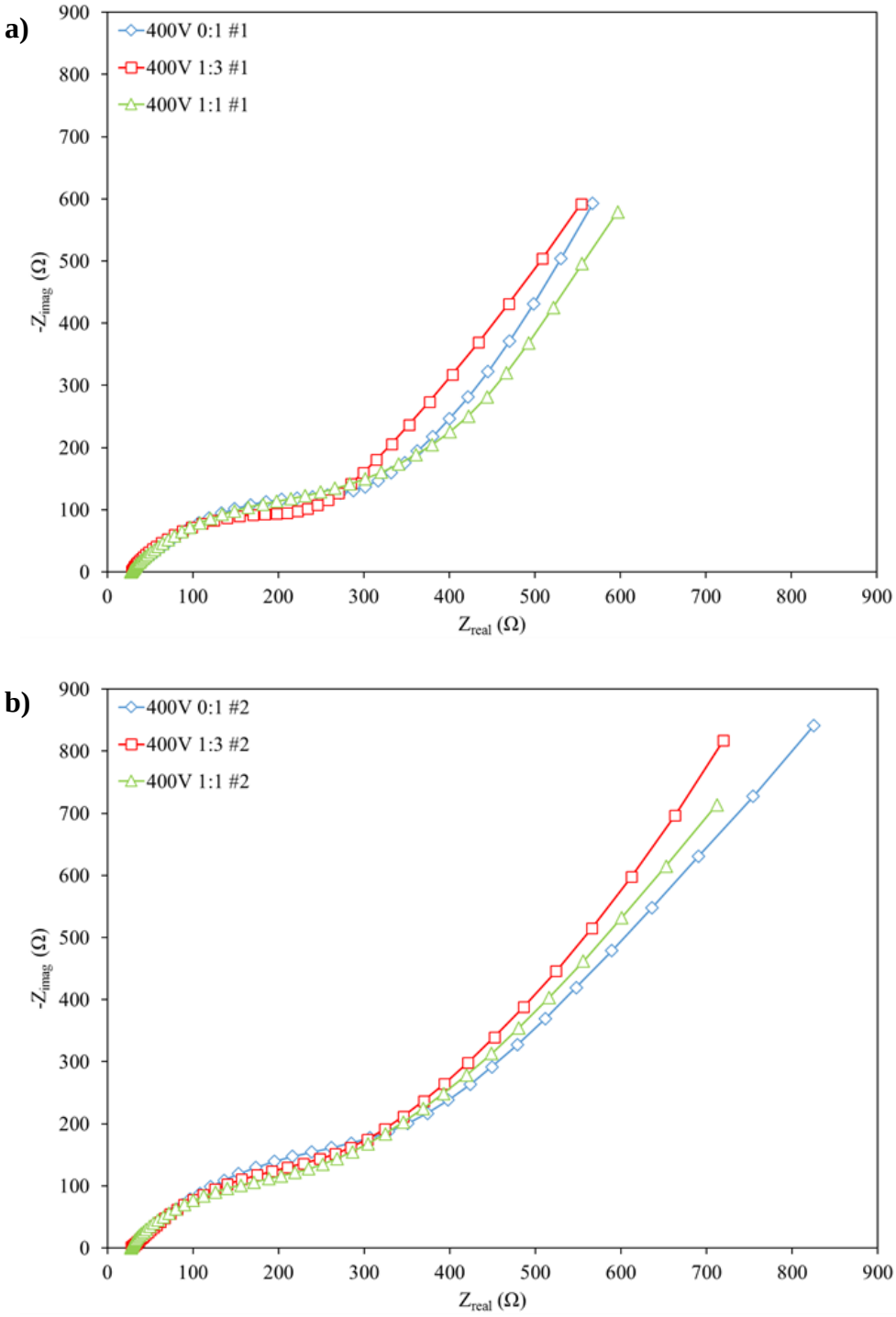

Figure 8: Abiotic EIS of a) SSS MFC Set #1 and b) SSS MFC Set #2

The start-up and subsequent repeatable cycle amended wastewater voltage curves of all stainless steel sheet anodes configurations can be seen in Figure 9 in their duplicity. All cells with CNT depositions were able to demonstrate inoculation and repeatable cycling in amended wastewater within 15 days of the initial addition of wastewater to the cell. Cells from set #1 were able to demonstrate maximum cell voltages between 350 mV and 430 mV with the voltage increasing as the nickel nanoparticle content increased and the nickel hydroxide content decreased. For the second set of MFCs, the 1:3 sample greatly outperformed the other two cell comparisons by reaching a 3 cycle repeatable voltage of 415 mV while both the pure ethanol and 1:1 cells only reached 360 mV. This variability between voltages, well as start-up times, is expected due to the nature of wastewater inoculation of MFCs, hence the necessity to run this, and all MFC studies, with at least duplicate cells[63].

Overall, there was a decrease in the start-up time for the pure ethanol anodes when comparted to the 1:1 anodes, while an even further decrease in start-up time was seen for the 1:3 anodes. In set #1, the pure ethanol MFC began more quickly than its counterpart in set #2, by approximately 7 hours, while the 1:3 anode from set #2 started up almost 17 hours faster than its set #1 companion. There is also indication that there is an optimal wettability for MFC start-up, given from the fact that the most hydrophilic anode was not the quickest to reach the 200 mV threshold in either of the MFC sets. While this trend has not be fully investigated here or in literature, there is indications that bacteria will change the wettability of even the most hydrophobic of samples, making the final anode-bacteria interface more hydrophilic, which may also be happening in this study[40]. Further studies would be needed to pinpoint the exact preferential contact angle of mixed-culture bacteria

colonies growing on MFC anodes, but for the context of this study, the 1:3 samples and their average contact angle of ~74^{o} provided the fastest start-up times.

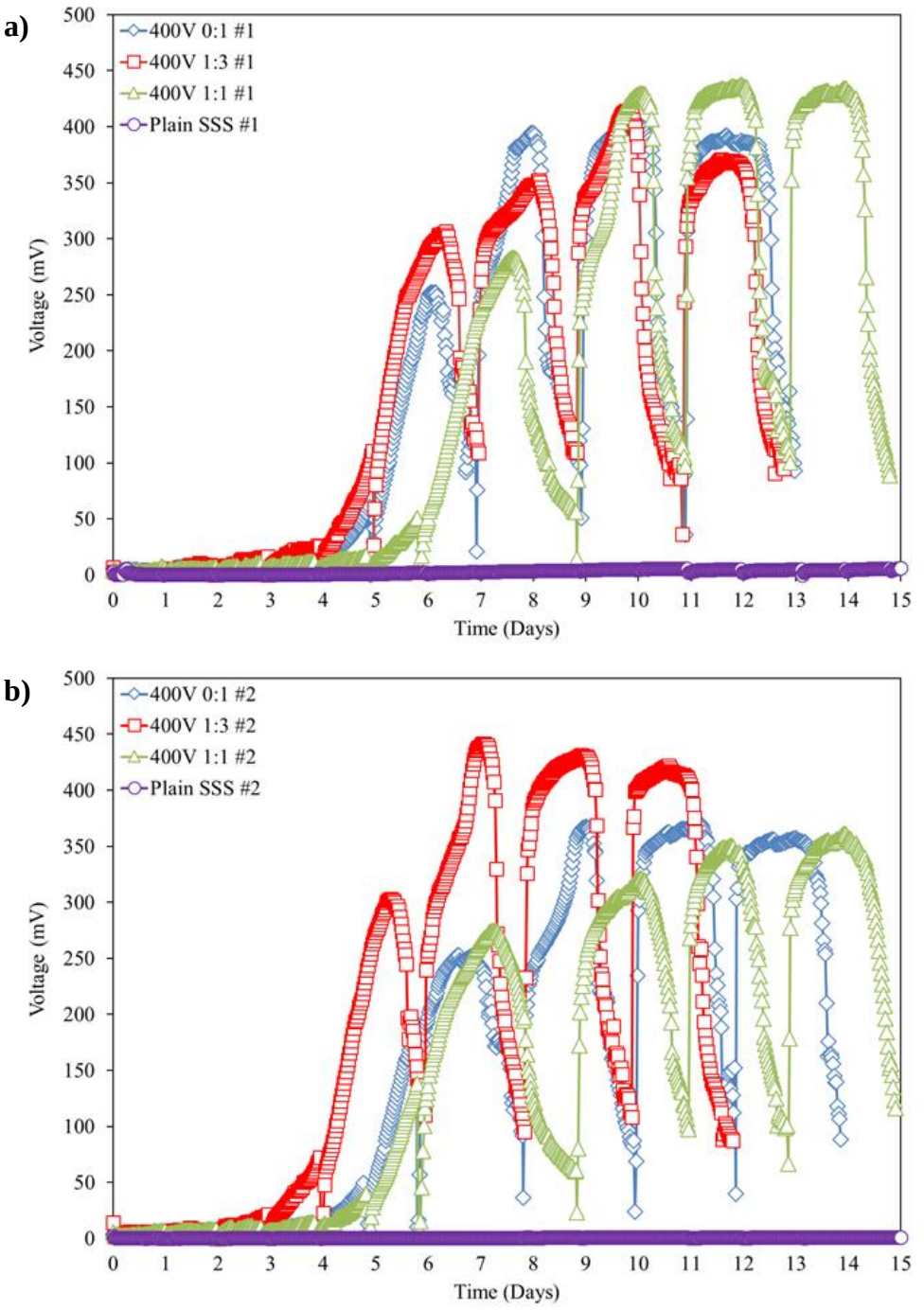

Figure 9: Inoculation Curves of a) SSS MFC Set #1 and b) SSS MFC Set #2 at 1000Ω

As was expected based on previous literature review, the plain stainless steel anodes were not an effective electrode for MFCs. The plain SSS anode never reached the start-up threshold of 200 mV within the same given 15 day window and instead plateaued at approximately 6 mV for the first set of cells and just 1 mV for the second set of cells. The internal resistances can be seen in Figure 10, which both the abiotic EIS curves as well as the post-inoculation comparison.

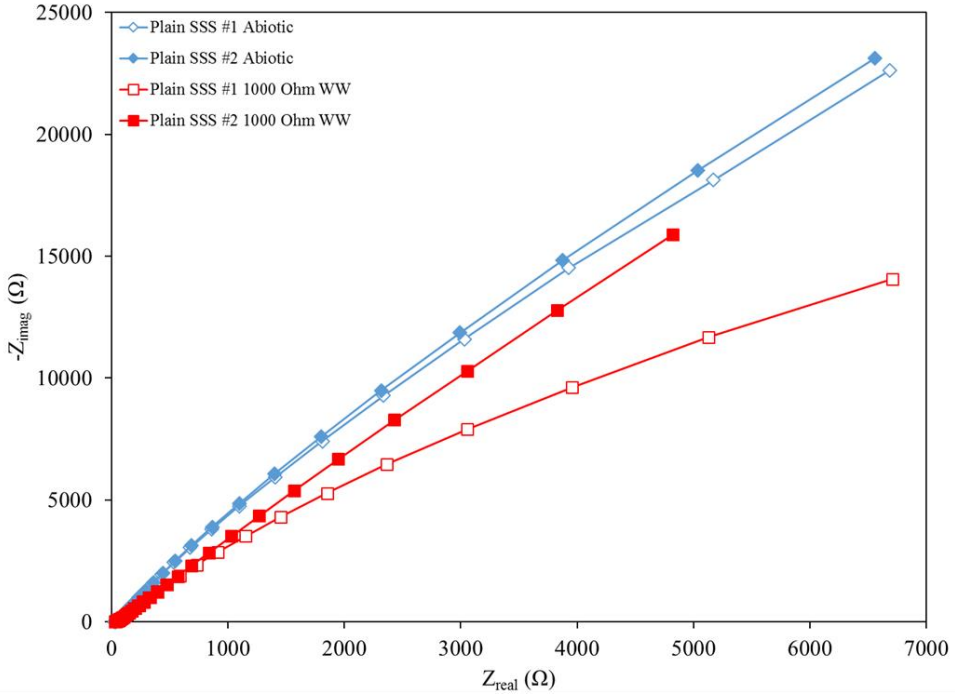

Figure 10: EIS of Plain SSS MFCs Before and After WW Inoculation at 1000Ω

For the plain SSS anode in set #1, the overall cell internal resistance remains much higher than what was seen in the CNT deposition anodes. Where the total resistance was between 600-800Ω as seen in Figure 5, the plain SSS anodes were an order of magnitude higher in the 5000-7000Ω range both before and after inoculation. This high internal resistance, coupled with the known biocompatibility issues of the bare metal, makes it unsurprising why the plain SSS anodes were unable to start-up. While there was a small increase in the electrochemical activity from the CV

curves show in Figure 11, this increase paled in comparison to the significant current generation provided by the CNT anodes.

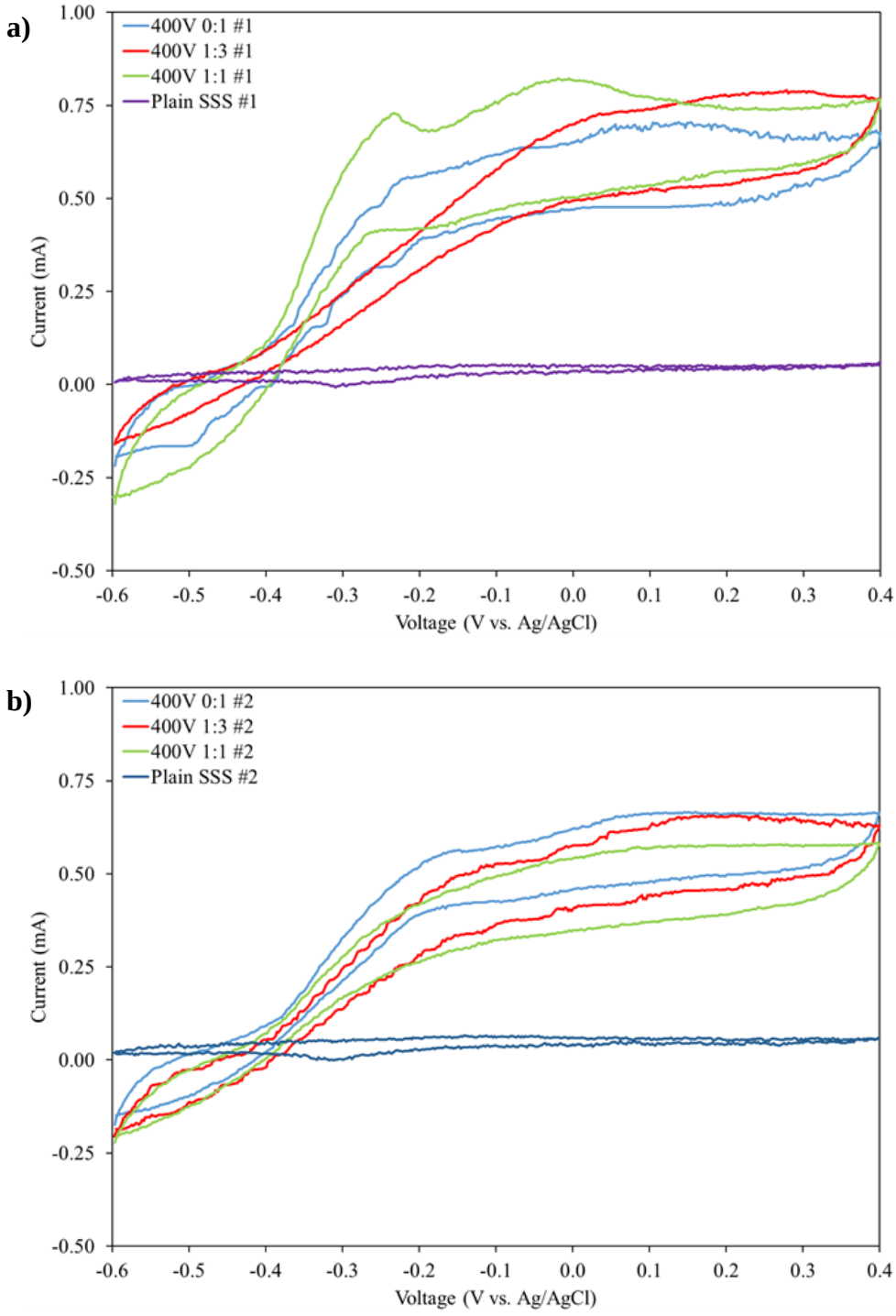

Figure 11: Cyclic Voltammetry of a) SSS MFC Set #1 and b) SSS MFC Set #2 After 1000Ω Wastewater Inoculation

Overall, the CNT depositions provided two orders magnitude higher current generation in the cyclic voltammetry curves when compared to the plain SSS anodes. As was discussed in Chapter 2, the shape of the CV curve in Figure 11 is what is known as a reverse-catalytic curve, which indicates that as the catalyst or reactive element of the system gains or loses electrons, the catalyst is regenerated by its operation in the system itself. For MFCs, the bacteria continually emit electrons and from c-type cytochromes in their outer cell membrane, which are replenished by the break-down of the sodium acetate. This anodic reaction can be seen in the following equation:

$$CH_3COO^- + 4H_2O \rightarrow 2HCO_3^- + 9H^+ + 8e^-, \qquad E_0 = 0.187V \qquad (12)[58]$$

The constant emission of electrons drives the catalytic reversible curve towards its characteristic "S" shape until the point where bacterial electron production can no longer sustain the increase in current where the current will fall and later plateau. If one was to take the first derivative of the CV curve, a peak near 370 mV versus Ag/AgCl can be seen, which corresponds to the of the reduction potential of c-type cytochromes in the cell bacteria outer membrane that are producing the electrons[24]. Taking the first derivative of the curves for the CNT deposition anodes show a peak between -350 and -355 mV vs. Ag/AgCl, within the acceptable range of mixed-culture colonies dominated by *Geobacter sulfurreducens*[53],[65].

As seen in the EIS curves in Figure 12, all CNT deposition anodes, experienced a decrease in the internal resistance of the cells after inoculation occurred compared to their abiotic states, which has been reported previously and is explained by the exoelectrogens decreasing the anode polarization resistance as the MFC is inoculated[93].

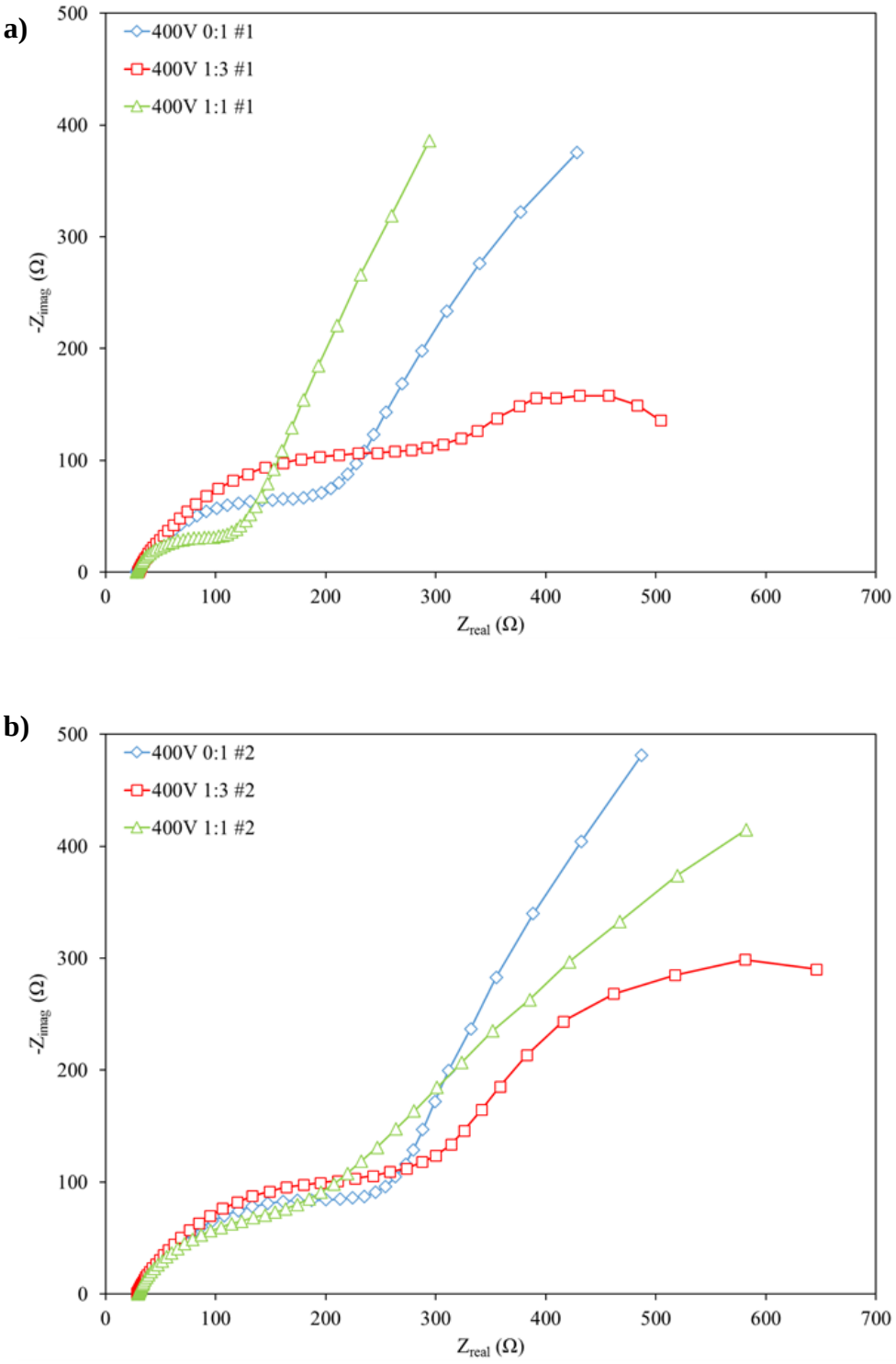

Figure 12: EIS of a) SSS MFC Set #1 and b) SSS MFC Set #2 After 1000Ω Wastewater Inoculation

For both sets of the 0:1 and 1:1 anodes, the shapes of the EIS curves are similar to those of their abiotic states, where there is a solution resistance near 30Ω due to the 50 mM PBs infused with 1 g/L acetate, the charge-transfer resistance pleateau, and finally followed by the increasing resistance of the Warburg diffusion. The charge-transfer resistance for the 1:1 anode is approximately 75Ω less for both sets when compared to the pure ethanol anodes. The 1:3 anodes however provide a much different EIS curve, where there is a much higher charge-transfer resistance plateau of nearly 300Ω, but also an almost fully developed Warburg diffusion semi-circle. One possible reason for the change in the EIS curve may come from the start-up time of the 1:3 anodes. Since the start-up time is much faster for these particular anodes, the bacterial colonies could be more developed and affect the anode polarization differently than either the 0:1 and 1:1 anodes. Additionally, faster start-up time could mean an accelerated bio-fouling of the cathode, as waste products from the bacteria and the inoculation media itself could change the Warburg diffusion portion of the EIS and make it look much different than that of the of other two anode types.

3.3.4 PBS Operation and Polarization Curves

The output cell voltages of both sets of MFCs operated at steady-state, i.e. only 50 mM PBS infused with 1 g/L sodium acetate, can be seen in Figure 13. All cells exhibited decays in voltages throughout the course of their operation in PBS, which is not uncommon due to increased biofouling of the cathode and decreased bacteria regeneration without the presence of wastewater. For both sets of MFCs, the 1:1 anodes exhibited higher maximum voltages, 384 mV for 1:1 #1 and 328 mV for 1:1 #2, and produced the most stable voltage curves as 1:1 #1 decreased by only 14.4% over the four cycles while 1:1 #2 decreased by 13.8%. For comparison, the 1:3 anodes decreased

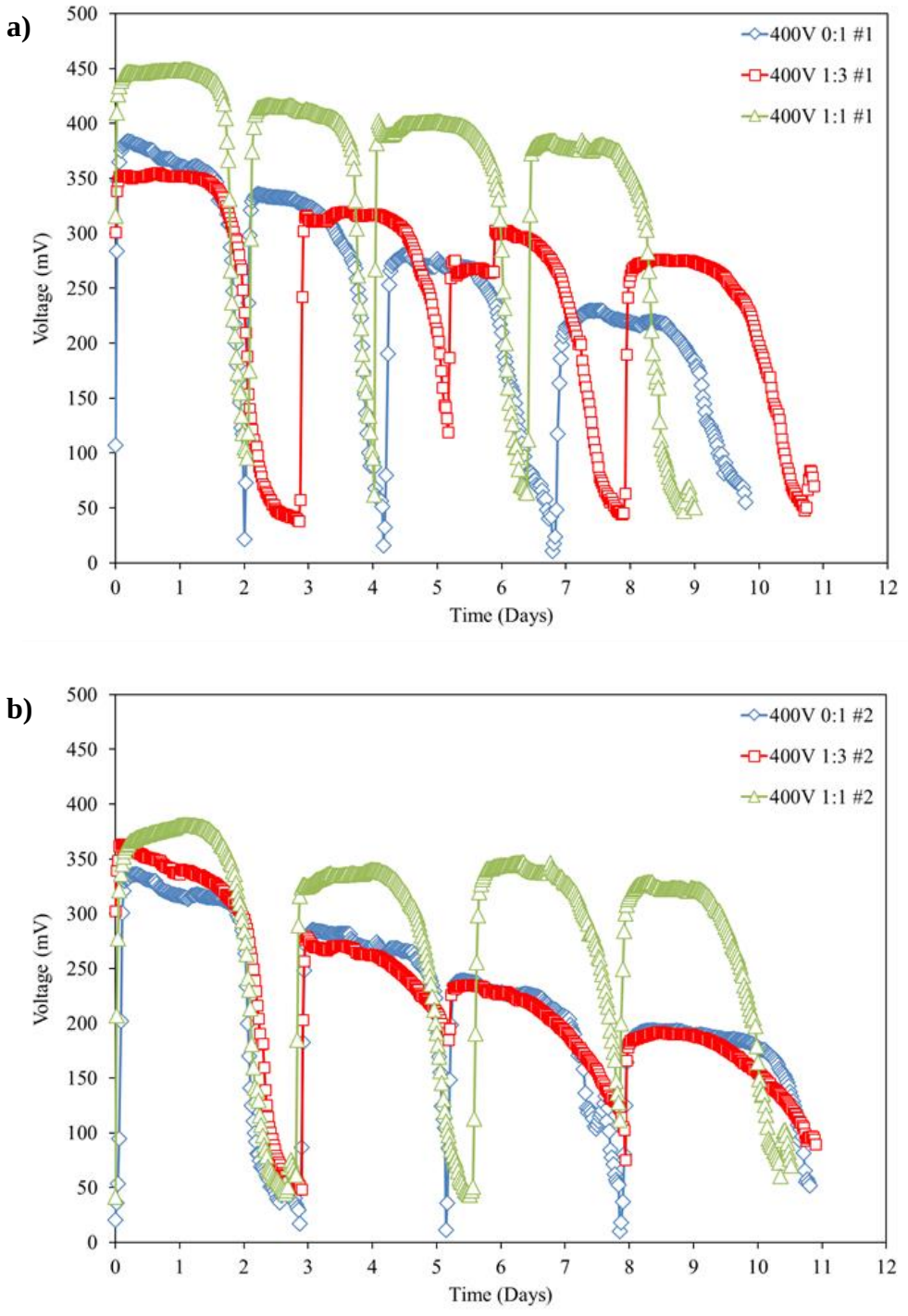

Figure 13: 50 mM PBS Voltage Curves of a) SSS MFC Set #1 and b) SSS MFC Set #2 at a Fixed 1000Ω Resistance

by 22.1% and 47.2% for set #1 and #2 respectively, while the pure ethanol anodes decreased by 40.1% and 42.3% for set #1 and #2 respectively. The Coulombic efficiencies for MFC set #1 can be seen in Table 2 while those for set #2 can be seen in Table 3.

Table 2: Coulombic Efficiencies of Set #1 MFCs

	0:1 #1 CE (%)	**1:3 #1 CE (%)**	**1:1 #1 CE (%)**
Cycle 1	19.3	21.2	25.0
Cycle 2	17.5	19.5	20.1
Cycle 3	16.5	18.0	22.7
Cycle 4	15.8	18.0	22.6

Table 3: Coulombic Efficiencies of Set #2 MFCs

	0:1 #1 CE (%)	**1:3 #1 CE (%)**	**1:1 #1 CE (%)**
Cycle 1	19.6	22.0	24.5
Cycle 2	17.5	16.7	21.3
Cycle 3	15.3	15.8	21.1
Cycle 4	14.7	13.8	20.2

As was with the cell voltages, the 1:1 anodes provided the highest Coulombic efficiency, followed by the 1:3 anodes and finally the 0:1. Higher Coulombic efficiencies would denote that there is higher electrochemical activity occurring on the anod, or better charge-transfer between the

bacteria and the anode surface. The electrochemical activity can again be verified using cyclic voltammetry, and can be seen in Figure 14. The cyclic voltammetry curves after the 50 mM PBS operation are much different than those directly after the inoculation cycles. While the maximum current generated for the 1:1 #1 cell is approximately the same as it was in Figure 14, all of the other cells show reduced maximum currents as well and significantly less area between the reduction and oxidation curves. Given that there is still significant current generation from the anodes, and since the Coulombic efficiencies do not catastrophically decrease over the course of the four cycles, bacteria death is not considered a full reason for the decrease in either the electrochemical performance or the output cell voltage.

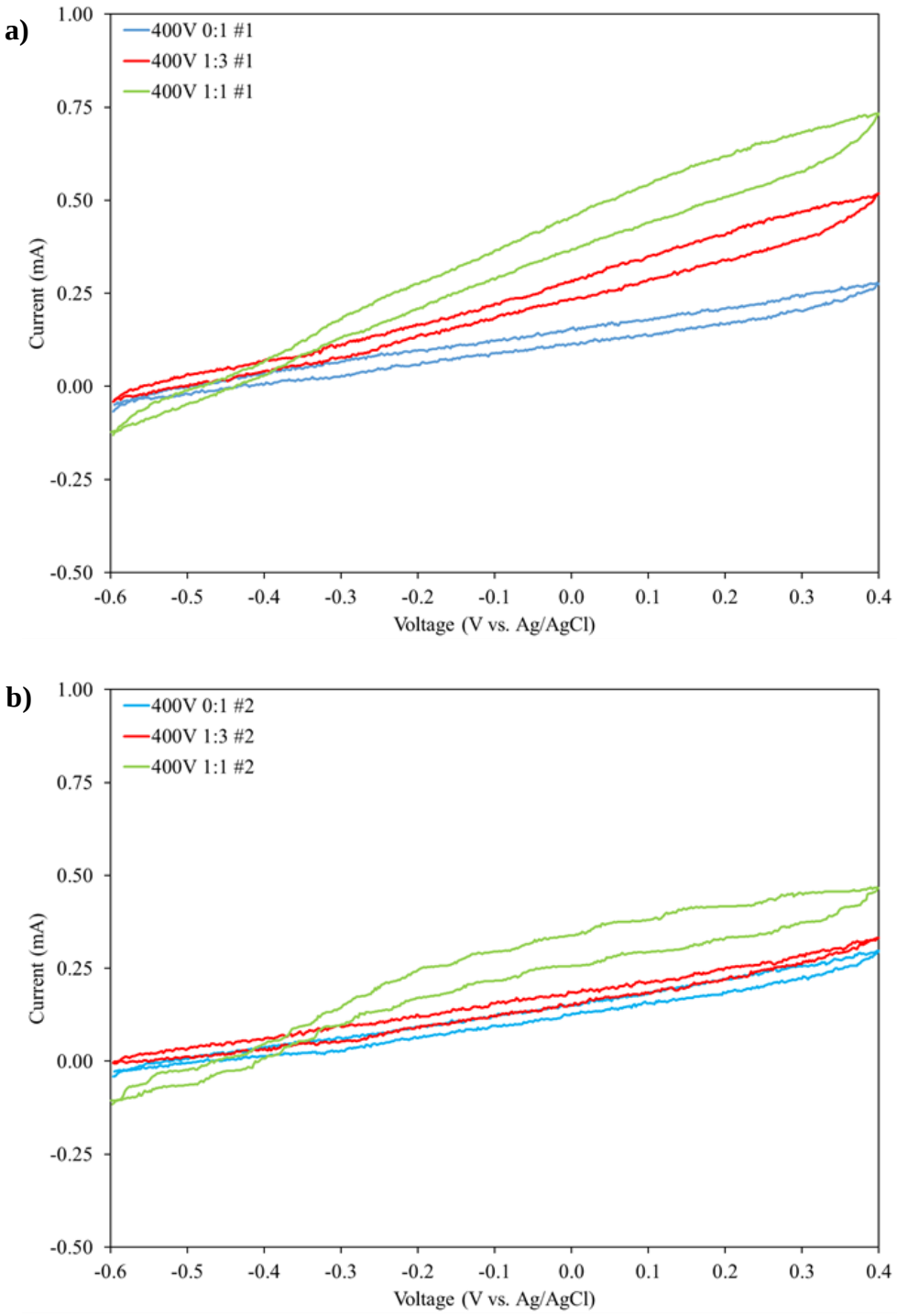

Figure 14: Cyclic Voltammetry of a) SSS MFC Set #1 and b) SSS MFC Set #2 After 50 mM PBS Operation at 1000Ω

Interactions between the PBS and the anode could be occurring or there could be a significant change in the internal resistance of the cells, the latter which is shown in Figure 15. The internal resistance of the cells dramatically increased over the course of the PBS operation with internal resistances now in the range of 1000 to 2000Ω for most of the cells and can be seen in Figure 15. The resistances in set #1 corroborate with the output voltages in the set as the lowest resistances, the 1:1 cell, provides the highest voltage at a fixed external resistor while the highest resistance 0:1 cell provides the lowest resistance. For set #2, again the lowest resistance 1:1 matches the highest voltage output and while both the 0:1 and 1:1 provide similar maximum voltages, the higher resistance of the 1:3 cell manifests itself with earlier cycle voltage degradation and lower Coulombic efficiency at the end of the four cycle testing.

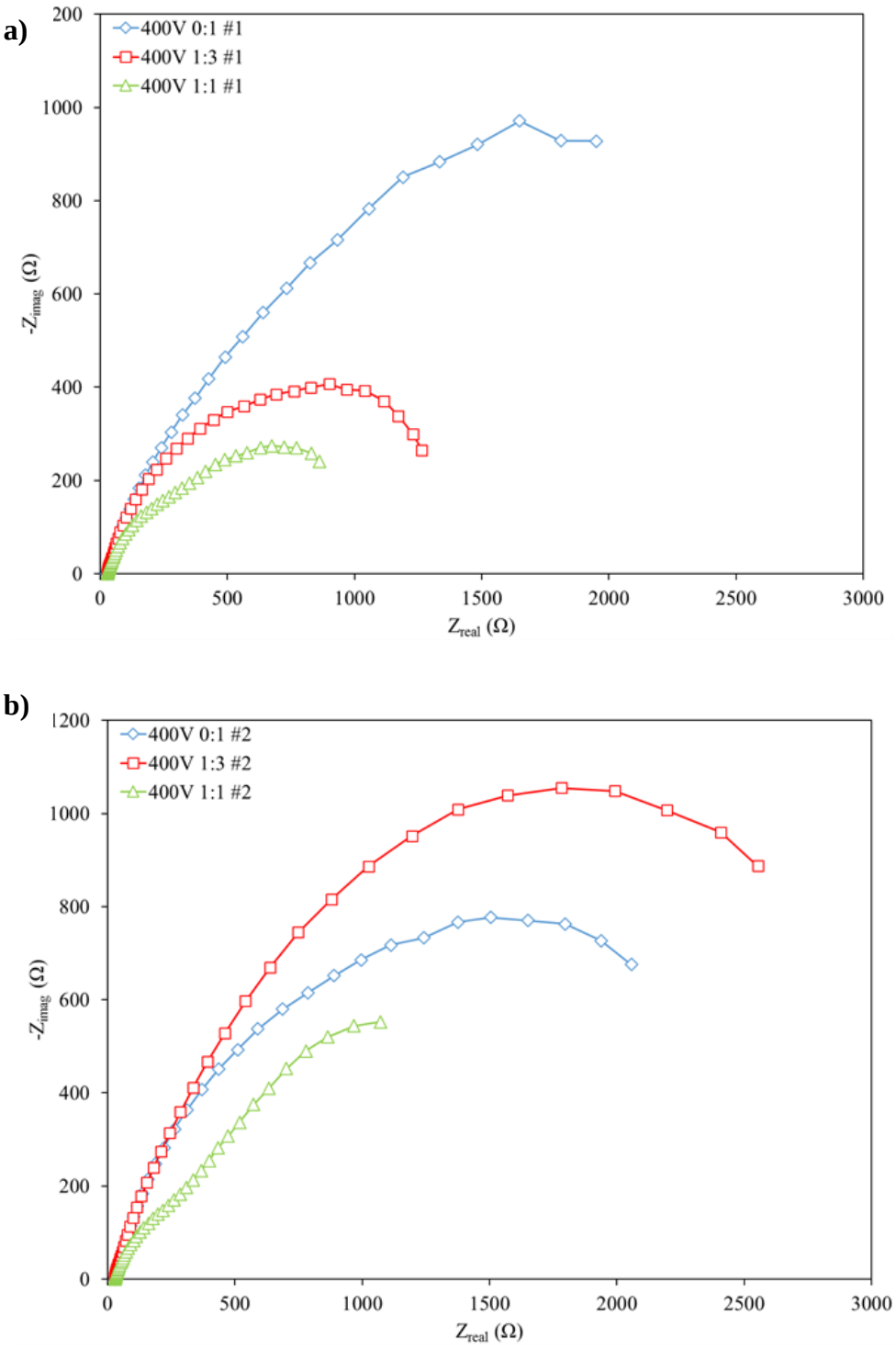

Figure 15: EIS of a) SSS MFC Set #1 and b) SSS MFC Set #2 After 50 mM PBS Operation at 1000Ω

For the polarization curves in Figure 16, the plain SSS anodes performed the worst out of all the cells with maximum volumetric power densities of 0.02 and 0.01 W/m^3 for set #1 and set #2 respectively, primarily due to their inability to produce any voltage during start-up. The addition of the CNTs significantly improved the power performance of the MFCs, with the pure ethanol cells and the 1:3 cells performing similar, which is unsurprising since both sets of anode configurations generated similar voltages during the PBS operation. When comparing the best performing and worst performing cells in set #1, not including the plain SSS, the 1:1 anode had a maximum current increase of 197% over the 0:1 cell and a maximum power increase of 269%. This trend was similar for set #2 where the 1:1 anode had a maximum current increase of 162% and a maximum power increase of 262%. Maximum volumetric power density and areal current densities can be seen in Table 4.

Table 4: Current and Power Density of MFC Set #1

	Current Density (mA/m^2)	**Power Density (W/m^3)**
Plain SSS #1	0.001	0.02
Plain SSS #2	0.001	0.01
0:1 #1	0.038	1.58
0:1 #2	0.032	1.01
1:3 #1	0.044	1.65
1:3 #2	0.030	0.99
1:1 #1	0.095	3.73
1:1 #2	0.080	3.57

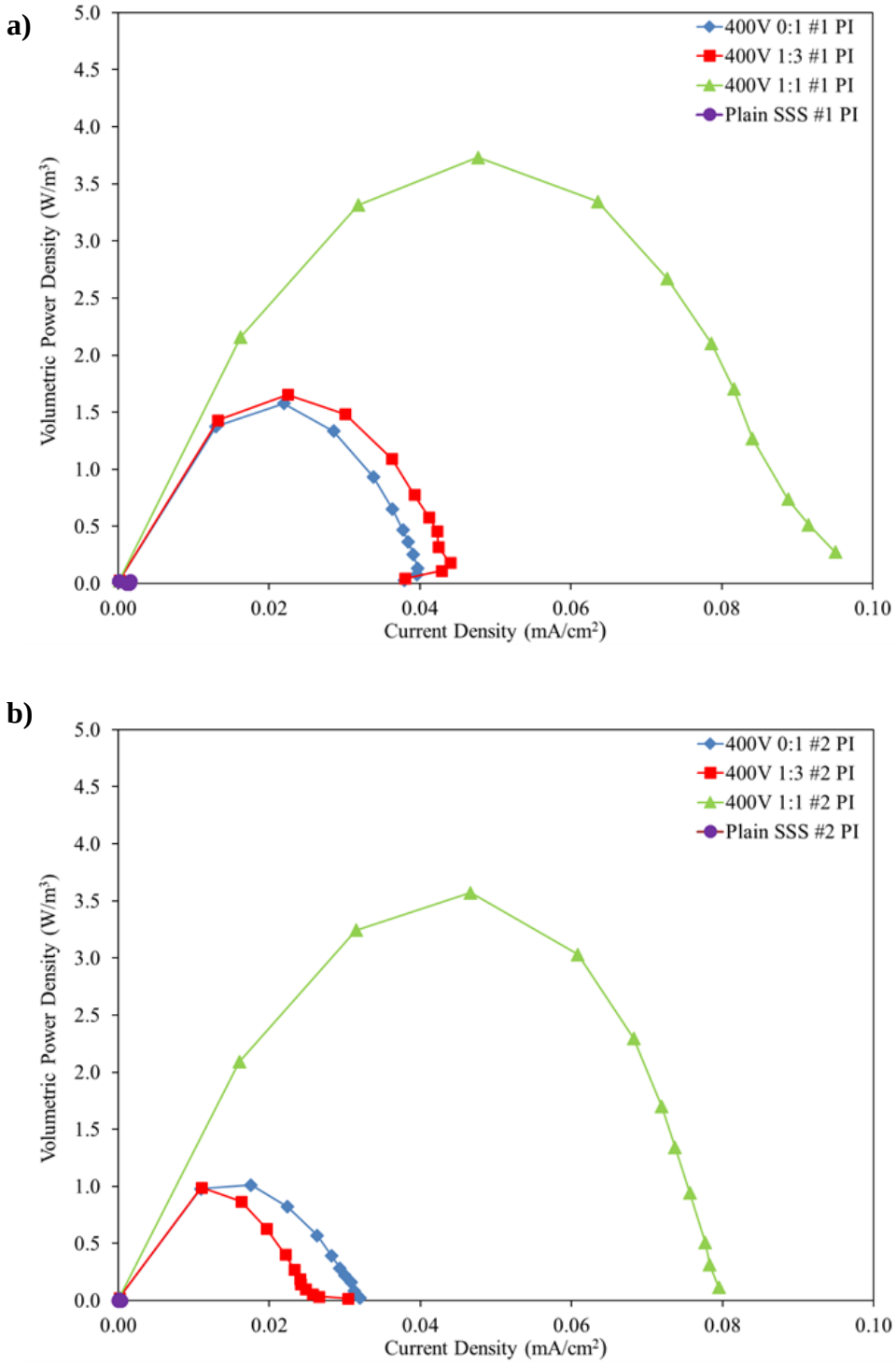

Figure 16: Polarization Curves of a) SSS MFC Set #1 and b) SSS MFC Set #2

3.4 Conclusion

By using different combinations of organic solvents, varying degrees of wettability were obtained for Nanoamor CNTs deposited electrophoretically onto stainless steel sheet, which were used as anodes for microbial fuel cells. A correlation between start-up time and initial deposition contact angle was inferred, with anodes having more hydrophilic contact angles reaching the start-up threshold voltage of 200 mV more quickly than hydrophobic ones. Cyclic voltammetry and electrochemical impedance spectroscopy were used to characterize the start-up and steady-state operation of these anodes and show the complex interactions between cell performance, electrochemical activity, and internal resistance.

IV. Chapter 4: Versatility of Developed Electrophoretic Deposition Technique to Fabricate Scalable Anodes for Microbial Fuel Cells

4.1 Introduction

In order to solve the previously described limitations and allow stainless steel to become a viable MFC anode electrode, various techniques are currently in the development stage. These techniques range from flame-oxidation to acid-treatment to the deposition of carbon nanomaterials, notably carbon black, graphene, and carbon nanotubes (CNTs), of the stainless steel surface with the ultimate goal to be able to increase the anode's surface area or functionalize the anode to attain improved bacterial adhesion and extracellular electron transport[30], [33], [34], [39], [94]. Notable high-performance stainless steel/graphene anodes have been made that are on par with graphite brushes. However, current surface deposition techniques rely primarily on pasting or dip-coating the nanomaterial mixed with a Nafion or polytetrafluoroethylene (PTFE) binder onto the stainless steel anode[39], [94]. Such binders should be avoided for stainless steel anodes since these non-conductive binders increase the internal resistance of the MFC and cause irregularities between devices. Thusly, the elimination of non-conductive binders, while using a repeatable, uniform deposition technique for the addition of nanomaterials, is necessary for the continued use of stainless steel as a MFC electrode.

As was shown in the previous study, EPD of carbon nanotubes can make stainless steel a viable substrate for MFC anodes. The results of the wettability study indicated that a combination of a highly conductive deposition and a contact angle of approximately 50-60^{o} appears to an optimal combination for developing a pathway to high performance MFC anodes. The increased

conductivity, demonstrated from the lower internal cell resistance, led to higher output voltages and the more hydrophilic anodes had noticeably increased start-up times compared to their hydrophobic counterparts. However, despite the increased viability of the stainless steel due to the CNT depositions, the formation of salt crystals from the phosphate buffer solution over the course of the cell life leads to an accelerated decrease in cell performance but aggressively changing the internal resistance of the cells. This salt formation needs to be remedied, or removed entirely, for stainless steel to become truly viable in wastewater treatment plants or other locations with accessible organic-rich runoff.

Therefore, in this study, a two-part approach is taken to demonstrate the scalability of stainless steel MFC anodes and the versatility of the EPD process. First, hydrophilic, highly conductive CNT-Ni deposits are created on the previously used planar stainless steel sheet and stainless steel mesh (SSM) based upon the information learned in the wettability study. Then, a radial EPD of CNTs is performed in order to deposit the nanomaterial onto commercially available stainless steel brushes (SSBs), in total giving three different anode types in order to compare the effect of the CNT depositions on anode hierarchies in 30 mL cells. Using commercially available SSBs allows for the combined use of a high surface area electrode, even more so than stainless steel mesh, with the additional benefit of low-cost scalability. After this is completed, larger scale 275 mL MFCs are made with larger SSBs and a characterization study of how varying EPD parameters can provide very different deposition morphologies. Both parts of this study incorporate much longer amended or pure wastewater run times in order show the long-term viability of CNT-based depositions in wastewater for future commercial applications.

4.2 Experimental

4.2.1 Chemicals and Materials

All chemicals were purchased from Sigma-Aldrich (MO, USA) and deionized (DI) water was collected from a Barnstead Smart2Pure system (Thermo-Fisher Scientific, MA, USA). Commercially available SSBs, 316 stainless steel sheet, 304 stainless steel mesh, and 3 mm thick acrylic sheet were purchased (McMaster-Carr, GA, USA) and used in the creation of MFC anodes and cells in this study.

Multi-walled CNTs, 140±20 nm in diameter and 5±2 μm in length, were purchased (denoted MRCNTs, MER Corporation, AZ, USA) and mild refluxed in a 10% nitric acid solution for 40 minutes at room temperature. After the refluxing, the CNTs were filtered in DI water until the filtered solution returned to a neutral pH, then dispersed in isopropyl alcohol (IPA), and dried at 80^{o}C in a convection oven (Thermo-Fisher Scientific, MA, USA).

Aligned multi-walled CNTs, 15±5 nm in diameter and 10±5 μm in length, were purchased (denoted Nanoamor CNTs, Nanoamor, Nanostructured & Amorphous Materials, Inc.) and used for the construction of the anodes. Nanoamor CNTs were refluxed in a 3:1 nitric: sulfuric acid solution for 40 minutes in a round bottom flask in a 90^{o}C heated water bath as previously described [52]. After the refluxing, the CNTs were filtered in DI water until the filtered solution returned to a neutral pH, then dispersed in isopropyl alcohol (IPA), and dried at 80^{o}C in a convection oven (Thermo-Fisher Scientific, MA, USA).

4.2.2 SSS and SSM Anode Preparation

As purchased SSS anodes were first cut from a 24” x 12” (length x width) bulk sheet into 4” x 1” blanks, which were then sequentially cleaned in acetone, isopropyl alcohol (IPA), and DI water for 30 minutes each via bath sonication (Branson Ultrasonics, CT, USA) in order to remove any residual organics and debris accumulated from the manufacturing and cutting process. A similar process was used to cut and clean the stainless steel mesh from its original 12” x 12” bulk sheet. After cleaning, the SSS and SSM blanks were allowed to air dry for 30 minutes at room temperature before being used in other modifications (denoted plain SSS or plain SSM).

Plain SSS and SSM anodes were modified exclusively using planar EPD using Nanoamor CNTs. EPD of Nanoamor CNTs was conducted by creating a 40 mL organic solution of containing 0.05 mg/mL CNTs and 0.05 mg/mL $NiCl_2$, the latter of which was used as a charging salt for the CNTs. First, the Nanoamor CNTs were dispersed in a Pyrex beaker containing 20 mL of IPA via a probe ultrasonicator (Sonics & Materials, Inc., CT, USA) for 15 minutes. The Pyrex beaker was placed in a cooling bath of room temperature water in order to make sure none of the organic solution was boiled off during sonication. After the CNTs were dispersed, 20 mL of IPA containing the necessary amount of $NiCl_2$ was added and the solution was then re-dispersed for 15 minutes via the probe ultrasonicator to obtain a well dispersed 40 mL solution.

EPD of the depositions was conducted immediately after solutions were made via ultra-sonication. A voltage of 400V was applied via a high-voltage power source (Matsusada, Japan) and a stainless steel counter electrode was used for all anode depositions. The time of depositions began with 3 minutes for SSS anodes and was increased to 5 minutes for SSM anodes in order to maintain a similar mass loading for all anode depositions. After depositions were complete, anodes were

washed in IPA to remove any excess chloride ions and allowed to dry at room temperature before massing and further characterization.

4.2.3 SS Brush Anode Preparation

As purchased SSBs, both 2.5 cm diameter and length SSBs for 30 mL cells and 5 cm diameter by 7 cm length SSBs for 275 mL cells, were first sequentially cleaned in acetone, IPA, and DI water for 30 minutes each via bath sonication in order to remove any residual organics and debris accumulated from the manufacturing process. After cleaning, the brushes were allowed to air dry for 30 minutes at room temperature before being used in other modifications (denoted as plain SS brush).

Plain SS brushes for 275 mL cells were first modified by dip-coating using MRCNTs as the deposited nanomaterial similar as to what was previously described [94]. Dip-coating of MRCNTs consisted of using a 250 mL n-methyl-2-pyrrolidone (NMP) solution incorporated with 1 mg/mL MRCNTs and 5 μL/mL Nafion resin solution, which were homogenized for 15 minutes using the probe ultrasonicator. The plain SS brushes were then slowly dipped into the NMP/CNT/Nafion solution for 1 minute before removal and subsequent drying in a convection oven at 160^{o}C for 10 minutes. This dip-coating process was repeated until 5 layers had been deposited (denoted as dip-coated brush).

Plain SS brushes for 275 mL cells were alternatively modified by radial EPD with MRCNTs again being the deposited nanomaterial, which can be seen schematically in Figure 17. EPD of MRCNTs utilized a 400 mL solution of IPA consisting of 0.03 mg/mL MRCNTs and 0.015 mg/mL $NiCl_2$,

which was probe ultra-sonicated for 30 minutes and allowed to cool for 10 minutes before use. The plain SS brush was arranged concentrically 1 cm away from a cylindrical piece of 316 stainless steel sheet in a Pyrex beaker, at which point the IPA/MRCNT/$NiCl_2$ was poured in and a 760V potential was applied for 15 seconds using a high voltage power source (Matsusada, Japan). Brushes were then removed from the EPD solution and allowed to dry for 10 minutes in air at room temperature before being washed in DI water to remove any residual chloride ions and organic solvent (denoted as EPD-WW for wastewater only operation and EPD-PBS for 50 mM PBS operation).

4.2.4 MFC Construction

As was done in the wettability study, 30 mL-single chamber, air cathode MFCs were fabricated out of 3 mm acrylic sheet (McMaster-Carr, GA, USA) with fabricated SSS, SSM, or SSB anodes epoxied at the base end of the cell and spaced 3 cm from the cathode with the CNT deposition in parallel with the cathode. Cathodes with a 0.5 mg/cm^2 Pt loading and PTFE gas diffusion layer were constructed as previously described and had a diameter of 3 cm (7.1 cm^2 projected surface area, 23.6 m^2/m^3 cathode specific area), consistent with other standard construction of other 30 mL-single chamber MFCS [10]. MFCs were incorporated into the monitoring circuit by attaching sensing leads to either the enlarged tab section of the SSS/SSM anode or the stainless steel wire core of the SSB and a stainless steel lead wire pressed against the cathode

275 mL-single chamber, air cathode MFCs were fabricated out of 3 mm acrylic sheet with fabricated SSB anodes epoxied at the base end of the cell and spaced 1.5 cm from the cathode, similar to what has been done for smaller scale MFCs [10]. Cathodes with a 0.5 mg/cm^2 Pt loading

and PTFE gas diffusion layer were constructed as previously described and had a diameter of 5 cm (19.6 cm^2 projected surface area, 7.1 m^2/m^3 cathode specific area) to match the cross-sectional area of the SSBs [10]. MFCs were incorporated into the monitoring circuit by attaching sensing leads to the stainless steel wire core of the brush and a stainless steel lead wire pressed against the cathode.

4.2.5 MFC Operation

All 30 mL MFCs were first inoculated using amended domestic wastewater from a primary effluent clarifier (Village Creek Wastewater Treatment Plant, Arlington, TX) and operated in duplicate for repeatable results. Amended wastewater was created by adding equal parts wastewater and 50 mM phosphate buffer solution (PBS; 4.58 g/L Na_2HPO_4, 2.45 g/L $NaH_2PO_4 \cdot H_2O$, 0.31 g/L NH_4Cl, 0.13 g/L KCl, produced in-house) containing 1 g/L sodium acetate in order to boost the conductivity and organic content of the wastewater for faster, more repeatable inoculation of the anodes. No other pre-acclimation methods aside from the amended wastewater used to enrich the anodes for increased biocompatibility. Start-up time was defined as the time necessary for all cells to reach 200 mV as had been described previously[66]. After the start-up cycle(s), MFCs were continually fed amended wastewater until 5 steady voltage cycles were achieved, at which point the cells were switched to only being wastewater amended with 1 g/L sodium acetate in order to replicate long term operation at a wastewater treatment plant. All feed solutions were replaced once cells dropped below a threshold voltage of 100mV in order to create one full cycle and were operated at room temperature (21 ± 2^oC).

All 275 mL SSB MFCs were first inoculated using unmodified domestic wastewater from a primary effluent clarifier (Village Creek Wastewater Treatment Plant, Arlington, TX) and operated in duplicate for repeatable results. Fresh domestic wastewater was collected for each wastewater cycle and used immediately upon collection for each MFC cycle. Start-up time was defined as the time necessary for all cells to reach 200 mV as had been described previously[66]. After the start-up cycle(s), MFCs were continually fed wastewater until 3 steady voltage cycles were achieved, at which point the cells were fed a 50 mM phosphate buffer solution (PBS; 4.58 g/L Na_2HPO_4, 2.45 g/L $NaH_2PO_4 \cdot H_2O$, 0.31 g/L NH_4Cl, 0.13 g/L KCl) containing 1 g/L sodium acetate as the consumable organic material. All feed solutions were replaced once cells dropped below a threshold voltage of 50mV in order to create one full cycle and were also operated at room temperature (21±2^oC).

4.2.6 Calculations and Measurements

Surface morphologies of the SSBs were taken before and after nanomaterial deposition using a Hitachi S-4800 II field-emission scanning electron microscope (FE-SEM) at a working distance of 8 mm and an accelerating voltage of 5kV. For FE-SEM imaging, bristles 2.5 cm in length were cut from each of the three anode configurations. The sections of the bristles were denoted as either exposed, middle, or cut, corresponding to the section of the bristle exposed to the deposition solution, the section of the bristle in the middle, and the section of the bristle near the steel wire core where it was cut, respectively.

The voltage across an external resistor box (1000Ω unless noted, Elenco Electronics, IL, USA) was measured at 10 minute intervals using an OM-CP-Quadvolt-2.5V data logger and

accompanying software (Omega Engineering, Inc., CT, USA) connected to a personal laptop. From the collected voltage, current (normalized to cathode projected area), power (normalized to the volume of the cell chamber), and Coulombic efficiency (CE) were calculated as have been previously described [10]. For polarization and power density determination, cells were first filled with the appropriate feed media and given 8 hours to reach open-circuit voltage (OCV), which was measured with a Keithley 2110 digital multimeter (Tektronix, Inc., OR, USA). Polarization and power densities were then constructed by placing the cell in the data logging circuit with 5000, 2500, 1000, 500, 300, 200, 150, 100, 50, and 30 ohm resistances, with each resistance lasting 1 hour in order to give the voltage time to stabilize. Polarization testing was conducted after 3 cycles of 50 mM PBS feeding for all configurations and after 3 repeatable cycles of only wastewater feeding for the EPD-WW cells.

Potentiostatic electrochemical impedance spectroscopy (EIS) was conducted using a Gamry Reference 3000 potentiostat/galvnostat (Gamry Instruments, PA, USA) using a frequency of 100 kHz to 10 mHz with an AC voltage of 10 mV and zero DC voltage component. EIS was performed on the MFCs when they were hooked up to a 1000 Ω resistor to see how the cells behave under steady-state conditions.

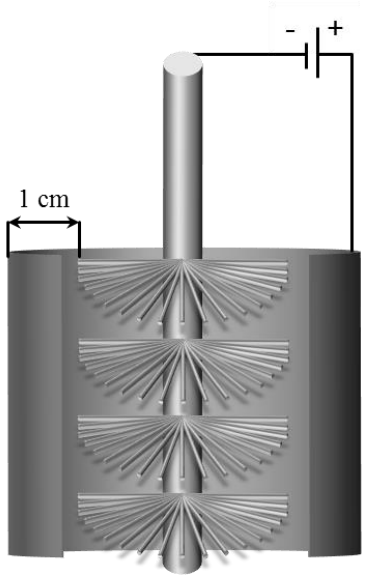

Figure 17: Graphical representation of the radial EPD process. Stainless steel brush, the negative electrode, is concentrically held in a stainless steel sheet cylinder, the positive electrode, with brush bristle ends 1 cm from the surface of the sheet. CNT/Ni solution is then poured into the set-up and a potential is applied.

4.3 Results and Discussion

4.3.1 Morphology of 30 mL Stainless Steel Anodes

For the surface modification study shown in Chapter 3 of this work, using a graphite counter electrode in coordination with increasing the IPA content of the dispersion media increased the contact angle of the CNT anode depositions. This was due to decreasing the amount of nickel hydroxide, which is hydrophilic, since less ethanol is present to provide the –OH functional groups for the formation of the hydroxide compound. In turn, more nickel metal nanoparticles were present in the deposition, which replace hydrophilic groups on the CNTs, making the overall surface more hydrophobic.

While the higher lower nickel hydroxide content led to better voltage and power performance in MFCs, there was a trade off in longer start-up times and slower bacterial colony development. As such, it was important for practical applications, where large electrodes need to be inoculated as quickly as possible for monetary reasons, to have both a conductive deposition and a hydrophilic surface contact angle. This marriage of conductivity and contact angle was achieved via changing the counter electrode from graphite foil to stainless steel in a pure IPA dispersion, which can be seen in Figure 18.

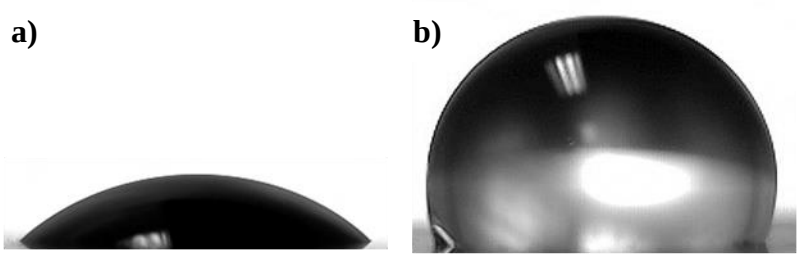

Figure 18: Contact Angles of CNT-Ni Anode Depositions Made from Only IPA with a) Stainless Steel and b) Graphite Foil Counter Electrodes

The stainless steel counter electrode gave a contact angle of 40.5° ± 2.6° while the graphite foil counter electrode gave a contact angle of 102.2° ± 8.1°. It is hypothesized that the changing of the contact angle from changing the counter electrode is related to the deposition current, as the current generated during the deposition using the graphite foil counter electrode was double that when the stainless steel counter electrode was used. As a result, the higher current may have deposited more nickel onto the CNTs, resulting in a more hydrophilic deposition. This phenomenon has not been seen previously and requires further experimentation to be understood fully.

Regardless of the mechanism, it is now possible to achieve high conductivity, hydrophilic surfaces on stainless steel for use as anodes in MFCs. The hydrophilic CNT-Ni deposition was applied to three types of stainless steel architectures: sheet, mesh, and brush. FE-SEM images showed that CNT depositions using only an IPA dispersion appear similar to those in Figures 4 and 5, again underlying the statement that all of these depositions give good, dense coverage of the stainless steel sheet. FE-SEM images of the mesh can be seen in Figure 19, with dense coverage covering the entirety of the wires that make up the mesh.

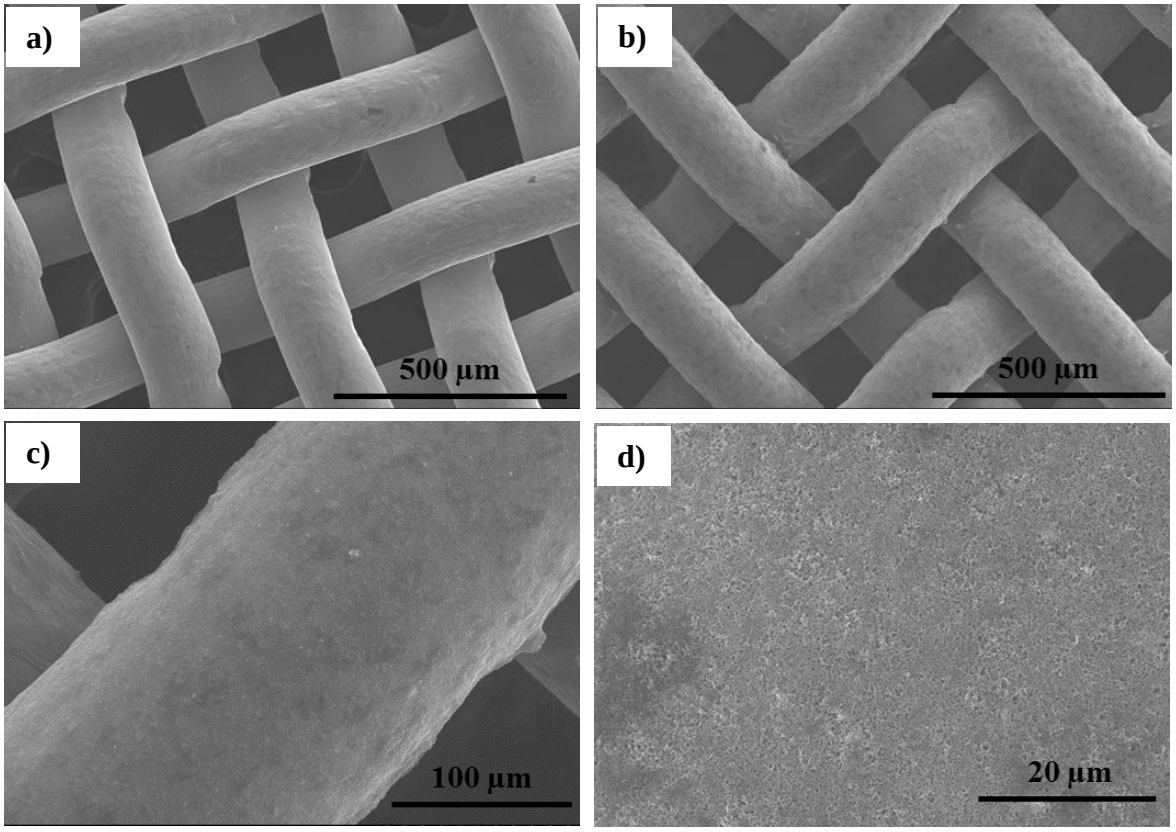

Figure 19: FE-SEM of a) Bare Stainless Steel Mesh and CNT-Ni Deposition at b) 100X, c) 400X, and d) 2000X magnification.

Due to the difficulty of removing individual bristles from the stainless steel brushes without damaging the CNTs, only optical images taken before and after the depositions. As can be seen

in Figure 20, the brushes show dense coverage along the entirety of the bristles and the higher surface area for the same volume should lead to higher performance when operated as MFCs.

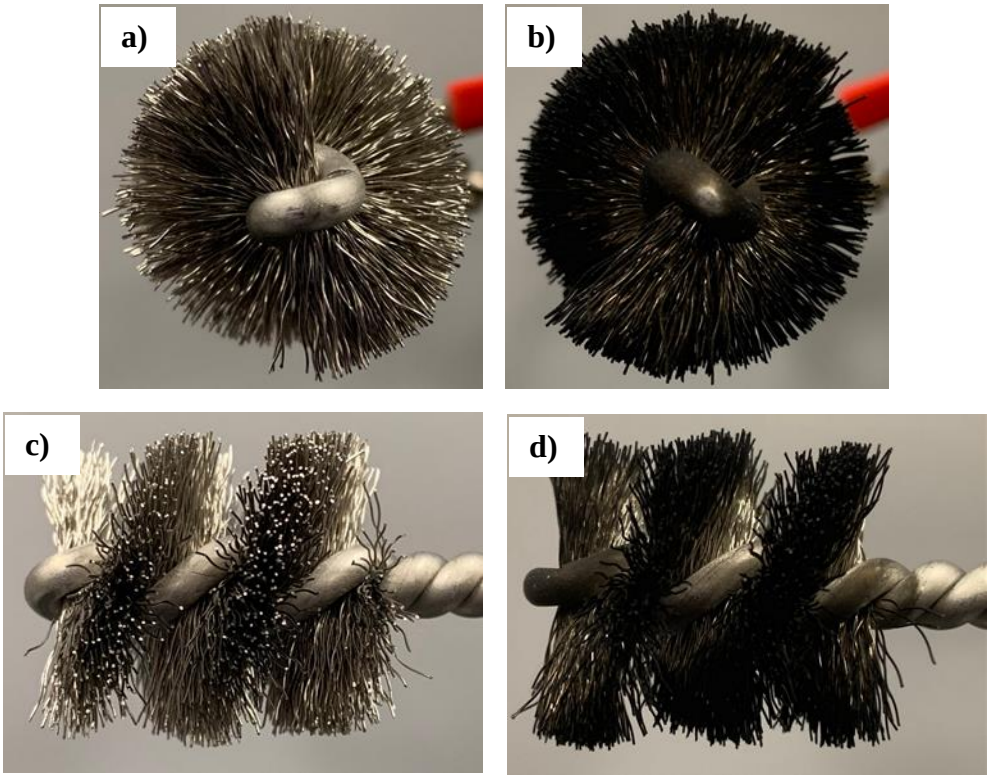

Figure 20: Optical Images of the Cross-Sectional Views a,c) Before and b,d) After CNT-Ni Deposition

4.3.2 Abiotic Testing and Wastewater Start-up of 30mL Stainless Steel Anodes

The abiotic cyclic voltammetry curves for the various stainless steel electrodes can be seen in Figure 21. As is expected, an increase in the surface area of the anode, especially going from the SSM to the SSB, shows a dramatic increase in the electrochemical activity of the anode as a quick integration of the brush curve in Figure 17a gives a total charge of 280 mC while the stainless steel mesh curve only gives 46 mC. Unlike the abiotic curves for the wettability study that were shown

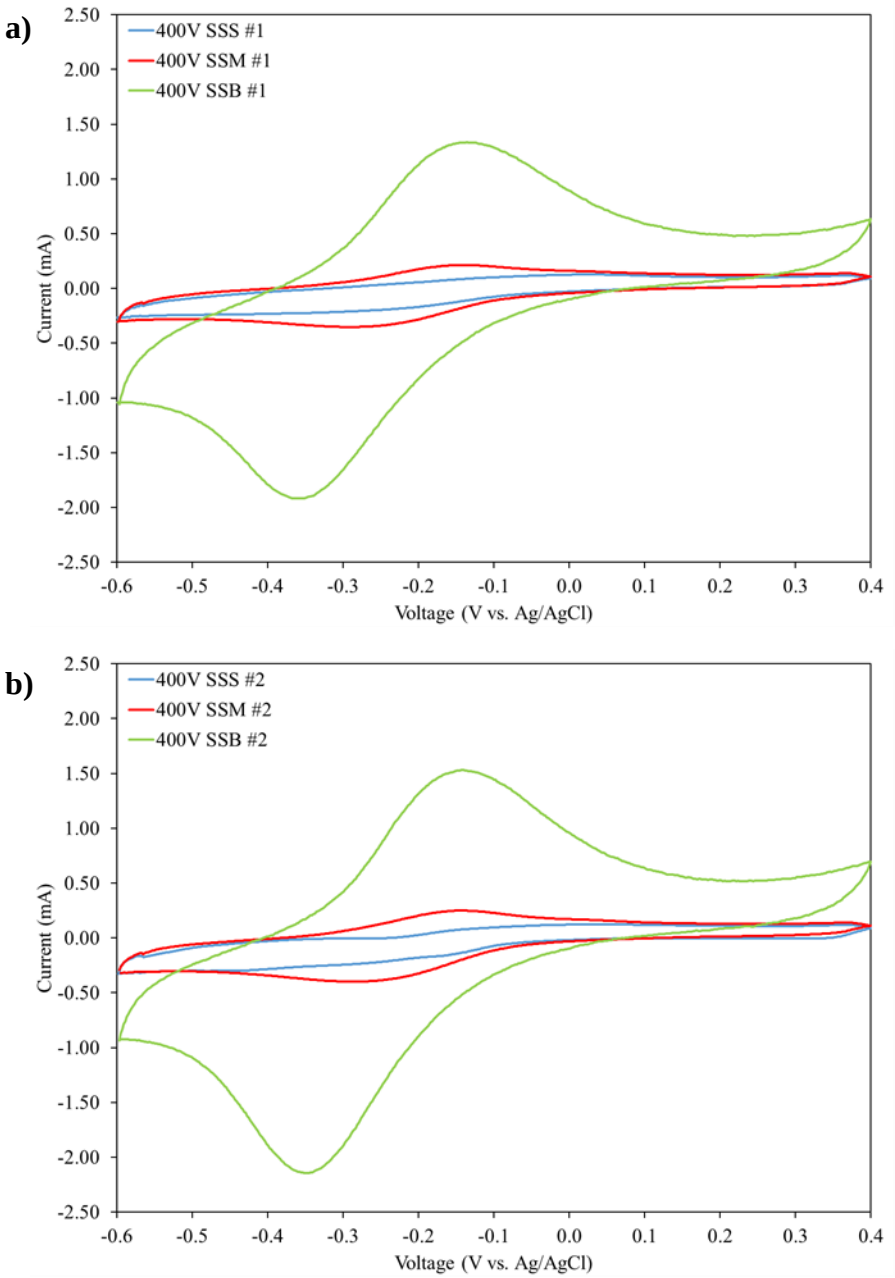

Figure 21: Abiotic Cyclic Voltammetry of a) Set #1 and b) Set #2 of Varied Stainless Steel Electrodes

in Figure 7, the IPA only depositions used for this study show a strong interaction with one of the ions present in the PBS, with reduction peaks for the SSM and SSB at approximately -150 mV vs. Ag/AgCl and a shifting oxidation peak as from -260 mV for the stainless steel mesh to -350 mV

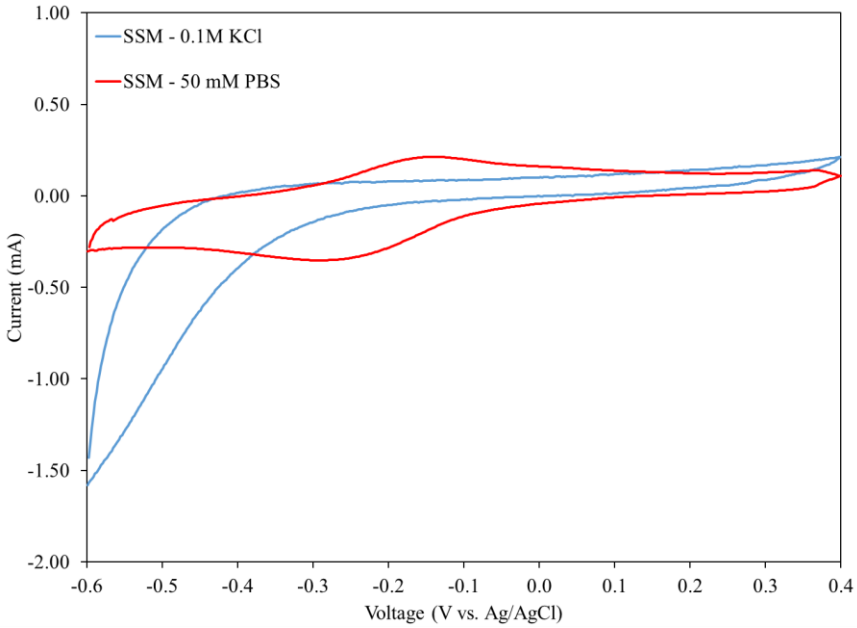

Figure 22: Comparison of SSM CNT Depositions Electrochemical Activity in PBS and KCl Solutions

for the stainless steel brush. These peaks are likely from either the sodium or phosphate ion present in the PBS as CV testing for the same stainless steel mesh in a 0.1M KCl solution reveals only capacitive behavior in the same voltage window, which can be seen in Figure 22.

Potassium chloride and ammonium chloride are small components of the 50 mM PBS, but most of the solution is comprised of sodium phosphate dibasic and sodium phosphate monobasic monohydrate, and since the KCl did not show redox reactions with the depositions, it stands to reason that the likely culprit is a component of the sodium phosphate compounds.

The accompanying abiotic EIS curves can be seen in Figure 23. For the pure IPA SSS anode, the charge-transfer resistance is approximately 30Ω for set #1 and approximately 40Ω for set #2, both lower than the same resistances seen in the 1:1 samples as shown in Figure 8 in Chapter 3. The stainless steel mesh and brushes both have even lower resistances than the sheet, even though all anodes use approximately a 0.4 mg/cm^2 mass loading for the depositions.

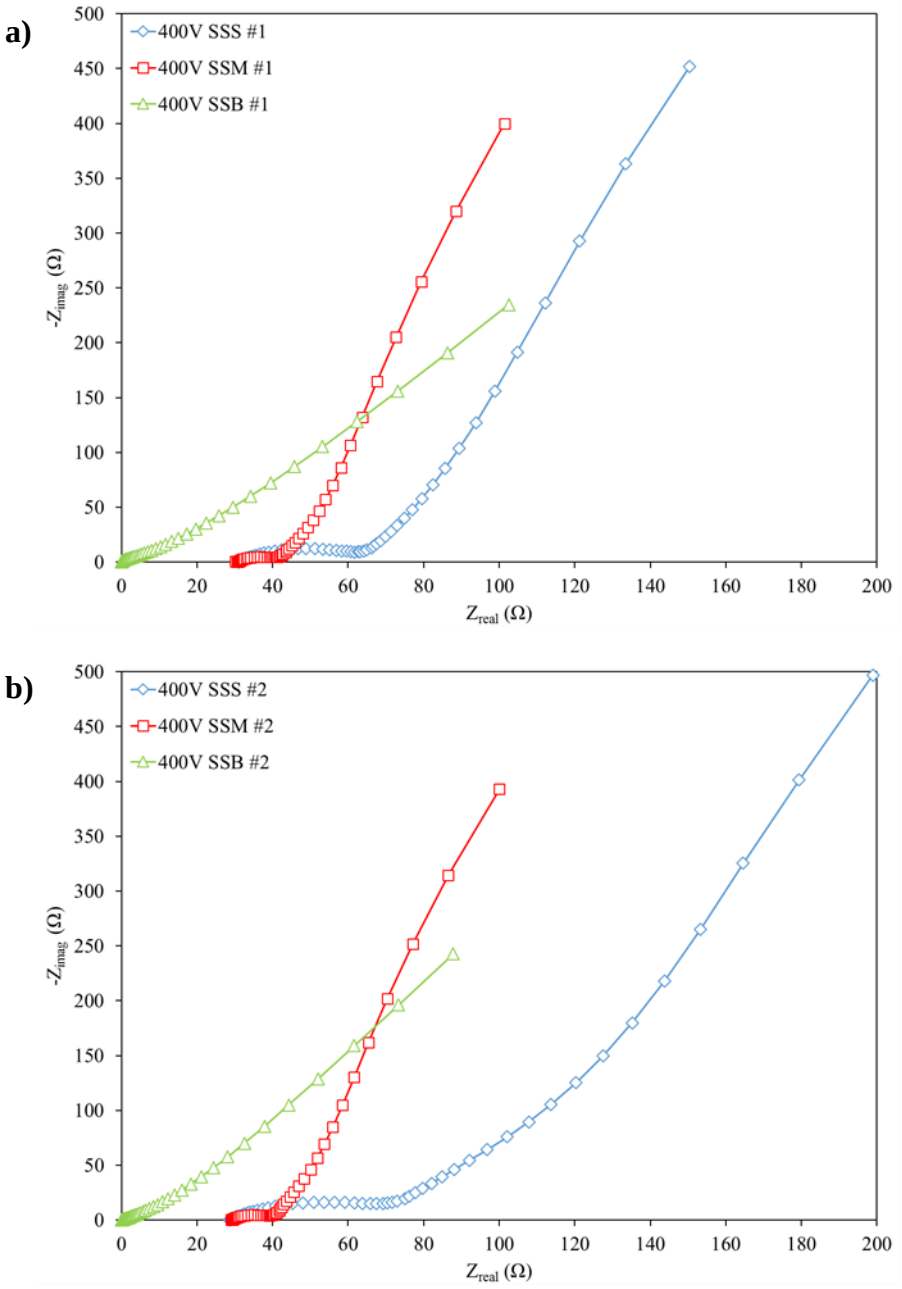

Figure 23: Abiotic EIS of a) Set #1 and b) Set #2 of Varied Stainless Steel Anodes

The reduction in charge-transfer is most likely due to the decreased nanomaterial thickness on the mesh and brush, since the mesh has increased surface area due to the mesh porosity given the same cross-sectional area of the sheet, and the brush has hundreds of bristles that are being used as the deposition surface instead of the planar configuration of the other two anode types. While both of the two planar configurations give similar solution resistances, the brush anodes have solution resistances on the order of 0.1Ω. Since the brush has the hundreds of bristles that act as its electrochemical surface, all of these surfaces are readily in contact with the introduced media, unlike the sheet where two surfaces are primarily in contact with the media. Additionally, the brush anode, unlike the sheet and mesh anodes that are placed 3 cm away from the cathode, takes up the entire volume of the 30 mL chamber, and displacing approximately 10 mL of solution, thereby placing the many of the bristles much closer to the cathode and in turn reducing diffusion resistance.

The start-up cell voltages can be seen in Figure 24. There was a general trend, especially noticeable in Figure 24b, where increasing the surface area of the anodes led to faster start-up times for the MFCs. This is to be expected where the increased surface area of the bristles, as long as there are biocompatible, should allow more bacteria to grow earlier in the inoculation phase and thereby produce a higher voltage from the larger amount of electrons being harvested when compared to the planar electrodes. Voltage wise, the SSM anode outperformed the SSS anode by approximately 20 mV per cycle for set #1 and approximately 40 mV per cycle for set #2, likely from a combination of higher surface area due to the mesh porosity and the decreased internal resistance of the cells. The SSB MFC in set #1 displayed on average the highest maximum voltages for the three cell set, with voltages in excess of 490 mV achieved with the SSM anode

lagging behind with a maximum of 460 mV. The SSB MFC in set #2 slightly underperformed the SSM anode, though did produce a similar maximal voltage of 455 mV near the end of its inoculation phase.

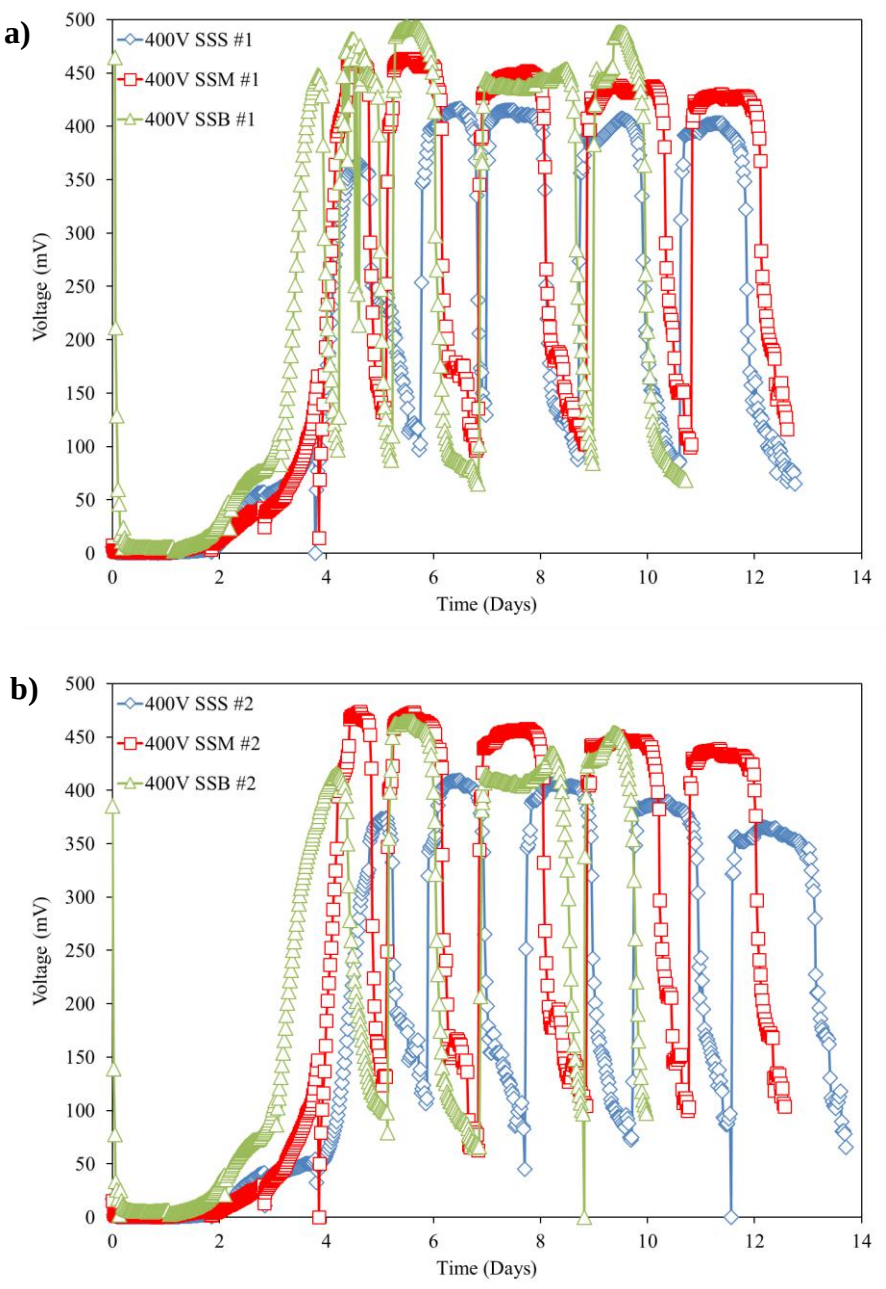

Figure 24: Inoculation Curves of a) Set #1 and b) Set #2 Varied Stainless Steel Anodes at 1000Ω

As was mentioned for the abiotic EIS, the SSB MFCs only received approximately 20 mL of inoculation media since the brush itself displaced approximately 10 mL in the 30 mL chamber, a problem that did not occur with the planar anodes due to their lower areal cross-section. It should be noted that SSB MFC #1 had a circuit connection issue during its day 4 cycle, an issue that was corrected and not repeated in following cycles.

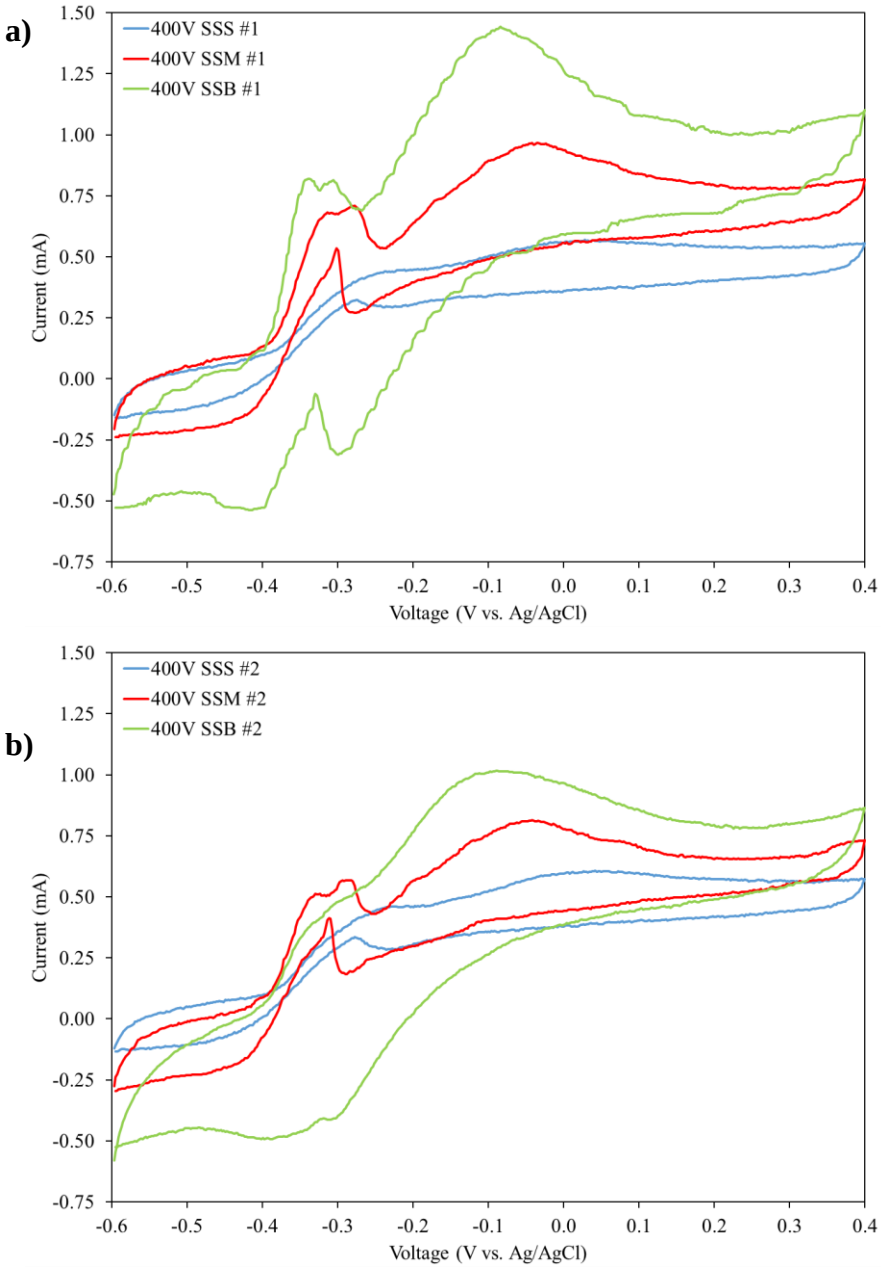

Figure 25: Cyclic Voltammetry of a) Set #1 and b) Set #2 Varied Stainless Steel Anodes After Inoculation at 1000Ω

Aside from the typical reversible catalytic curve previously seen for MFCs, the cyclic voltammetry curves in Figure 25 show a significant reduction peak for the SSB anode near -350 mV vs. Ag/AgCl along with the oxidation peak near -300 mV vs. Ag/AgCl. These peaks shift as the surface area of the anode decreases, to the point where it is barely noticeable for the SSS anode. This peak can be seen somewhat for the 1:1 anode in Figure 11a, the more conductive of the two 1:1 anodes, but not for the 0:1 or 1:3 anodes. It is believed, since the peak is occurring during the voltages between -0.4V and -0.2 V where the bacteria are most active, that the higher electrochemical activity of the bacteria on the more conductive stainless steel mesh and brush anodes contributes to the distinct peak.

The EIS of the various SS anodes can be seen in Figure 26. When compared to the abiotic curves in Figure 23, little differentiation can be seen, with only a noticeable increased in the charge-transfer resistance of the SSS anodes present. The overall resistance of SSB #2 is higher than its set #1 counterpart and, when coupled with its lower electrochemical activity compared to SSB #1, could be why the secondary brush was underperforming during the voltage study.

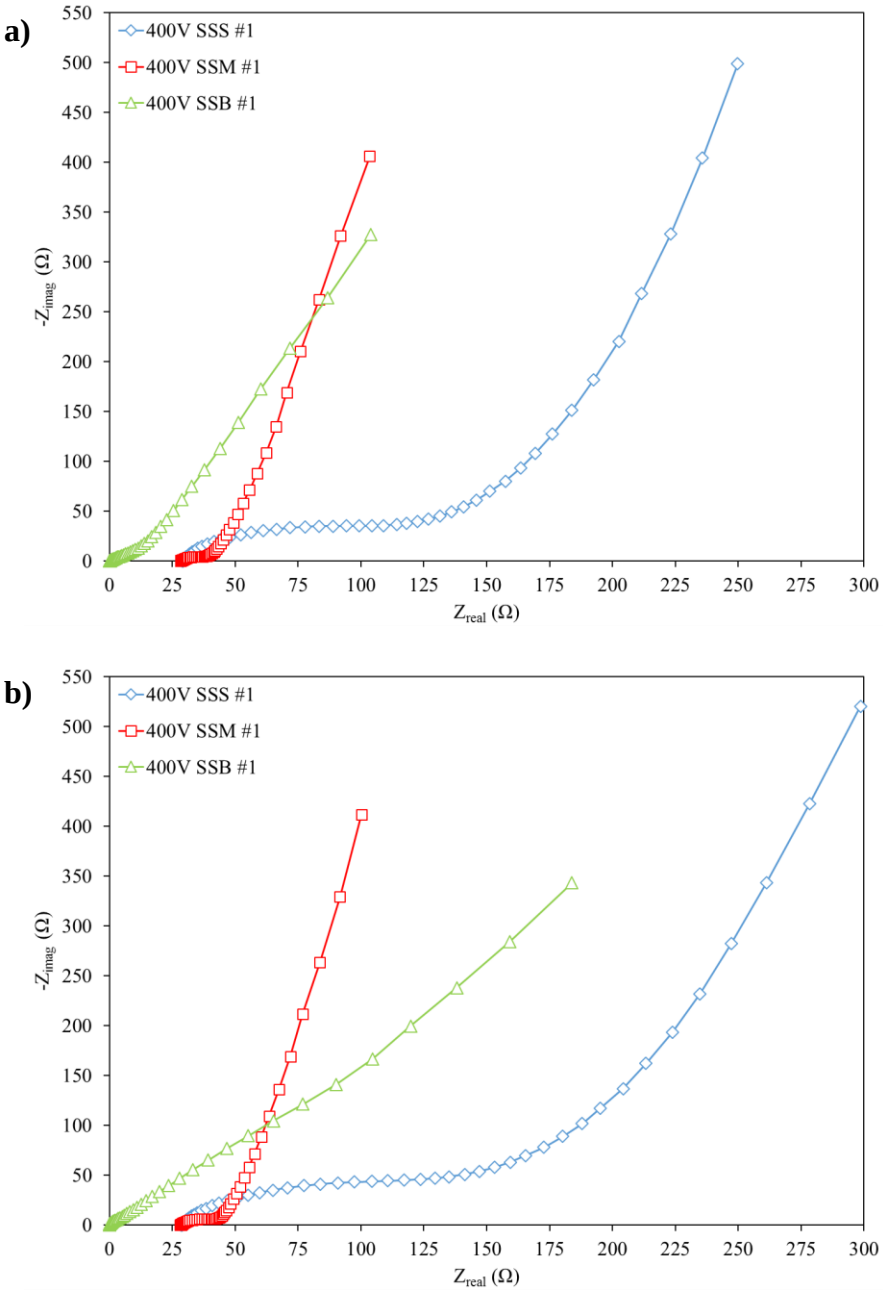

Figure 26: EIS of a) Set #1 and b) Set #2 Varied Stainless Steel Anodes After Inoculation at 1000Ω

4.3.3 Initial Radial EPD Refinement of Large SSBs

After the initial use of radial EPD for SSBs in 30 mL cells, some extended characterization of the EPD process was done in order to better understand how good coverage along the entirety of the brush bristle was achievable. For this task, a more open 5 cm by 7 cm brush was selected in order to build a much larger MFC than had previously been explored so to show additional scalability of the EPD process, as well as making it more feasible to study under the FE-SEM.

For this study, the main EPD parameters of voltage and time were selected to be characterized. These parameters are generally two of the three the easiest parameters to modulate when conducting EPD. For this study, nanomaterial concentration, the typically third of the easiest parameters, was not selected due to the fact that the 400 mL of solution necessary to deposit on the brush was quite conductive and made the high-voltage power source deposit in a current-limited mode for concentrations above the 0.03 mg/mL CNTs and 0.015 mg/mL $NiCl_2$. Therefore, a fixed concentration was used and for each of the voltage and time studies, a low, middle, and high setting were chosen in order to show the exaggerated effect of each parameter on the MRCNT deposition.

For the effect of voltage and subsequently voltage control on MRCNT deposition onto SSBs, 30V, 400V, and 760V were selected as the studied voltages. The highest voltage of 760V was selected, even though the high voltage power source is rated up to 2kV, was because this voltage allowed for a meaningful deposition time of up to 1 minute before the power source self-regulated itself and switched over to a current-limited state. The other two voltages were selected since 400V had been used in the previous iteration of EPD for MFCs and 30V is a traditionally low voltage for

EPD, especially for aqueous media. For these depositions, a quick deposition of 10 seconds at a concentration of 0.03 mg/mL for both the MRCNTs and $NiCl_2$ charging salt was used.

The images of the MRCNT depositions describing the effect of voltage on radial EPD can be seen in Figure 27.

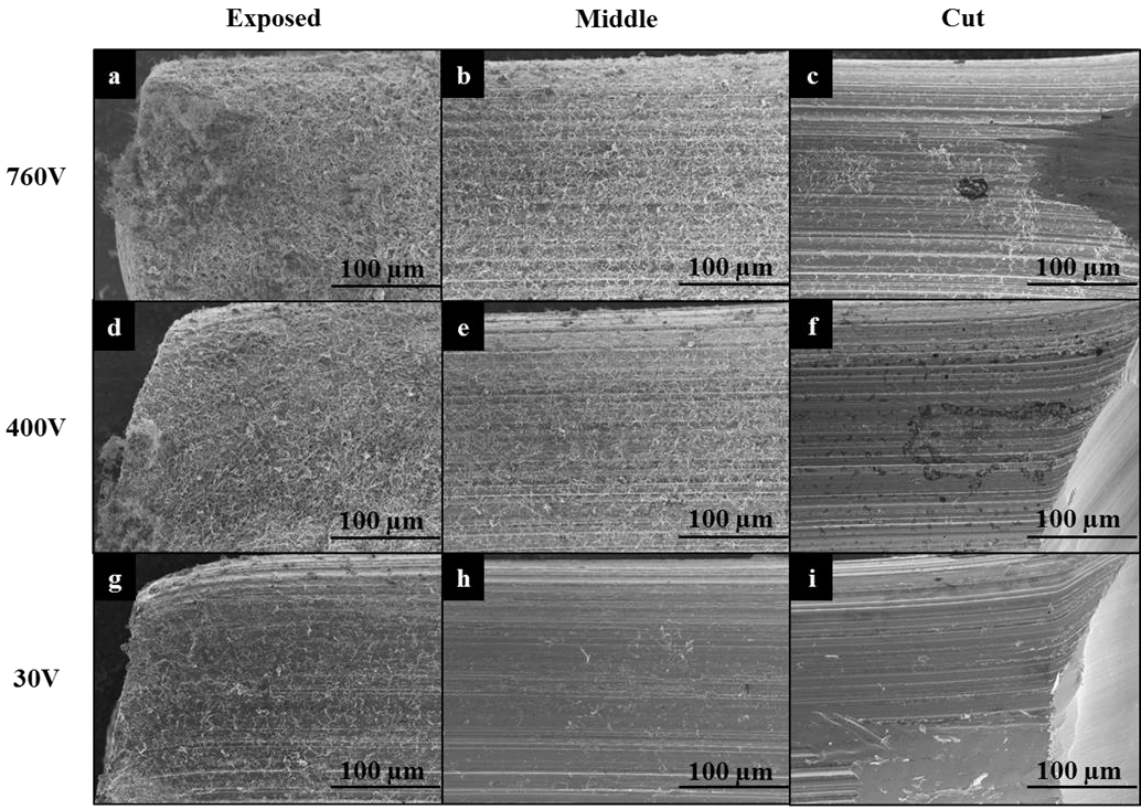

Figure 27: FE-SEM characterization of the effect of voltage on radial EPD for deposition of MRCNTs onto SSBs. Micrographs depict sequentially the exposed, middle, and cut ends of (a-c) plain stainless steel after acetone/IPA/DI water cleaning, (d-f) CNT/NMP/Nafion dip-coating, and (g-i) CNT/Ni EPD at 760V.

The first noteworthy observation of the FE-SEM images is the production of a gradient across the entirety of the SS bristle. This is not typically the case for planar substrates such as the stainless steel sheet or the mesh used in the 30 mL MFCs. As the electric field is applied further down the bristle, the electric field becomes weaker, making the total deposition mass lower the further away the electrode gets from the steel shim counter electrode at the edge of the beaker. It is believed that for radial EPD, each of the exposed ends of the bristles act as points of electric field concentration, similar to the edge-effect buildup of CNTs when conducting planar EPD. As such, a larger amount of CNTs are deposited in the exposed sections for all the EPD voltages, with the higher voltages corresponding to denser CNT depositions.

Unsurprisingly, the low voltage deposition for a short 10 second deposition provided the least amount of CNTs to the bristle and thereby the worst coverage of the three selected voltages. The 400V and 760V bristles showed good coverage at the exposed ends while the 760V bristle had denser CNT deposition in both the middle and cut sections. This increased deposition can be attributed to the higher voltage, which allowed CNTs to be deposited more quickly onto the bristle when compared to the 400V setting. For the cut ends, some localized CNT deposition, i.e. the immediate deposition of CNTs present in the solution in the vicinity of that bristle section, can be seen for the 760V setting in Figure 27c, but it seems that most of the CNTs in the dispersion near cut end of the bristle migrate towards the middle and exposed ends of the brush bristle for all three voltages shown in this study. This migration can be attributed to the electric field concentration as well as the CNT concentration gradient.

If the time is increased, as seen in Figure 28, a much more dense deposit is seen at both the exposed and middle sections of the bristle for the 45 second time setting of the 760V deposition. Again, as the time is increased, CNTs from the "reservoir" on the outer edges of the beaker, and seemingly the cut section of the bristle, are drawn in by the concentration gradient created from initial deposition of CNTs.

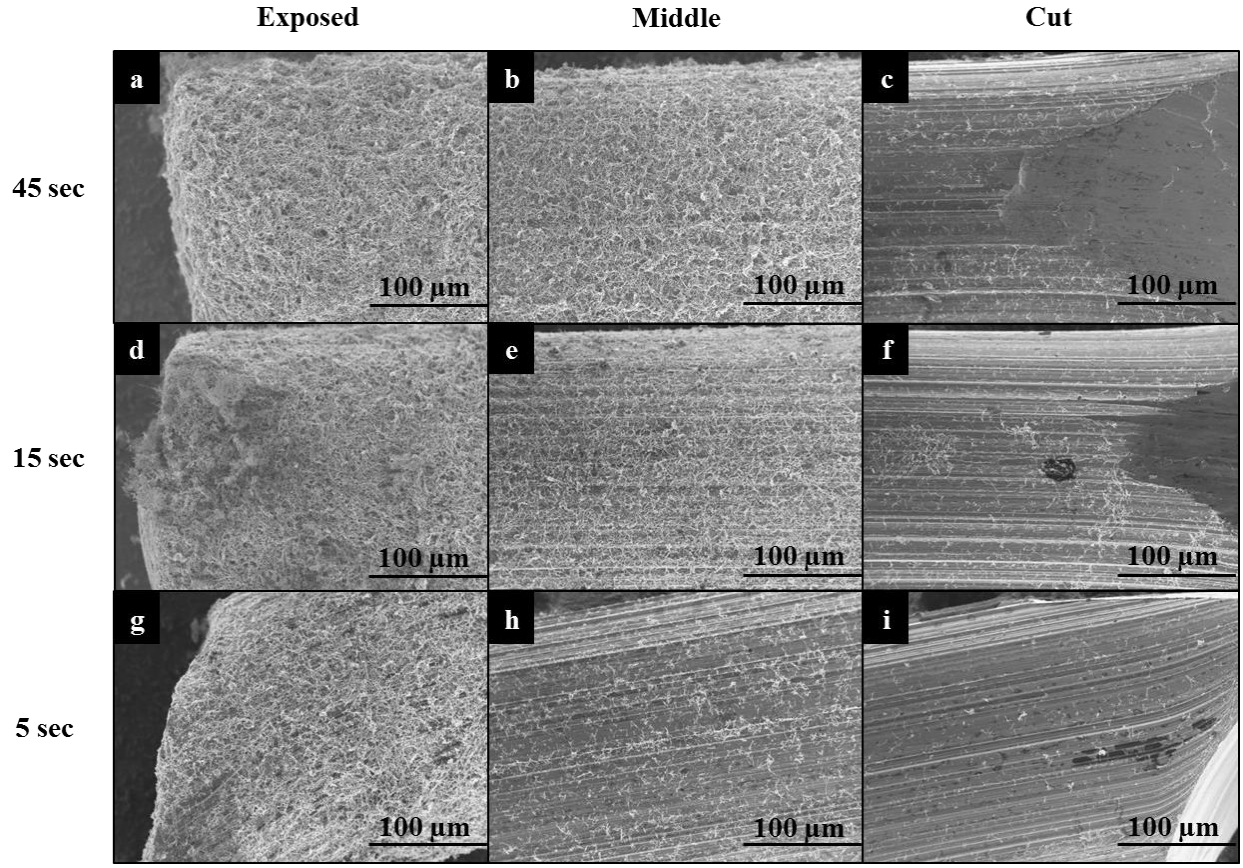

Figure 28: FE-SEM characterization of the effect of time on radial EPD for deposition of MRCNTs onto SSBs. Micrographs depict sequentially the exposed, middle, and cut ends of (a-c) plain stainless steel after acetone/IPA/DI water cleaning, (d-f) CNT/NMP/Nafion dip-coating, and (g-i) CNT/Ni EPD at 760V.

4.3.4 Morphology Analysis of 275mL MFC SSBs

Figures 29a-c shows the smooth surface of the plain SS brush, which is problematic for biocompatibility since there are no distinct surface features for the bacteria to attach to during inoculation of the anodes, which can cause a dramatic increase in cell start-up time or incomplete inoculation. Due to the smoothness seen in the plain SS images, the passive oxidation layer seems to be intact and the acetone/IPA/DI water washing does not seem to affect the steel aside from the removal of organics and manufacturing debris.

Figures 29d-f show the results of the dip-coating of the MRCNTs from the MRCNT/Nafion/NMP solution. The MRCNT dip-coating technique has a slight preferential for the exposed ends of the SS bristles, but otherwise generates a patchy, sporadic deposition throughout the entirety of the bristle with large sections having no MRCNTs while other sections having dense sections of bundled MRCNTs. On some bristles, dense agglomerations of MRCNTs develop and are large enough to be seen optically as black spots in Figure 30b. Adhesion of the MRCNTs is attributed to a Nafion coating and holding layer that binds the nanomaterial to the surface of the SS bristle, similar to what occurs in the 10% Pt/C cathode production.

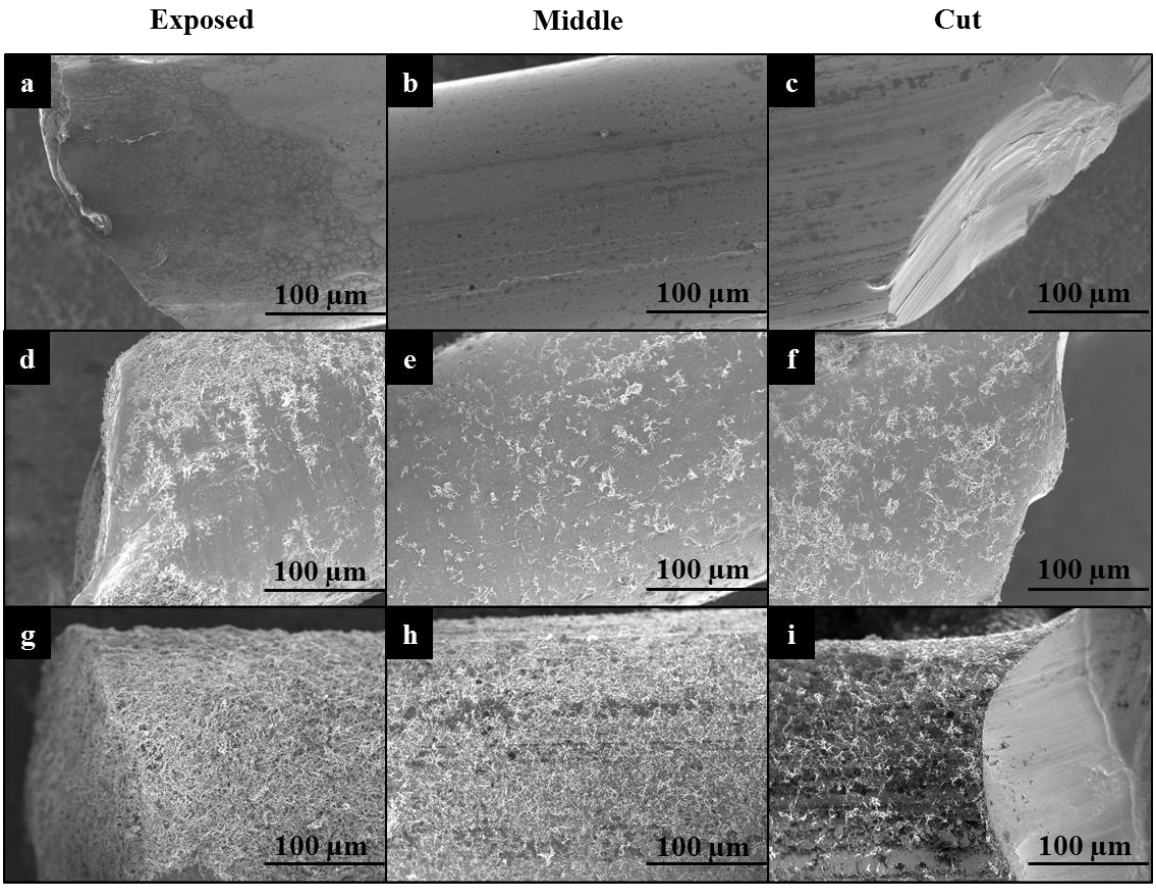

Figure 29: FE-SEM images of 2.5 cm length stainless steel bristles taken from brush anodes. Micrographs depict sequentially the exposed, middle, and cut ends of (a-c) plain stainless steel after acetone/IPA/DI water cleaning, (d-f) CNT/NMP/Nafion dip-coating, and (g-i) CNT/Ni EPD at 760V.

Figures 29g-i show the results of the radial EPD of the MRCNTs from the MRCNT/Ni/IPA solution. As was explained previously, due to the electric field line concentration generated at the exposed end of the SS bristles during EPD, a dense, dark deposit of interconnected MRCNTs about 2-5 mm in length and can be seen optically in Figure 25c. Along the length of the bristle, radial electric field lines cause interference between the bristles caused a small reduction in the amount of MRCNTs deposited, culminating at the cut end of the bristle. However, even with this interference, the EPD anode shows a much denser deposit throughout the entirety of the SS bristle than that of the Nafion dip-coating technique. The MRCNTs remain attached to the SS bristle via the introduction of the nickel ions present in the deposition solution. The nickel ions attach to the surface defects given to the MRCNTs during the mild-refluxing process, giving the MRCNTs an overall net positive charge. This positive charging of the MRCNTs causes, in the presence of an electric field, them to electrostatically deposit onto the negatively poised brush during EPD. Additionally, free nickel ions in the deposition solution will also deposit onto the MRCNTs, forming a conductive holding layer that also serves as a conductive pathway from the MRCNTs to the SS bristle, similar as to what happens with the planar EPD of SSS and SSM anodes.

For both the dip-coating and EPD MRCNT depositions, the coating is robust and survives multiple DI water washings even immediately after the deposition, indicating that it was likely that the MRCNTs would survive bacterial adhesion as well as continual removing of the feed solutions. Laboratory photographs of the completed brushes can be seen in Figure 30.

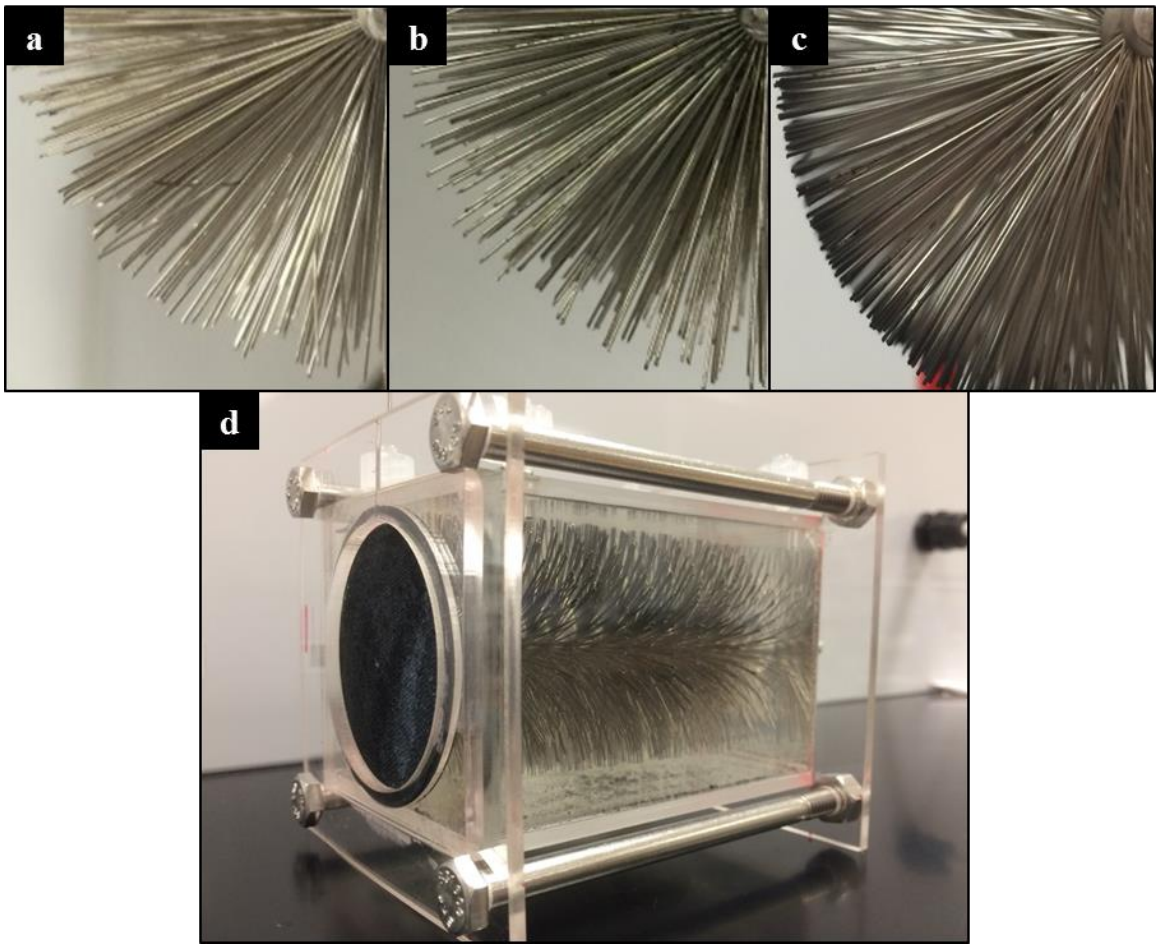

Figure 30: Stainless steel brush anodes used in 275 mL MFCs. Photographs depict (a) plain brush after acetone/IPA/DI water cleaning, (b) brush after CNT/NMP/Nafion dip-coating (c) brush after CNT/Ni EPD at 760V, and (d) full assembly of MFC cell.

4.3.5 Wastewater Start-up and Operation of 275mL Cells

The start-up and subsequent operation of all stainless steel brush anodes configurations can be seen in Figure 31. As was expected due to its poor biocompatibility, the plain SS brush took 288 hours over multiple wastewater replacements to reach the start-up criterion, however, this threshold was not maintained over subsequent wastewater cycles. The plain SS brush reached a maximum voltage 205 mV before degrading performance over the next two cycles prior to its operation in PBS likely due to the poor biocompatibility and the inability of the plain SS brush to maintain the continual growth and death of the bacterial colony. The dip-coated brush took only two cycles to reach the 200 mV start-up threshold and did so in 98 hours. Repeatable maximum voltages of 402 ± 29 mV were recorded for the dip-coated brush however cycles only maintained the maximum voltages for 9 ± 3 hours before steady decline in the output voltage, likely due to high charge transfer resistance of the Nafion holding layer.

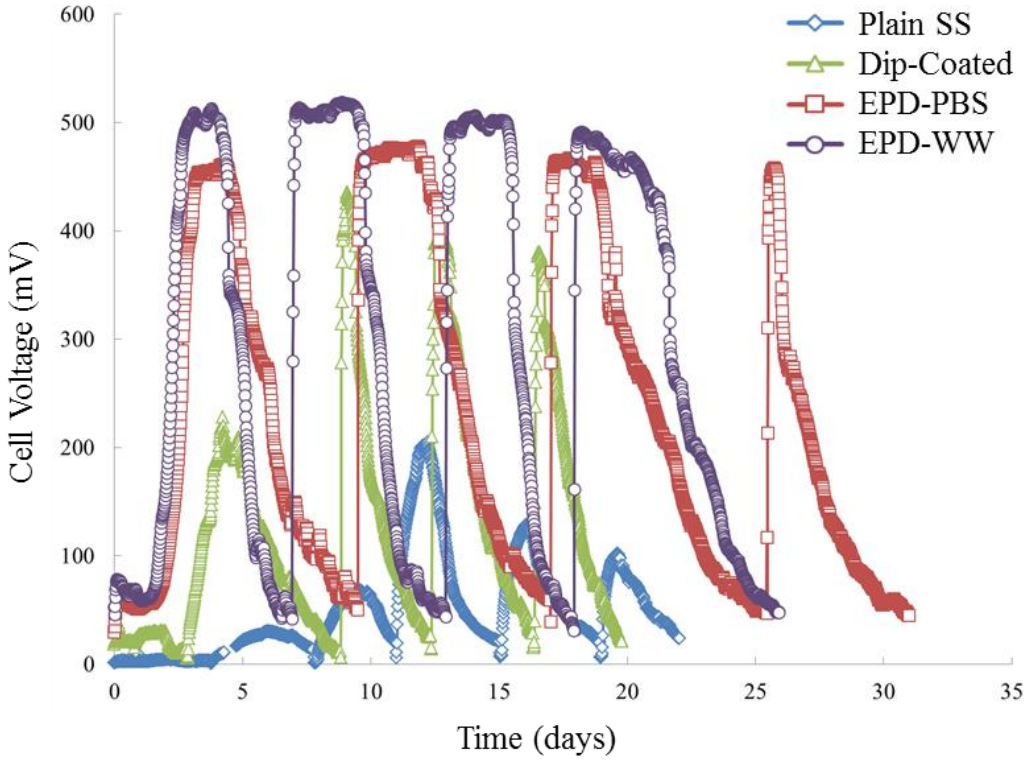

Figure 31: Initial start-up and operation cycles of stainless steel brush anodes in unmodified domestic wastewater (1000Ω resistor).

Both of the EPD-WW and EPD-PBS anodes reached the start-up threshold of 200 mV in their first cycle with wastewater, at 52 hours and 61 hours respectively. This start-up time is 45-53% reduction in what is typically seen for reactor volumes in excess of 250 mL and start-up of time of approximately 60 hours has only been previously seen in the start-up of 28 mL MFCs utilizing ammonia-gas treated carbon fiber brushes[31]. As was the case with the ammonia-treated brush, the EPD process introduces a large amount of positive surface charge to the MRCNTs from the dissolved nickel ions, which is necessary for the deposition process. This excess positive surface charge is maintained after deposition and provides a highly preferential surface for bacteria to adhere and grow on during the initial start-up cycle. Unlike the ammonia-treated brush however, the maximum voltage of the start-up cycle was on par with the repeatable maximum voltages, 507 ± 12 mV and 466 ± 9 mV for EPD-WW and EPD-PBS respectively. The voltage outputs for both of these brush anodes are some of the highest reported values for unmodified domestic wastewater, with reported values typically ranging between 275-400 mV, and the EPD-WW brush anode is one of the few reported cases of a singular MFC anode outputting a voltage in excess of 500 mV in unmodified domestic wastewater.

4.3.6 PBS Operation of 275mL Cells

For PBS voltage cycles, 3 repeatable maximum voltage cycles were obtained starting with the first media feeding for all configurations, due to the extended inoculation and operation in domestic wastewater. The voltage curves for the plain SS, dip-coated, and EPD-PBS brushes can be seen in Figure 32. Unlike the wastewater cycles, all brush configurations exhibited extended plateaus at maximum voltage for multiple days of operation. Plain SS brushes performed at lower voltages than those seen in wastewater operation with a maximum voltage of 76 ± 9 mV and a CE of 1.8 ± 0.3%. While galvanic current onset from the corrosion of the stainless steel may have led to over-

exaggerated performance in wastewater, the voltage curve of the plain SS brush is similar in both shape and maximum voltage when compared to previous works. The previously discussed low biocompatibility, high overpotential, and low electron transport of the stainless steel are the main factors that cause poor steady-state MFC performance in 50 mM PBS. The cycle time for the plain SS brushes of 229 ± 24 hours drove the columbic efficiency to be has high as 2.0% for the configuration's first cycle, despite the inherent limitations of the material.

The dip-coated brush provided a maximum voltage of 577 ± 21 mV and a CE of 11.9 ± 0.6%, a corresponding 659% increase in the voltage and 561% increase in CE when compared to the plain SS brush configuration. The dip-coated brush had the shortest cycle time of the three configurations of 175 ± 16 hours. The maximum voltage of 596 mV for the first cycle of the dip-coated brush was the highest recorded voltage for all brush configurations, however, subsequent cycles decreased steadily in maximum voltage by approximately 15 mV per cycle. This voltage decrease was likely due to increasing charge transfer resistances attributed to the Nafion holding layer, decreasing biocompatibility with the Nafion coating on the MRCNTs, and/or the increasing presence of aerobic bacteria as the cell continued its extended operation.

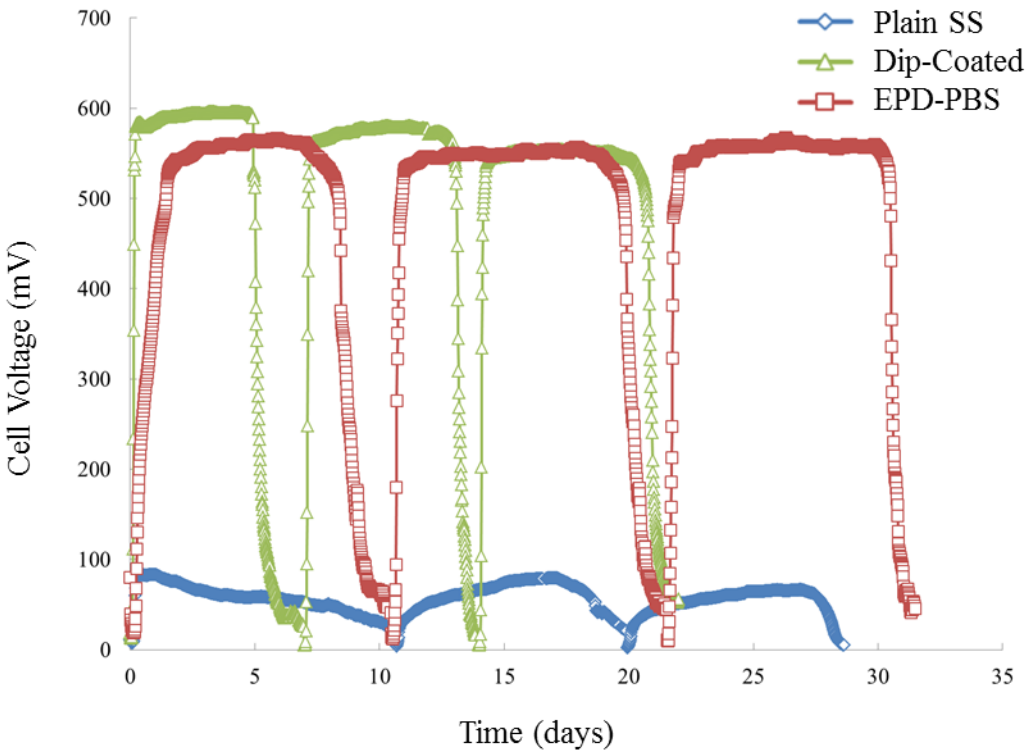

Figure 32: Steady-state operation of stainless steel brush anode configurations in 50 mM PBS (1000Ω resistor) after operation in wastewater.

The EPD-PBS brush had a maximum voltage of 564 ± 6 mV and a CE of 16.4 ± 1.2%, a corresponding 642% increase in the voltage and 811% increase in CE when compared to the plain SS brush configuration. The EPD-PBS brush provided the least variation in the maximum voltage output and, when combined with the longest cycle times of 250 ± 13 hours, produced the highest columbic efficiencies of this study. The reduction in voltage variance and CE of the EPD-PBS brush is a continuation of the phenomenon seen during the domestic wastewater operation. The high uniformity of the MRCNT deposit along the length of the SS bristles provides an adequate scaffold for continued large colony bacterial growth and proliferation in the high organic concentration of the sodium acetate PBS and the nickel conductive holding layer provided better electron transport than that of the Nafion holding layer for the dip-coated brush. Considering that

the EPD-PBS brush maintained its maximum operation voltage for in excess of one month, the results are very promising for extended use in actual wastewater plants in the future.

4.3.7 Polarization Curves of 275 mL Cells

The plain SS brush performed the worst out of all the brush configurations with a 60 mW/m^3 (8.5 mW/m^2) maximum volumetric power density, as can be seen in Figure 33. The addition of nanomaterials significantly improved the power performance of the MFCs, even with the passive oxidation layer remaining after the deposition processes. The dip-coated brush output a power density of 1297 mW/m^3 (182 mW/m^2) and the EPD brushes performed even better, outputting power densities of 1556 mW/m^3 (218 mW/m^2) in domestic wastewater and 2702 mW/m^3 (379 mW/m^2) in 50 mM PBS. The EPD-PBS brush had a 108% increase in the power density when compared to the dip-coated brush and even the EPD-WW brush outperformed the dip-coated brush by 20%. The volumetric power density for the EPD-PBS brush is on par with unmodified (estimated 650 mW/m^3) and ammonia-treated (estimated 1000 mW/m^3) carbon fiber brushes of the same size operated in 50 mM PBS. The EPD-PBS brush was even comparable to unmodified (1200 mW/m^3) and ammonia-treated (2300 mW/m^3) carbon fiber brushes operated in 200 mM PBS [9].

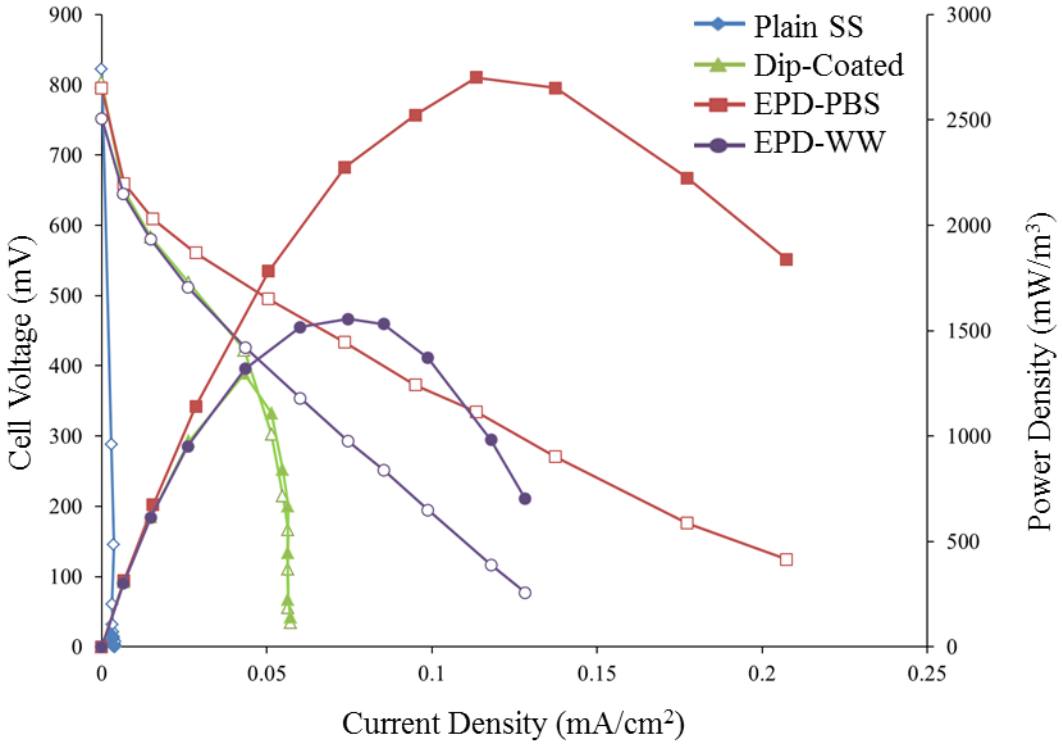

Figure 33: Polarization and power density curves for stainless steel brush anodes.

However, the EPD-PBS was outperformed when compared to carbon brush anode MFCs of similar reactor size with higher cathodic specific areas due to the lower anodic surface area available for the bacteria to grow on (0.024 m^2 to 1.06 m^2 for EPD-PBS and carbon fiber brushes respectively) [11]. Additionally, the EPD-PBS brush performed lower than other modified-stainless steel anodes, especially in terms of the cell current density (typical values 1.5 to 5 mA/cm^2), for a few reasons. First, many stainless steel anodes in previous studies had their passive oxidation layer removed either through an acid treatment process or flame-oxidation method, unlike this study that deliberately attempted to preserve the oxidation layer [33], [34]. Both the acid-treatment and flame-oxidation techniques inherently increase the conductivity of the stainless steel via the removal of the oxidation layer and create a micro-textured surface for the bacteria to grow on, which are preferential for high-power MFCs. The addition of nanomaterials further increases these

effects. Secondly, many stainless steel anode MFCs have been developed as two-chamber systems and are inherently unrealistic comparisons to our EPD-PBS brush anode. In the future, it is likely that removal of the passive oxidation layer by acid-treatment, in combination with the radial EPD process, will lead to high performance current and power densities that rival currently developed stainless steel anodes.

4.3.8 EIS of 275 mL Cells

The differences between the solution resistance of the 50 mM PBS, 14 ± 2 ohms, and the unmodified wastewater, 63 ± 4 ohms, was apparent given the initial offsets of the EIS curves seen in Figure 34. The large semi-circle seen in the zoomed-out view denotes the diffusion resistance of the MFCs while the inset shows the smaller semi-circles of the charge transfer resistance. The EPD-WW brush has a high charge transfer resistance due to the low conductivity of the wastewater and this high resistance manifests itself as the lower voltages displayed in both the voltage and power density curves. The dip-coated brush showed both a higher charge transfer and diffusion resistance than the plain SS brush and the EPD-PBS brush due to its larger diameters and in turn, the EPD-PBS brush has a lower resistance than that of the plain SS brush.

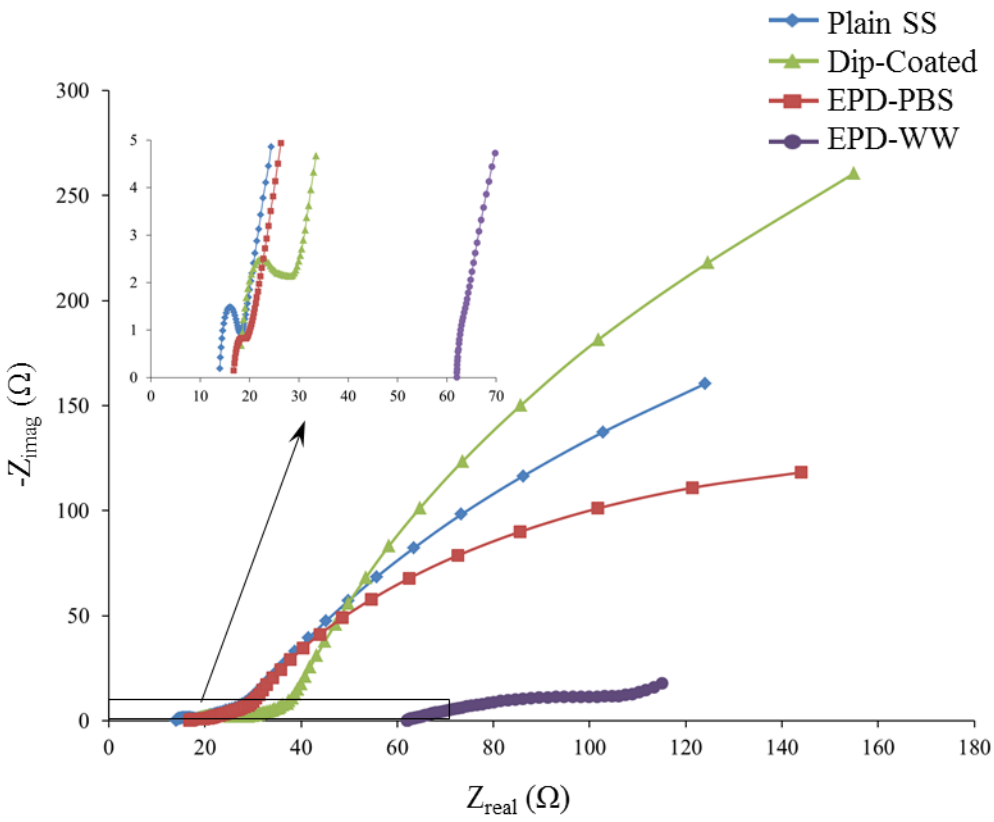

Figure 34: Electrochemical impedance spectroscopy (EIS) curves of 275 mL stainless steel brush anodes.

Both the increase in the charge transfer resistance and the diffusion resistance for the modified brushes can be explained from their production methodology, with the increase in the dip-coated brush attributed to the Nafion holding layer and the decrease for the EPD brush attributed to the nanomaterial and metal nanoparticle-holding layer. It should be noted that even though the diffusion and charge transfer resistance are much higher for the dip-coated brush due to the Nafion, the improved surface roughness given by the MRCNTs enhanced the biocompatibility of the stainless steel brush enough for decent MFC performance. Therefore, EPD modification of high biocompatible, low conductivity substrates could potentially lead to high performance anodes in future works.

4.4 Conclusion

For the first time a radial electrophoretic deposition of carbon nanotubes have been deposited onto a commercially available stainless steel brush for the anode of a microbial fuel cell. In this study, a comparison of different stainless steel anodes in 30 mL MFCs was initially explored following the EPD process previously developed by the wettability study. A short characterization of the radial EPD process for large-scale stainless steel brushes was conducted that showed, for a specific nanomaterial concentration, higher voltages and longer depositions allowed for better coverage of CNTs onto the brush bristles. For the 275 mL SSB, with a total bristle surface area of 0.024 m^2, achieved start-up in 52 hours in unmodified domestic wastewater and had a maximum power density of 2.7 W/m^3 in 50 mM PBS, a 108% increase over a dip-coated comparison. Electrochemical impedance spectroscopy showed that the addition of MRCNTs caused a reduction in the charge transfer and diffusion resistances inside the cell during operation with a 1000Ω resistor when comparted to the dip-coated brush.

V. Chapter 5: Controlled Wettability via Electrophoretic Deposition and the Effect on Catalytic Performance for Microbial Electrolysis Cell Cathodes

5.1 Introduction

While a majority of this work has explored the use of electrophoretically deposited carbon nanotubes for improving anode performance in microbial fuel cells, the same EPD process can also be applied to the cathode for either MFCs or MECs. There has been limited work on the effect of EPD created catalysts for MFC cathodes however there has been no study of the same catalysts for MEC cathodes[37], [95]. Therefore, this chapter details a brief exploratory study has been conducted to show the effect of wettability of electrophoretically deposited CNTs previously shown in Chapter 2 on hydrogen evolution for MECs and initial attempts into optimizing catalytic activity using the galvanic replacement of nickel nanoparticles with platinum.

5.2 Stainless Steel Sheet Wettability on Hydrogen Evolution

Adapting the method used in Chapter 2 for the wettability of anodes in microbial fuel cells, both hydrophobic and hydrophilic CNT-Ni deposits were made solely in IPA to establish the effect of wettability on hydrogen evolution for MECs. Both of these depositions were compared to a bare stainless steel electrode with the wettabilities shown in Figure 35.

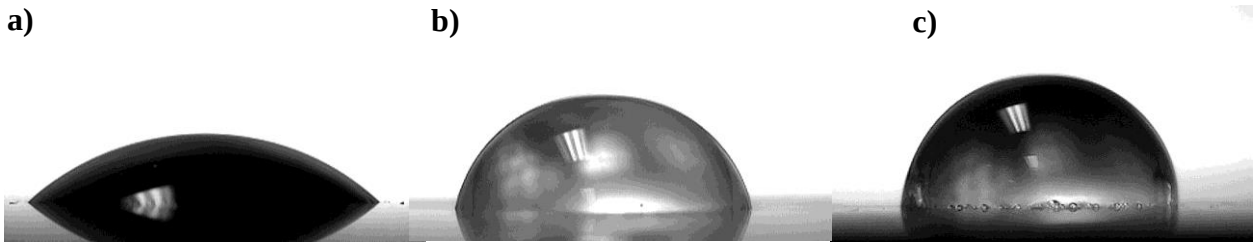

Figure 35: Wettabilities of a) Hydrophilic CNT-Ni, b) Bare SSS, and c) Hydrophobic CNT-Ni

All catalytic tests were performed using linear sweep voltammetry (LSV) with samples submerged in 0.1M KCl. A graphite rod and Ag/AgCl electrode were used as the counter electrode and reference electrode respectively, and the KCl solution was degassed with nitrogen for 20 minutes before LSV was conducted. The fifth run of each sample is presented in Figure 36.

From both Figures 36a and 36b, it is evident that the hydrophobic CNT-Ni sample performed the worst out of the three wettabilities as it gave the lowest maximal current density at -1.6V vs. Ag/AgCl and had the highest overpotential when evaluated at 1 mA/cm^2. The 1 mA/cm^2 current density is particularly important because most MECs operate with current densities in the 0.1 to 1 mA/cm^2 regime and as such, can be used as the figure of merit when comparing MEC catalytic performance. The hydrophilic CNT-Ni performed the best at the 1 mA/cm^2 current density, outperforming the hydrophobic comparison by 30mV and the bare SSS by 10 mV. This is due to the fact that the hydrophilic CNT-Ni was able to remove hydrogen bubbles more quickly during LSV testing and there were much fewer pinned bubbles on the catalyst, especially on the edges of the stainless steel sheet.

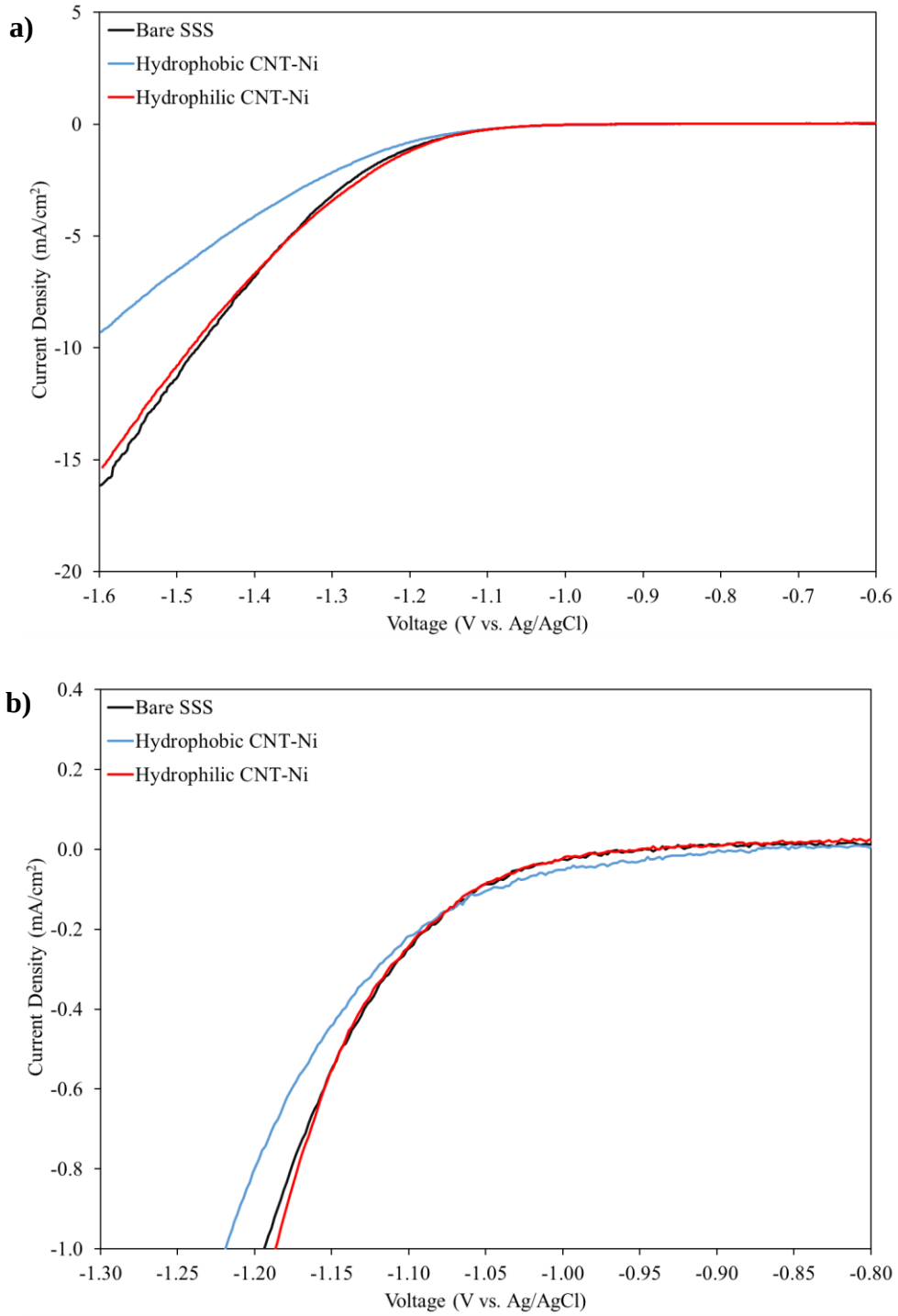

Figure 36: LSV of Stainless Steel Sheet Wettability for a) 1V Window and b) 1 mA/cm^2 Current Density

5.3 Stainless Steel Mesh Galvanic Replacement

In order to improve upon the catalytic performance of the hydrophilic electrophoretic depositions made on the stainless steel sheet, two optimizations were made. The first was to make the hydrophilic depositions on stainless steel mesh to improve the electrolyte interaction with the electrode due to the porosity of the mesh. The effect of going from the sheet to the mesh can be seen in Figure 37. The legend denotes the nanomaterial and present metal nanoparticles for each deposition, as well as the dispersion solution used for each.

For the 1 mA/cm^2 current density regime important for MEC hydrogen generation, the both the CNT-Ni depositions outperformed the bare SSM, with the CNT-Ni in IPA reaching the threshold current density at -1.17V vs. Ag/AgCl while the CNT-Ni in ethanol reached it at -1.21V vs. Ag/AgCl. The CNT-Ni deposition made in the ethanol dispersion was outperformed by its IPA counterpart again likely due to the presence of the more non-conductive $Ni(OH)_2$ as was explained in Chapter 2 of this work. At the maximum current densities generated at -1.6V vs. Ag/AgCl, the CNT-Ni in IPA generated far higher current densities than the other two samples and the ethanol deposition was unable to catalytically outperform the bare SSM.

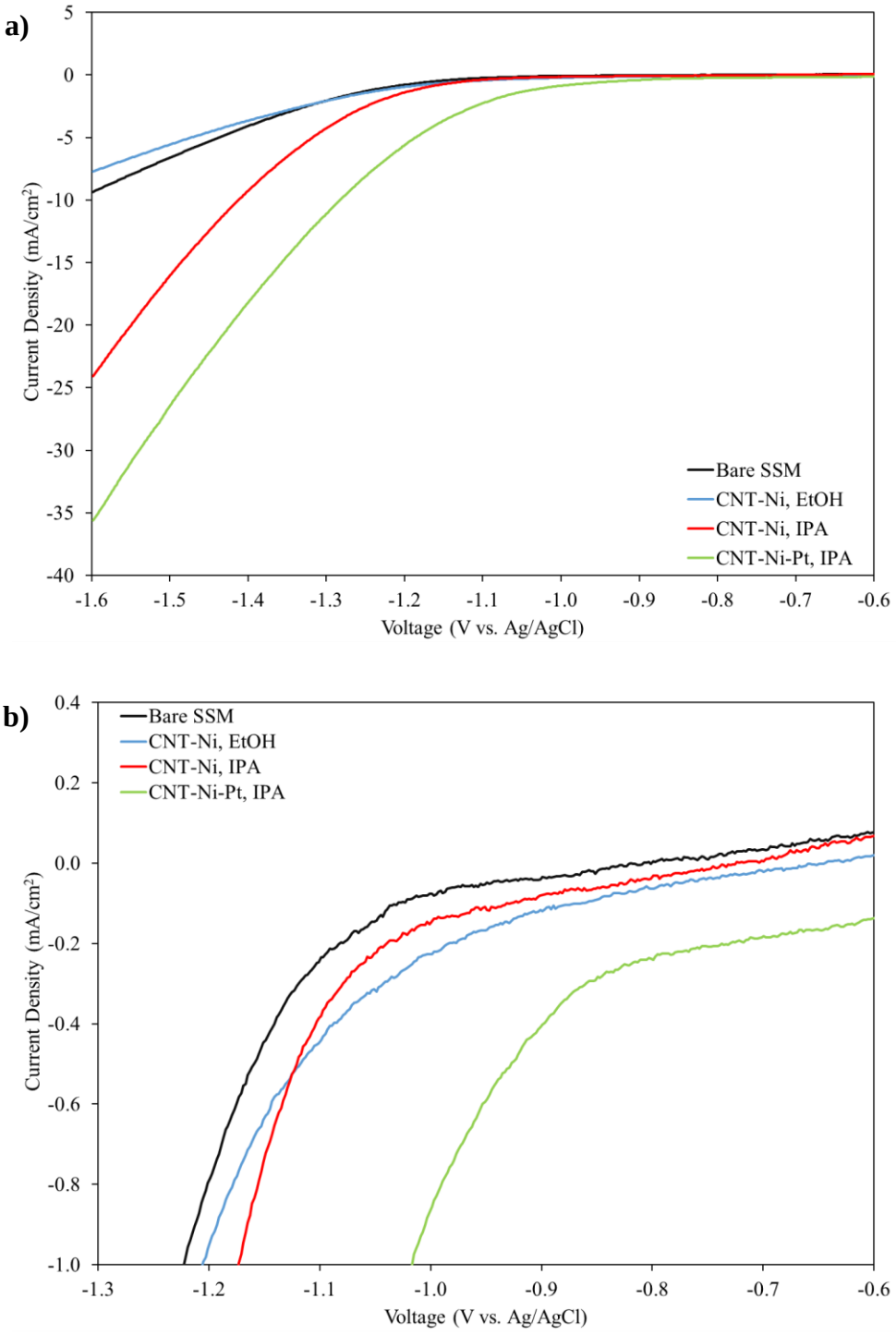

Figure 37: LSV of Stainless Steel Mesh for a a) 1V Window and b) 1 mA/cm^2 Current Density

The second optimization, shown as the CNT-Ni-Pt curve in Figure 37, was to take the best performing hydrophilic catalyst, in this case the CNT-Ni made in an IPA dispersion, and perform a platinum galvanic replacement of the nickel metal nanoparticles on the CNTs. The galvanic replacement of the platinum in the CNT-Ni-Pt deposition reduced the necessary voltage to reach the 1 mA/cm^2 current density criteria by 115 mV when compared to the only CNT-Ni one and increased the maximum current density seen at -1.6V by 48%. In order to perform the galvanic replacement, a duplicate CNT-Ni deposition was submerged in 0.025 mg/mL $PtCl_4$ dissolved in ethanol for 18 hours. After the submersion, the sample was triple rinsed in fresh ethanol to remove any excess ions, at which point EDS was conducted on galvanic replacement deposition before and after the replacement to show the change in the elemental components due to the process. As seen in Figure 38, only the after the galvanic replacement is conducted is there the presence of platinum, along with some adsorption of chlorine due to the fact that $PtCl_4$ was used as the source material for the platinum ions. The galvanic replacement process replaced some of the nickel metal nanoparticles with platinum ones due to the fact nickel ions are oxidized and dissolved out in the present of the more reactive platinum ion, which in turn allows the platinum ion to become reduced onto the CNT surface. This galvanic replacement process is well known and has been demonstrated for silver/gold nanoparticle replacement, as well as for the general formation of bimetallic nanotubes[96], [97].

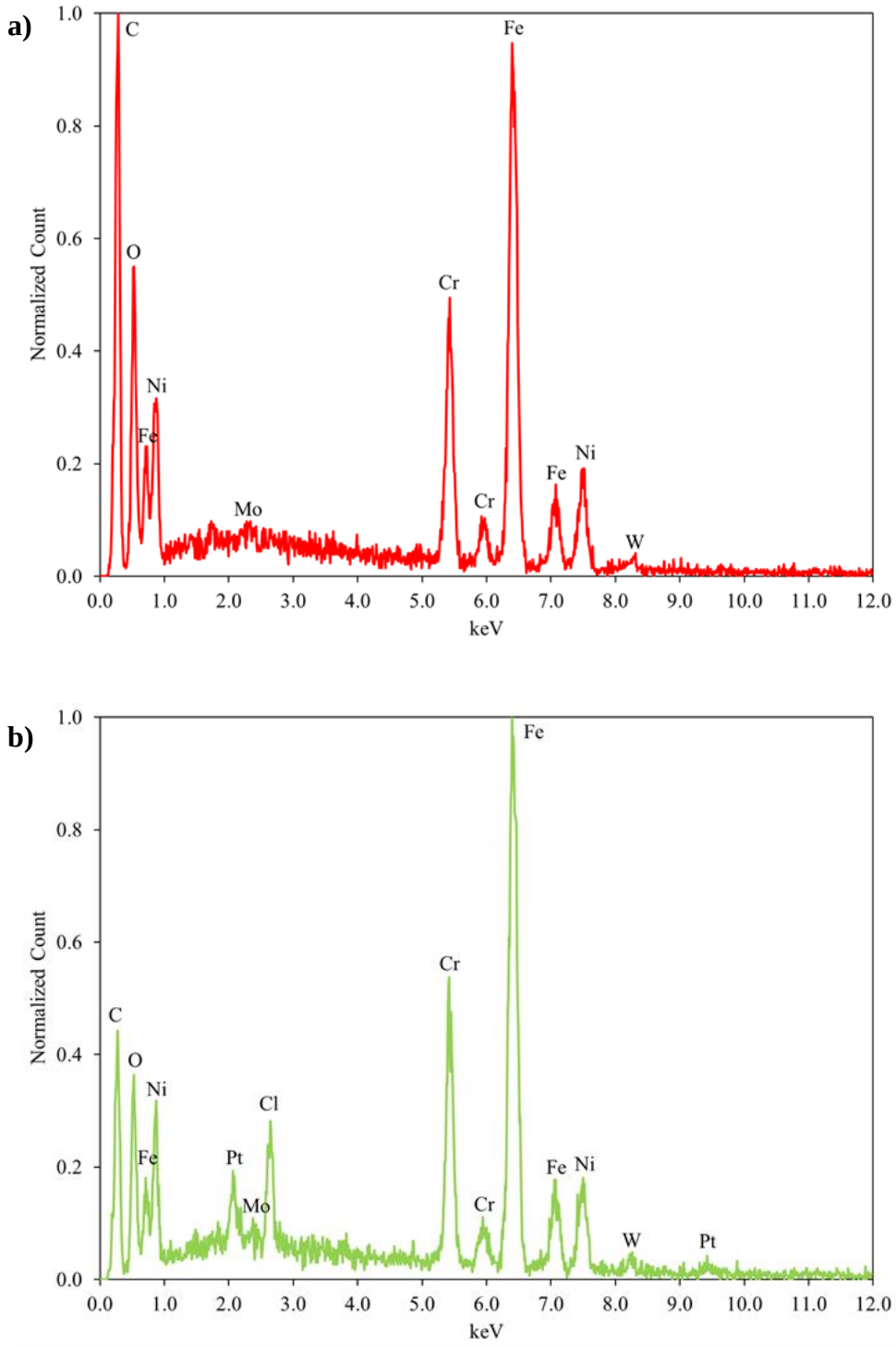

Figure 38: EDS of CNT-Ni Depositions a) Before and b) After Galvanic Replacement in a $PtCl_4$ Solution

5.4 Conclusion

An exploratory study of the use of EPD to create HER catalysts for MECs was conducted, which showed that hydrophilicity is important in order to improve catalytic performance. The galvanic replacement of nickel with platinum has been demonstrated for these particular EPD deposits as a quick, facile option to optimize the CNT-Ni catalytic activity in MECs.

VI. Overall Conclusions

6.1 Summary of Work

In summary, electrophoretic deposition was used as a method to deposit carbon nanotubes onto stainless steel for applications in microbial fuel cells and electrolysis cells. Some notable findings in this work include:

- The ability to control the hydrophilicity and hydrophobicity of CNT depositions made exclusively from EPD for MFC and MEC applications.
- The combined effect of anode surface wettability and conductivity on MFC start-up time and power density performance.
- The comparison of different types of stainless steel electrodes and how they perform as MFC anodes after the EPD of CNTs.
- The first use and characterization of radial EPD to develop stainless steel brushes with CNTs covering the length of their bristles for use as a high performance MFC anode.
- Demonstration of EPD for the deposition of HER catalysts for MECs and the effect of galvanic replacement of nickel with platinum on electrochemical performance.

For all of the anode studies listed in this work, extensive electrochemical testing, in particular cyclic voltammetry and electrochemical impedance spectroscopy, has been performed to provide an understanding of how the depositions made for each application change over the life cycle of the MFC.

6.2 Future Work

For future work, it would be beneficial to decouple the wettability from the conductivity to investigate how each parameter plays a role in, not just cell start-up, but also the long-term stability of EPD created anodes for MFCs. This could be done by changing from the smaller CNTs used in this study to a larger CNT, where alignment of CNTs could cause varying wettabilities, while maintaining the same anode conductivity. While some characterization at high voltages has been done for the radial EPD of CNTs onto stainless steel brushes, further refinement of the deposition process could be investigated for lower voltages and longer times in order to avoid the current limitation of the high-voltage power source. Lower voltages and longer times could lead to better coverage at the base of the brush bristles since the voltage gradient across each individual bristle would be much less than the high-voltage deposition. Further refinement of HER catalysts made via EPD is required, whether it be refinement in catalyst mass loading and subsequent platinum replacement or the development of new catalyst systems, and long-term testing of these catalysts in MECs is necessary.

VII. References

[1] R. E. Smalley, “Top Ten Problems of Humanity for Next 50 Years,” 2003.

[2] I. Dekanić, “Energy markets at the beginning of the second decade of the 21st century,” *Nafta*, vol. 62, no. 9–10, pp. 307–319, 2011.

[3] A. Dosio and E. M. Fischer, “Will Half a Degree Make a Difference? Robust Projections of Indices of Mean and Extreme Climate in Europe Under 1.5°C, 2°C, and 3°C Global Warming,” *Geophys. Res. Lett.*, vol. 45, no. 2, pp. 935–944, 2018.

[4] “New frontiers in sustainable energy production and storage,” *Vacuum*, vol. 122, pp. 369–375, 2015.

[5] “Sustainable development of road transportation sector using hydrogen energy system,” *Renew. Sustain. Energy Rev.*, vol. 51, pp. 1132–1155, 2015.

[6] W. T. Process and B. Use, “Cite as: Center for Sustainable Systems, University of Life Cycle Impacts Life Cycle Impact of Wastewater Treatment Systems 1,” 2018.

[7] W. Q. Guo, Q. L. Wu, S. S. Yang, S. M. Peng, and H. C. Luo, “The Promising Resource Utilization Methods of Excess Sludge: A Review,” *Appl. Mech. Mater.*, vol. 507, pp. 777–781, 2014.

[8] X. Li, I. Abu-Reesh, and Z. He, “Development of Bioelectrochemical Systems to Promote Sustainable Agriculture,” *Agriculture*, vol. 5, no. 3, pp. 367–388, 2015.

[9] D. R. Lovley, “The microbe electric: conversion of organic matter to electricity,” *Curr. Opin. Biotechnol.*, vol. 19, no. 6, pp. 564–571, 2008.

[10] B. E. Logan *et al.*, “Microbial fuel cells: Methodology and technology,” *Environ. Sci. Technol.*, vol. 40, no. 17, pp. 5181–5192, 2006.

[11] S. C. Barton, J. Gallaway, and P. Atanassov, “Enzymatic biofuel cells for implantable and

microscale devices," *Chem. Rev.*, vol. 104, no. 10, pp. 4867–4886, 2004.

[12] M. C. Potter, "Electrical Effects Accompanying the Decomposition of Organic Compounds," *Proc. R. Soc. B Biol. Sci.*, vol. 84, no. 571, pp. 260–276, 1911.

[13] J. R. Trapero, L. Horcajada, J. J. Linares, and J. Lobato, "Is microbial fuel cell technology ready? An economic answer towards industrial commercialization," *Appl. Energy*, vol. 185, pp. 698–707, 2017.

[14] D. Call and B. E. Logan, "Hydrogen production in a single chamber microbial electrolysis cell lacking a membrane," *Environ. Sci. Technol.*, vol. 42, no. 9, pp. 3401–3406, 2008.

[15] S. Cheng *et al.*, "Microbial electrolysis cells for high yield hydrogen gas production from organic matter," *Environ. Sci. Technol.*, vol. 42, no. 23, pp. 8630–8640, 2008.

[16] A. Kadier, Y. Simayi, P. Abdeshahian, N. F. Azman, K. Chandrasekhar, and M. S. Kalil, "A comprehensive review of microbial electrolysis cells (MEC) reactor designs and configurations for sustainable hydrogen gas production," *Alexandria Eng. J.*, vol. 55, no. 1, pp. 427–443, 2016.

[17] S. Oh, B. Min, and B. E. Logan, "Cathode performance as a factor in electricity generation in microbial fuel cells," *Environ. Sci. Technol.*, vol. 38, no. 18, pp. 4900–4904, 2004.

[18] H. Liu, S. Cheng, and B. E. Logan, "Power generation in fed-batch microbial fuel cells as a function of ionic strength, temperature, and reactor configuration," *Environ. Sci. Technol.*, vol. 39, no. 14, pp. 5488–5493, 2005.

[19] Y. Ahn and B. E. Logan, "Effectiveness of domestic wastewater treatment using microbial fuel cells at ambient and mesophilic temperatures," *Bioresour. Technol.*, vol. 101, no. 2, pp. 469–475, 2010.

[20] J. Wei, P. Liang, and X. Huang, "Recent progress in electrodes for microbial fuel cells,"

Bioresour. Technol., vol. 102, no. 20, pp. 9335–9344, 2011.

[21] A. ter Heijne, H. V. M. Hamelers, M. Saakes, and C. J. N. Buisman, "Performance of non-porous graphite and titanium-based anodes in microbial fuel cells," *Electrochim. Acta*, vol. 53, no. 18, pp. 5697–5703, 2008.

[22] F. Li, Y. Sharma, Y. Lei, B. Li, and Q. Zhou, "Microbial fuel cells: The effects of configurations, electrolyte solutions, and electrode materials on power generation," *Appl. Biochem. Biotechnol.*, vol. 160, no. 1, pp. 168–181, 2010.

[23] H. Liu, R. Ramnarayanan, and B. E. Logan, "Production of Electricity during Wastewater Treatment Using a Single Chamber Microbial Fuel Cell," *Environ. Sci. Technol.*, vol. 38, no. 7, pp. 2281–2285, 2004.

[24] J. M. Sonawane, A. Yadav, P. C. Ghosh, and S. B. Adeloju, "Recent advances in the development and utilization of modern anode materials for high performance microbial fuel cells," *Biosens. Bioelectron.*, vol. 90, no. September 2016, pp. 558–576, 2017.

[25] B. Logan, S. Cheng, V. Watson, and G. Estadt, "Graphite Fiber Brush Anodes for Increased Power Production in Air-Cathode Microbial Fuel Cells," *Environ. Sci. Technol.*, vol. 41, no. 9, pp. 3341–3346, 2007.

[26] D. Pocaznoi, A. Calmet, L. Etcheverry, B. Erable, and A. Bergel, "Stainless steel is a promising electrode material for anodes of microbial fuel cells," *Energy Environ. Sci.*, vol. 5, no. 11, p. 9645, 2012.

[27] H. Wang *et al.*, "High power density microbial fuel cell with flexible 3D graphene-nickel foam as anode," *Nanoscale*, vol. 5, no. 21, pp. 10283–10290, 2013.

[28] A. Baudler, I. Schmidt, M. Langner, A. Greiner, and U. Schröder, "Does it have to be carbon? Metal anodes in microbial fuel cells and related bioelectrochemical systems,"

Energy Environ. Sci., vol. 8, no. 7, pp. 2048–2055, 2015.

[29] X. Zhu and B. E. Logan, "Copper anode corrosion affects power generation in microbial fuel cells," *J. Chem. Technol. Biotechnol.*, vol. 89, no. 3, pp. 471–474, 2014.

[30] J. Hou, Z. Liu, S. Yang, and Y. Zhou, "Three-dimensional macroporous anodes based on stainless steel fiber felt for high-performance microbial fuel cells," *J. Power Sources*, vol. 258, no. July, pp. 204–209, 2014.

[31] S. Cheng and B. E. Logan, "Ammonia treatment of carbon cloth anodes to enhance power generation of microbial fuel cells," *Electrochem. commun.*, vol. 9, no. 3, pp. 492–496, 2007.

[32] Y. Feng, Q. Yang, X. Wang, and B. E. Logan, "Treatment of carbon fiber brush anodes for improving power generation in air-cathode microbial fuel cells," *J. Power Sources*, vol. 195, no. 7, pp. 1841–1844, 2010.

[33] K. Guo, D. Hidalgo, T. Tommasi, and K. Rabaey, "Pyrolytic carbon-coated stainless steel felt as a high-performance anode for bioelectrochemical systems," *Bioresour. Technol.*, vol. 211, pp. 664–668, 2016.

[34] J. L. Lamp *et al.*, "Flame synthesis of carbon nanostructures on stainless steel anodes for use in microbial fuel cells," *J. Power Sources*, vol. 196, no. 14, pp. 5829–5834, 2011.

[35] X. Zhang, M. Epifanio, and E. Marsili, "Electrochemical characteristics of Shewanella loihica on carbon nanotubes-modified graphite surfaces," *Electrochim. Acta*, vol. 102, pp. 252–258, 2013.

[36] H. F. Cui, L. Du, P. B. Guo, B. Zhu, and J. H. T. Luong, "Controlled modification of carbon nanotubes and polyaniline on macroporous graphite felt for high-performance microbial fuel cell anode," *J. Power Sources*, vol. 283, pp. 46–53, 2015.

[37] T. S. Song, Peng-Xiao, X. Y. Wu, and C. C. Zhou, “Electrophoretic deposition of multi-walled carbon nanotube on a stainless steel electrode for use in sediment microbial fuel cells,” *Appl. Biochem. Biotechnol.*, vol. 170, no. 5, pp. 1241–1250, 2013.

[38] D. Zhu *et al.*, “Effect of carbon nanotube modified cathode by electrophoretic deposition method on the performance of sediment microbial fuel cells,” *Biotechnol. Lett.*, vol. 37, no. 1, pp. 101–107, 2015.

[39] X. Peng, S. Chen, L. Liu, S. Zheng, and M. Li, “Modified stainless steel for high performance and stable anode in microbial fuel cells,” *Electrochim. Acta*, vol. 194, pp. 246–252, 2016.

[40] C. Santoro *et al.*, “The effects of carbon electrode surface properties on bacteria attachment and start up time of microbial fuel cells,” *Carbon N. Y.*, vol. 67, pp. 128–139, 2014.

[41] Y. Fu, J. Yu, Y. Zhang, and Y. Meng, “Graphite coated with manganese oxide/multiwall carbon nanotubes composites as anodes in marine benthic microbial fuel cells,” *Appl. Surf. Sci.*, vol. 317, pp. 84–89, 2014.

[42] X. yuan Wu *et al.*, “Effect of zeolite-coated anode on the performance of microbial fuel cells,” *J. Chem. Technol. Biotechnol.*, vol. 90, no. 1, pp. 87–92, 2015.

[43] H. O. Mohamed *et al.*, “Cobalt oxides-sheathed cobalt nano flakes to improve surface properties of carbonaceous electrodes utilized in microbial fuel cells,” *Chem. Eng. J.*, vol. 326, pp. 497–506, 2017.

[44] A. Choudhury *et al.*, “Effect of electrode surface properties on enhanced electron transfer activity in microbial fuel cells,” *Eng. Life Sci.*, vol. 17, no. 2, pp. 186–192, 2017.

[45] F. G. Boyaci San and I. Isik-Gulsac, “Effect of surface wettability of polymer composite

bipolar plates on polymer electrolyte membrane fuel cell performances," *Int. J. Hydrogen Energy*, vol. 38, no. 10, pp. 4089–4098, 2013.

[46] Z. Lu, C. Rath, G. Zhang, and S. G. Kandlikar, "Water management studies in PEM fuel cells, part IV: Effects of channel surface wettability, geometry and orientation on the two-phase flow in parallel gas channels," *Int. J. Hydrogen Energy*, vol. 36, no. 16, pp. 9864–9875, 2011.

[47] L. Besra and M. Liu, "A review on fundamentals and applications of electrophoretic deposition (EPD)," *Prog. Mater. Sci.*, vol. 52, no. 1, pp. 1–61, 2007.

[48] A. R. Boccaccini, J. A. Roether, B. J. C. Thomas, M. S. P. Shaffer, and E. Chavez, "The Electrophoretic Deposition of Inorganic Nanoscaled Materials," *J. Ceram. Soc. Japan*, vol. 14, 2006.

[49] a R. Boccaccini, S. Keim, R. Ma, Y. Li, and I. Zhitomirsky, "Electrophoretic deposition of biomaterials.," *J. R. Soc. Interface*, vol. 7 Suppl 5, no. May, pp. S581–S613, 2010.

[50] S. Santhanagopalan, F. Teng, and D. D. Meng, "High-voltage electrophoretic deposition for vertically aligned forests of one-dimensional nanoparticles," *Langmuir*, vol. 27, no. 2, pp. 561–569, 2011.

[51] S. Santhanagopalan, A. Balram, and D. D. Meng, "Scalable high-power redox capacitors with aligned nanoforests of crystalline MnO2 nanorods by high voltage electrophoretic deposition," *ACS Nano*, vol. 7, no. 3, pp. 2114–2125, 2013.

[52] A. Balram, S. Santhanagopalan, B. Hao, Y. K. Yap, and D. D. Meng, "Electrophoretically-Deposited Metal-Decorated CNT Nanoforests with High Thermal/Electric Conductivity and Wettability Tunable from Hydrophilic to Superhydrophobic," *Adv. Funct. Mater.*, vol. 26, no. 15, pp. 2571–2579, 2016.

[53] D. R. Bond, “Electricity Production by Geobacter sulfurreducens Attached to Electrodes,” *Appl. Environ. Microbiol.*, vol. 69, no. 3, pp. 1548–1555, 2003.

[54] V. G. Debabov, “Electricity from microorganisms,” *Microbiology*, vol. 77, no. 2, pp. 123–131, 2008.

[55] E. Marsili, J. B. Rollefson, D. B. Baron, R. M. Hozalski, and D. R. Bond, “Microbial biofilm voltammetry: Direct electrochemical characterization of catalytic electrode-attached biofilms,” *Appl. Environ. Microbiol.*, vol. 74, no. 23, pp. 7329–7337, 2008.

[56] K. Fricke, F. Harnisch, and U. Schröder, “On the use of cyclic voltammetry for the study of anodic electron transfer in microbial fuel cells,” *Energy Environ. Sci.*, vol. 1, no. 1, pp. 144–147, 2008.

[57] F. A. Armstrong, H. A. Heering, and J. Hirst, “Reaction of complex metalloproteins studied by protein-film voltammetry,” *Chem. Soc. Rev.*, vol. 26, no. 3, p. 169, 1997.

[58] B. E. Logan *et al.*, “Microbial Fuel Cells: Methodology and Technology,” *Environ. Sci. Technol.*, vol. 40, no. 17, pp. 1–9, 2006.

[59] T. S. Magnuson, “Isolation, characterization and gene sequence analysis of a membrane-associated 89 kDa Fe(III) reducing cytochrome c from Geobacter sulfurreducens,” *Biochem. J.*, vol. 359, no. 1, pp. 147–152, 2001.

[60] D. H. Park and J. G. Zeikus, “Utilization of electrically reduced neutral red by Actinobacillus succinogenes: Physiological function of neutral red in membrane-driven fumarate reduction and energy conservation,” *J. Bacteriol.*, vol. 181, no. 8, pp. 2403–2410, 1999.

[61] D. R. Bond, D. R. Bond, D. E. Holmes, and L. M. Tender, “Electrode-Reducing Microorganisms That Harvest Energy from Marine Sediments,” *Science (80-.).*, vol. 295,

no. 2002, pp. 483–485, 2002.

[62] B. Min, S. Cheng, and B. E. Logan, “Electricity generation using membrane and salt bridge microbial fuel cells,” *Water Res.*, vol. 39, no. 9, pp. 1675–1686, 2005.

[63] B. E. Logan, “Essential data and techniques for conducting microbial fuel cell and other types of bioelectrochemical system experiments,” *ChemSusChem*, vol. 5, no. 6, pp. 988–994, 2012.

[64] H. Liu, S. Cheng, and B. E. Logan, “Production of electricity from acetate or butyrate using a single-chamber microbial fuel cell,” *Environ. Sci. Technol.*, vol. 39, no. 2, pp. 658–662, 2005.

[65] H. Liu and B. E. Logan, “Electricity generation using an air-cathode single chamber microbial fuel cell in the presence and absence of a proton exchange membrane,” *Environ. Sci. Technol.*, vol. 38, no. 14, pp. 4040–4046, 2004.

[66] G. Liu, M. D. Yates, S. Cheng, D. F. Call, D. Sun, and B. E. Logan, “Examination of microbial fuel cell start-up times with domestic wastewater and additional amendments,” *Bioresour. Technol.*, vol. 102, no. 15, pp. 7301–7306, 2011.

[67] V. J. Watson and B. E. Logan, “Analysis of polarization methods for elimination of power overshoot in microbial fuel cells,” *Electrochem. commun.*, vol. 13, no. 1, pp. 54–56, 2011.

[68] Y. Hong, D. F. Call, C. M. Werner, and B. E. Logan, “Adaptation to high current using low external resistances eliminates power overshoot in microbial fuel cells,” *Biosens. Bioelectron.*, vol. 28, no. 1, pp. 71–76, 2011.

[69] J. Ge and H. Liu, “Experimental studies of a direct methanol fuel cell,” *J. Power Sources*, vol. 142, no. 1–2, pp. 56–69, 2005.

[70] X. Zhu, J. C. Tokash, Y. Hong, and B. E. Logan, “Controlling the occurrence of power

overshoot by adapting microbial fuel cells to high anode potentials," *Bioelectrochemistry*, vol. 90, pp. 30–35, 2013.

[71] H. Liu, S. Grot, and B. E. Logan, "Electrochemically assisted microbial production of hydrogen from acetate," *Environ. Sci. Technol.*, vol. 39, no. 11, pp. 4317–4320, 2005.

[72] R. A. Rozendal, H. V. M. Hamelers, G. J. W. Euverink, S. J. Metz, and C. J. N. Buisman, "Principle and perspectives of hydrogen production through biocatalyzed electrolysis," *Int. J. Hydrogen Energy*, vol. 31, no. 12, pp. 1632–1640, 2006.

[73] L. Lu and Z. J. Ren, "Microbial electrolysis cells for waste biorefinery: A state of the art review," *Bioresour. Technol.*, vol. 215, pp. 254–264, 2016.

[74] R. Karthikeyan, K. Y. Cheng, A. Selvam, A. Bose, and J. W. C. Wong, "Bioelectrohydrogenesis and inhibition of methanogenic activity in microbial electrolysis cells - A review," *Biotechnol. Adv.*, vol. 35, no. 6, pp. 758–771, 2017.

[75] J. Y. Nam and B. E. Logan, "Enhanced hydrogen generation using a saline catholyte in a two chamber microbial electrolysis cell," *Int. J. Hydrogen Energy*, vol. 36, no. 23, pp. 15105–15110, 2011.

[76] S. Cheng and B. E. Logan, "High hydrogen production rate of microbial electrolysis cell (MEC) with reduced electrode spacing," *Bioresour. Technol.*, vol. 102, no. 3, pp. 3571–3574, 2011.

[77] K. Rabaey and W. Verstraete, "Microbial fuel cells: Novel biotechnology for energy generation," *Trends Biotechnol.*, vol. 23, no. 6, pp. 291–298, 2005.

[78] R. A. Rozendal, H. V. M. Hamelers, K. Rabaey, J. Keller, and C. J. N. Buisman, "Towards practical implementation of bioelectrochemical wastewater treatment," *Trends Biotechnol.*, vol. 26, no. 8, pp. 450–459, 2008.

[79] B. E. Logan, “Scaling up microbial fuel cells and other bioelectrochemical systems,” *Appl. Microbiol. Biotechnol.*, vol. 85, no. 6, pp. 1665–1671, 2010.

[80] B. Zhang, C. Feng, J. Ni, J. Zhang, and W. Huang, “Simultaneous reduction of vanadium (V) and chromium (VI) with enhanced energy recovery based on microbial fuel cell technology,” *J. Power Sources*, vol. 204, pp. 34–39, 2012.

[81] I. S. Chang *et al.*, “Continuous determination of biochemical oxygen demand using microbial fuel cell type biosensor,” *Biosens. Bioelectron.*, vol. 19, no. 6, pp. 607–613, 2004.

[82] G. G. Kumar, V. G. S. Sarathi, and K. S. Nahm, “Recent advances and challenges in the anode architecture and their modifications for the applications of microbial fuel cells,” *Biosens. Bioelectron.*, vol. 43, no. 1, pp. 461–475, 2013.

[83] S. Cheng and B. E. Logan, “Increasing power generation for scaling up single-chamber air cathode microbial fuel cells,” *Bioresour. Technol.*, vol. 102, no. 6, pp. 4468–4473, 2011.

[84] J. J. Sun, H. Z. Zhao, Q. Z. Yang, J. Song, and A. Xue, “A novel layer-by-layer self-assembled carbon nanotube-based anode: Preparation, characterization, and application in microbial fuel cell,” *Electrochim. Acta*, vol. 55, no. 9, pp. 3041–3047, 2010.

[85] R. J. M. Logan, Bruce E., “Microbial Challenges and fuel cells applications,” *Environ. Sci. Technol.*, pp. 5172–5180, 2006.

[86] S. Santhanagopalan, A. Balram, E. Lucas, F. Marcano, and D. D. S. Meng, “High Voltage Electrophoretic Deposition of Aligned Nanoforests for Scalable Nanomanufacturing of Electrochemical Energy Storage Devices,” *Key Eng. Mater.*, vol. 507, pp. 67–72, 2012.

[87] A. F. Stalder, T. Melchior, M. Müller, D. Sage, T. Blu, and M. Unser, “Low-bond axisymmetric drop shape analysis for surface tension and contact angle measurements of

sessile drops," *Colloids Surfaces A Physicochem. Eng. Asp.*, vol. 364, no. 1–3, pp. 72–81, 2010.

[88] X. Tan, M. Fang, C. Chen, S. Yu, and X. Wang, "Counterion effects of nickel and sodium dodecylbenzene sulfonate adsorption to multiwalled carbon nanotubes in aqueous solution," *Carbon N. Y.*, vol. 46, no. 13, pp. 1741–1750, 2008.

[89] L. Zheng *et al.*, "Exceptional superhydrophobicity and low velocity impact icephobicity of acetone-functionalized carbon nanotube films," *Langmuir*, vol. 27, no. 16, pp. 9936–9943, 2011.

[90] G. H. A. Therese and P. V. Kamath, "Electrochemical synthesis of metal oxides and hydroxides," *Chem. Mater.*, vol. 12, no. 5, pp. 1195–1204, 2000.

[91] A. Balram, H. Zhang, and S. Santhanagopalan, "Enhanced Oxygen Evolution Reaction Electrocatalysis via Electrodeposited Amorphous α-Phase Nickel-Cobalt Hydroxide Nanodendrite Forests," *ACS Appl. Mater. Interfaces*, vol. 9, no. 34, pp. 28355–28365, 2017.

[92] N. Sekar and R. P. Ramasamy, "Electrochemical Impedance Spectroscopy for Microbial Fuel Cell Characterization," *J. Microb. Biochem. Technol.*, 2013.

[93] R. P. Ramasamy, Z. Ren, M. M. Mench, and J. M. Regan, "Impact of initial biofilm growth on the anode impedance of microbial fuel cells," *Biotechnol. Bioeng.*, vol. 101, no. 1, pp. 101–108, 2008.

[94] J. Hou, Z. Liu, Y. Li, S. Yang, and Y. Zhou, "A comparative study of graphene-coated stainless steel fiber felt and carbon cloth as anodes in MFCs," *Bioprocess Biosyst. Eng.*, vol. 38, no. 5, pp. 881–888, 2015.

[95] Y. J. Choi *et al.*, "Electrophoretically fabricated nickel/nickel oxides as cost effective

nanocatalysts for the oxygen reduction reaction in air-cathode microbial fuel cell," *Int. J. Hydrogen Energy*, no. xxxx, pp. 1–11, 2019.

[96] A. A. El Mel *et al.*, "Galvanic Replacement Reaction: A Route to Highly Ordered Bimetallic Nanotubes," *J. Phys. Chem. C*, vol. 120, no. 31, pp. 17652–17659, 2016.

[97] A. G. M. Da Silva, T. S. Rodrigues, S. J. Haigh, and P. H. C. Camargo, "Galvanic replacement reaction: Recent developments for engineering metal nanostructures towards catalytic applications," *Chem. Commun.*, vol. 53, no. 53, pp. 7135–7148, 2017.